VALIDATION OF THE RELAP5 CODE FOR LOHS EVENTS IN THE MNR

VALIDATION OF THE RELAP5 CODE FOR LOSS OF HEAT SINK EVENTS IN THE MCMASTER NUCLEAR REACTOR

By KEVIN SEBASTIAN RUIZ, BS, MASc

A Thesis Submitted to the School of Graduate Studies in Partial Fulfillment of the Requirements for the Degree Master of Applied Science

McMaster University
MASTER OF APPLIED SCIENCE (2024)
Hamilton, Ontario, Canada (Engineering Physics)

TITLE:	Validation of the RELAP5 Code for Loss of Heat Sink Events in the McMaster Nuclear Reactor
AUTHOR:	Kevin Sebastian Ruiz BS, MASc (Nuclear Engineering), Instituto Balseiro, Bariloche, Argentina
SUPERVISOR:	Dr. David Novog
NUMBER OF PAGES:	xix, 154

Abstract

Open pool research reactors play a crucial role in industry, medicine, scientific research and training. Ensuring its safety involves the use of widely accepted computer codes, such as RELAP5, that can predict the progression of accidents and evaluate reactor performance during transient events. These codes need a continuous validation process against various accident scenarios to ensure the reliability of the results. Two Loss of Heat Sink events (LOHS) took place previously in the McMaster Nuclear Reactor. One is the Loss of Forced Circulation in the Secondary Side event that happened in the year 2020, and the second is the Pool Temperature Experiment conducted at the McMaster Nuclear Reactor (MNR) in March 2023. These two events became a perfect opportunity to validate the safety analysis tools used by the NOF (Nuclear Operations and Facilities) staff. The focus was on validating the MNR RELAP5 model, particularly on the simulation of a loss of heat sink (LOHS) accident caused by the loss of the secondary pump. This study elucidates the validation results of the RELAP5 code for these two events and also under steady state conditions. A particular finding of this research was that reactor pool cooling transients prior to the start of a loss of heat sink accident (LOHS) can have an impact on the pool heating rate due to the pool thermal stratification. In these cases, the common assumption of an initial homogeneous temperature profile in the pool might not be

accurate and could lead to underestimating the core temperature. With the help of CFD simulations it was possible to adjust the RELAP5 model, by providing a stratified temperature profile of the pool to be used as initial condition for the simulations. This led to more accurate estimations of the pool heating rate during the LOHS. Moreover, a sensitivity analysis on the pool nodalization showed that a minimum of two vertical pipes interconnected laterally by cross flow junctions is needed for the accurate analysis of this kind of transients.

To my family

Acknowledgements

I extend my heartfelt appreciation to the contributors who played key roles in this research endeavor.

Dr. David Novog, my dedicated supervisor, provided invaluable guidance, expertise, and unwavering support throughout this study. His mentorship was integral to the success and depth of this research.

Dr. Simon Day, the lead analyst at McMaster Nuclear Reactor, offered essential guidance and assistance, providing crucial insights and expertise that were indispensable to this research.

I express gratitude to my colleagues from the Technical University of Munich, particularly Dr. Christian Reiter, Dr. Kaltrina Shehu, Tilmann Schlitt, Ronja Schoenecker, Lorenzo Nastasi and Lukas Kuhnemann for their valuable discussions, support, and contributions.

The McMaster Nuclear Reactor staff, including operators, managers, and technical services personnel, are acknowledged for their cooperation, assistance, and provision of essential experimental data.

My beloved family who always motivates me to give my best. My eternal gratitude for your unconditional support and for always being there for me. No matter how great the distance is that separates us, I will always carry you in my heart.

Table of Contents

Abstract **iii**

Acknowledgements **vi**

Notation, Definitions, and Abbreviations **xvii**

1 Introduction **1**

1.1 Background 1

1.2 Objectives 3

1.3 Thesis structure 4

2 Literature Review **6**

2.1 McMaster Nuclear Reactor (MNR) 6

2.2 Loss of Heat Sink Events in the MNR 14

2.3 Instrumentation in the MNR 22

2.4 The RELAP5 code 28

3 Theory **33**

3.1 Conservation of Mass 35

3.2 Conservation of Momentum 35

3.3 Conservation of Energy 37
3.4 Heat transfer 38

4 Model Development **40**
4.1 RELAP5 model of the MNR 40
4.2 Reactor nodalization 41
4.3 Reactor Pool 44
4.4 Reactor core 52
4.5 Primary piping and valves 71
4.6 Hold-up tank 77
4.7 Primary pump 81
4.8 Heat exchanger 82
4.9 Secondary Heat Transport System 88

5 Results and Discussion **90**
5.1 Simulation of the loss of forced circulation in the secondary side in 2020 90
5.2 Simulation of the Pool Temperature Experiment in 2023 100
5.3 Sensitivity analysis 111

6 Conclusion **140**

7 Future Work **144**

A CFD model of the MNR pool **147**

List of Figures

2.1 Schematic of the McMaster Nuclear Reactor primary loop. 7

2.2 McMaster Nuclear Reactor heat transport system. Taken from MNR Facility Specification Thermal-Hydraulics [20]. 10

2.3 MNR pool layout (picture and diagram). 14

2.4 Temperature readings during the loss of forced circulation in the secondary side in 2020. 17

2.5 Temperature and power readings during the Pool Temperature Experiment. 19

2.6 Derivative of the core inlet temperature over time. 21

2.7 Schematic of the Primary Heat Transport System including the position of the flow and temperature sensors. 25

4.1 Nodalization of the MNR RELAP5 model. 43

4.2 Top view of the Pool with dimensions and positions of structures. Taken from MNR Safety Analysis Report [1] 45

4.3 Pool nodalization with two vertical pipes interconnected through cross-flow lateral junctions. 47

4.4 Cross section of the Pool with dimensions. 50

4.5 Slab thermal model used in the heat structures of the Pool wall. . . . 51

4.6 Typical Core Layout. Taken from MNR Safe Operating Envelope [2]. 53
4.7 Perspective of an MSFA (left) and a typical core configuration (right). Schematic provided by MNR analysis team. 55
4.8 Axial view of the MSFA. Taken from MNR Reactor Specification technical report [9]. 55
4.9 Cross section of the MSFA with dimensions. Taken from MNR Safe Operating Envelope [2]. 56
4.10 Axial view of the MCA. Taken from MNR Reactor Specification technical report [9]. 58
4.11 Cross section of the MCA with dimensions. Taken from MNR Safe Operating Envelope [2]. 59
4.12 Schematic of the MNR graphite reflector assembly. Taken from MNR Safe Operating Envelope [2]. 60
4.13 Schematic of the MNR beryllium reflector assembly. Taken from MNR Safe Operating Envelope [2]. 61
4.14 Upstream flow paths to open bypass hole. Taken from MNR Safe Operating Envelope [2]. 62
4.15 Core configuration 62P. 64
4.16 Core nodalization. 65
4.17 Core power distribution. 68
4.18 Core power per axial node. 69
4.19 Slab thermal model used in the heat structures of the core. 70
4.20 Example of how the piping system is nodalized in the RELAP5 model. 75
4.21 Radial thermal model used in the heat structures of the piping. . . . 76

4.22 Top view of the HUT "U" shaped geometry. 78
4.23 Representation of the HUT nodalization. 79
4.24 Cross section of the HUT showing concrete wall thickness. 81
4.25 Pictures showing the heat exchanger sides. 84
4.26 Picture of the two heat exchangers assembled in series. 84
4.27 Schematic showing the design of the heat exchanger. 85
4.28 Illustration showing the primary and secondary flow paths within the 2 heat exchangers in series. 85
4.29 Nodalization of the MNR Heat Exchanger. 86
4.30 Radial thermal model used in the heat structures of the Heat Exchanger tubes. 88
5.1 Steady State core inlet and outlet temperatures (Loss of secondary, 2020). 92
5.2 Steady State HEX inlet and outlet temperatures (Loss of secondary, 2020). 93
5.3 Steady State primary and secondary flow (Loss of secondary, 2020). . 94
5.4 Primary and secondary flow over time (Loss of secondary, 2020). . . . 96
5.5 Transient core inlet and outlet temperatures (Loss of secondary, 2020). 97
5.6 Core inlet temperature derivative over time (Loss of secondary, 2020). 98
5.7 Transient HEX inlet and outlet temperatures (Loss of secondary, 2020). 99
5.8 Evolution of the outlet Heat Exchanger temperature used as inlet condition for the pool cooling simulation. 102
5.9 CAD model pool used for the CFD simulation. Indications denote the boundary conditions for the model. 103

5.10 Pool temperature results from CFD simulations. 105
5.11 Average pool temperature axial profile at the end of the cooling process. 106
5.12 Pool temperature profile over the first 1000 seconds (∼0.27 hours) of simulation. 107
5.13 Core inlet and outlet temperature over time. 108
5.14 Core inlet temperature derivative over time. 109
5.15 Pool temperature across multiple heights from RELAP. 110
5.16 Core inlet and outlet temperature over time, with uniform pool temperature as initial condition. 113
5.17 Derivative of the core inlet temperature over time, with uniform pool temperature as initial condition. 114
5.18 Core inlet and outlet temperature over time, considering the pool cooling process. 116
5.19 Derivative of the core inlet temperature over time, considering the pool cooling process. 117
5.20 Comparison of the core inlet temperature over time with the different assumptions. 119
5.21 Comparison of the core inlet derivative over time with the different assumptions. 120
5.22 Representation of the 1-pipe nodalization of the Pool. 124
5.23 Pool temperature across height with a 1-pipe nodalization. 125
5.24 Representation of the 2-pipe nodalization of the Pool. 126
5.26 Pool temperature across height with 4-pipe nodalization. 129

5.27 Comparison of the Pool average temperature obtained with the three different nodalizations. 130
5.28 Comparison of the core inlet temperature obtained with the three different nodalizations and the experimental measurements. 131
5.29 Comparison of the derivative of the core inlet temperature obtained with the three different nodalizations and the experimental measurements. 132
5.30 HUT nodalization considering a single vertical pipe. 134
5.31 HUT nodalization considering a 2 vertical pipes connected laterally with cross-flow junctions. 134
5.32 Comparison of the coolant time delay in the HUT with three different nodalizations; considering 1, 2 and 7 vertical pipes. 136
5.33 Core temperature evolution with and without heat losses. 138
5.34 Evolution of the core inlet derivative with and without heat losses. . . 139
A.1 CAD model of the MNR pool. The core is shown in red. The Inlet of the pool is shown both figures, while the outlet is only shown on the left-hand side figure. In the right-hand side figure, the outlet is located below the core. 149

List of Tables

2.1 Uncertainties of the reactor measurements. 26

3.1 Boundary condition options for the heat transfer problem in RELAP5. 39

4.1 MNR Pool operational parameters. 45

4.2 Axial position and static pressure of the pool nodes. 49

4.3 Thermal properties of concrete. 52

4.4 Geometric parameters of the MSFA for constructing the core model. . 57

4.5 Averaged hydraulic parameters for the core model. 67

4.6 Relative and absolute axial power distribution. 68

4.7 Thermal properties of the fuel meat. 71

4.8 Thermal properties of the cladding. 71

4.9 Primary piping information. 72

4.10 Thermal properties of Stainless Steel (type 304). 76

4.11 Parameters used for the primary pump model. 82

4.12 Design specifications of the heat exchanger. 83

5.1 Steady-State results and comparison with experimental measurements in the secondary loss simulation. *Note: the window of uncertainty in the orifice flowmeter measurements represents the standard deviation of the data recorded during the steady state period under consideration. The random uncertainty associated with the instrument was not accounted for. 95

5.2 Transient results and comparison with experimental measurements in the secondary loss simulation. *Note: the window of uncertainty in the heating rate denotes the standard deviation of the temperature derivative during the stable period (from $t = 0.5h$ to $t = 1.5h$). 100

5.3 RELAP results and comparison with experimental measurements in the Pool Temperature Experiment simulation. *Note: the window of uncertainty in the orifice flowmeter measurements represents the standard deviation of the data recorded during the first heating cycle of the experiment. The random uncertainty associated with the instrument was not accounted for. 111

5.4 RELAP results and comparison with experimental measurements in the Pool Temperature Experiment simulation assuming initial uniform pool temperature. 114

5.5 RELAP results and comparison with experimental measurements in the Pool Temperature Experiment simulation considering the pool cooldown process previous to the start of the experiment. 117

5.6 RELAP results and comparison with experimental measurements considering the effect of heat losses. 139

A.1 Mesh sensitivity analysis parameters for three meshes. 149

Notation, Definitions, and Abbreviations

Definitions

Reactor Core The arrangement of fuel assemblies, control assemblies and reflectors in a certain geometry where the nuclear fission chain reaction takes place.

Primary Heat Tansport System

The light water heat transfer circuit that includes the Pool and enclosed piping circuit via which light water coolant exits the Reactor Pool, flows through the Heat Exchanger and is returned to the Reactor Pool. Water in the Primary Loop flows through the Reactor Core, removing heat from the fuel, and passes this to the Secondary Loop via the Heat Exchanger.

Secondary Heat Transport System

The light water heat transfer circuit that collects heat from the Primary Loop through the Heat Exchanger and transports this water to

the Cooling Towers where the heat is dissipated to the atmosphere.

Reactor Pool Large concrete structure that houses the core and contains enough water to provide cooling, moderation and biological shielding.

Hold-Up Tank

Large volume tank whose function is to delay the coolant flow before it reaches the primary pump, allowing the decay of short-lived radioisotopes.

Abbreviations

MNR McMaster Nuclear Reactor

MTR Materials Testing Reactor, a term typically used to indicate use of rectangular plate-fuel assemblies

MSFA MNR Standard Fuel Assembly

MCFA MNR Control Fuel Assembly

CIF Central Irradiation Facility

HTS Heat Transport System

LOHS Loss of Heat Sink

HEX Heat Exchanger

HUT Hold-Up Tank

LEU	Low Enriched Uranium (< 20% U-235)
SAR	Safety Analysis Report
OLCs	Operating Limits and Conditions
SOE	Safe Operating Envelope

Chapter 1

Introduction

1.1 Background

To ensure the safety and reliability of nuclear reactors, comprehensive modeling and analysis of various operational and transient scenarios is needed. Among the key tools used for such evaluations is the RELAP (Reactor Excursion and Leak Analysis Program) code, distinguished for its exceptional capabilities to simulate thermohydraulic systems and used for deterministic safety analysis [4]. This code plays a key role in the development, licensing, and operation of nuclear power plants by providing valuable insights into complex thermal-hydraulic phenomena and enhancing the overall safety and efficiency of nuclear reactor systems [3].

Validating the RELAP code for research reactors such as the McMaster Nuclear Reactor (MNR) holds immense importance in ensuring the accuracy and reliability of predictive simulations. Regulatory requirements demand that codes used in safety assessments for specific reactors undergo validation against relevant experimental

data. This process helps verify the code capability to simulate various thermal-hydraulic scenarios and transient events that could occur within nuclear reactors and also defines the accuracy of code predictions [16].

Many verification and validation studies of the RELAP code for research reactor safety analysis have been conducted and are available in the literature. These studies focus on postulated scenarios such as loss-of-coolant accidents (LOCA) [8], loss-of-flow accidents (LOFA) [21][18][15], reactivity insertion accidents (RIA) [15][12][7], blockage of the cooling channels in a fuel assembly [6][5], and loss-of-heat sink accidents (LOHS) [7]. The work being carried out by the nuclear community regarding code verification and validation is highly important and necessary. Increased validation efforts directly correlate with enhanced reliability in the outcomes generated by these codes.

This thesis presents an in-depth analysis of heat sink loss events at the MNR (McMaster Nuclear Reactor) employing the RELAP5 code. Loss of heat sink accidents present critical scenarios where the secondary heat transport system fails to adequately remove heat generated in the reactor core. These accidents can arise from various causes, such as the failure of a valve or a pump, or a piping rupture in the secondary system. Without proper heat removal, the reactor core temperature rise, potentially leading to fuel overheating, core damage and the release of radioactive materials. Validation for these events gives credibility for applications of RELAP to other similar system level events such as Loss of Flow Accidents (LOFA).

The MNR provides an exemplary case to explore reactor behavior in transients of this nature. This study focuses on two important data sources from the MNR: the loss of forced circulation in the secondary side event that happened in 2020 and the Pool Temperature Experiment carried out in 2023. These transients, both involving

heat sink loss in the secondary cooling system, offer invaluable insights into the reactor behavior during this type of accidental scenario and provide full scale data for validation.

1.2 Objectives

This thesis aims to study the predictive capabilities of RELAP5 in replicating reactor behaviors under steady-state operations and transient heat sink loss events. The analysis involves detailed comparisons between RELAP5 simulations and experimental data, examining system temperatures and flow rates to evaluate the code's capabilities. Furthermore, this study explores the complexities of thermal stratification within the reactor pool and its impact on transient events. Through the integration of Computational Fluid Dynamics (CFD) with RELAP5, this research aims to improve the understanding of three-dimensional thermal mixing effects within the pool, and how it affects the safety analysis.

By examining the strengths and limitations of RELAP5 in simulating diverse operational conditions and transient events, this thesis underscores the significance of robust modeling tools in ensuring nuclear reactor safety. The comprehensive analyses performed aim to refine the current understanding of reactor behavior during heat sink loss events and pave the way for enhanced safety assessments and predictive capabilities in nuclear reactors.

1.3 Thesis structure

The thesis is divided into 6 chapters, which will be briefly described below:

- Chapter 1: This chapter serves as the introduction to the thesis. It briefly outlines the structure of the thesis, emphasizing the motivation behind the work and the proposed objectives. It provides a short overview of what will be covered in the rest of the document and also presents a concise bibliographic analysis of relevant publications that form the scientific basis of this research.

- Chapter 2: In this chapter the literature review is presented. It starts with a detailed description of the McMaster Nuclear Reactor (MNR), followed by a specific description of Loss of Heat Sink accidents and their importance for this reactor. This chapter concludes with an overview of the RELAP5 code used in this research for the thermohydraulic simulation of the reactor. The main characteristics of the code are analyzed, as well as its modeling capabilities, calculation scope, and thermohydraulic models.

- Chapter 3: This chapter provides a review of theoretical concepts essential for the subsequent analysis in the thesis. It presents the conservation equations for mass, momentum, and energy, which are internally solved using numerical methods by the RELAP5 code.

- Chapter 4: This chapter illustrates the development of the McMaster Nuclear Reactor model in the RELAP5 code. It unveils details and features of each hydraulic and thermal model developed for the different reactor components, along with a thorough description of the nodalizations performed.

- Chapter 5: This section presents the simulation results and outlines the findings from the testing and validation procedures conducted on the model, covering steady-state operational scenarios as well as Loss of Heat Sink transients.
- Chapter 6: This chapter presents the conclusions drawn from the research.

Chapter 2

Literature Review

2.1 McMaster Nuclear Reactor (MNR)

2.1.1 Reactor general specifications

The McMaster Nuclear Reactor is a research reactor located on the campus of McMaster University in Hamilton, Ontario, Canada. It is a light-water cooled and moderated pool type reactor and is one of the largest and most powerful university-based research reactors in the world. The reactor was built in the late 1950s and began operations in 1959. It has undergone numerous upgrades and improvements over the years, and currently it is licensed to operate at a maximum power of 5 MW. The reactor is used for a wide range of research applications, including materials science, nuclear physics, and medical research [1].

The reactor currently operates at 3 MW with low-enriched uranium fuel (19.75%wt). A simplified representation of the MNR Heat Transport System is depicted in Figure 2.1. The reactor features a large pool segmented into two halves, a reactor core,

Hold-Up Tank (HUT), pump, heat exchanger (HEX), valves, and connecting piping of various diameters.

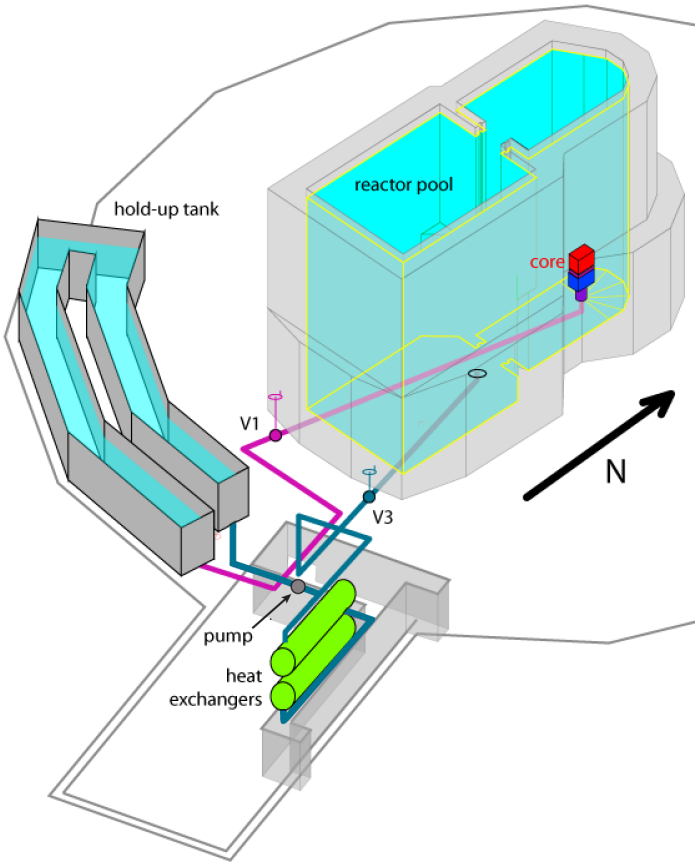

Figure 2.1: Schematic of the McMaster Nuclear Reactor primary loop.

The MNR core consists of a 9x6 rectangular array of fuel, control, reflector, and irradiation assemblies. The grid plate in the reactor core typically holds 32 low-enriched uranium fuel assemblies (MSFAs), 7 graphite reflector assemblies (G), 6 control fuel assemblies (MCA), 1 beryllium reflector assembly (Be), and 8 empty water sites (W). The MNR uses MTR type fuel. The fuel assemblies contain 18 fuel plates and the outer two are 'dummy' plates containing no fuel. The fuel is made from Low Enriched Uranium (LEU) in the form of sintered powder mixture of uranium

silicide and aluminum, containing about 73% uranium by weight. The plates are rectangular with a small curvature radius to ensure that each of the two plates do not bend towards each other should they start deforming. The cladding over the fuel meat is made of aluminum. Detailed specifications regarding core components, configuration, and surrounding structures can be consulted in the reference [9].

The energy generated by nuclear fission is removed from the core by the heat transport system, designed to maintain safe temperatures for the fuel and other components. This system consists of a primary loop, including the Pool acting as a large heat sink in direct contact with the fuel, and a secondary loop responsible for transferring heat from the primary circuit to the atmosphere. Sub-systems are associated with each major loop, serving non-thermal purposes such as purification and loss makeup.

In the MNR, coolant flow is driven by a pressure difference of 70 kPa between the reactor core and the Hold-Up Tank (HUT), which is maintained at atmospheric pressure. The coolant enters the reactor core, flows downward, and exits Pool 1 through an outlet piping system that directs it to the HUT. Within the HUT, the coolant is held for a sufficient duration to allow for the decay of short-lived radionuclide N16. Subsequently, the coolant moves to the Heat Exchanger (HEX), where excess heat is removed, before being returned to Pool 2 via a centrifugal pump.

The secondary system extracts the heat from the primary system through the HEX structure. Key components of the secondary system include twin cooling towers, two fans and motors, and a pump with associated piping. The secondary system receives heat via the HEX and transports it to the cooling towers. Within the towers, the heat is removed from the secondary system and the cooled water is returned to the

HEX forming a closed secondary loop. The atmosphere serves as the ultimate heat sink.

2.1.2 Primary Heat Transport System specifications

This section provides an overview of the operation and key components of the MNR Primary Heat Transport System. The main source of information for this section was the MNR technical report [20].

The Primary Loop serves the crucial function of transferring heat from the reactor core to a heat exchanger, from where it is subsequently removed to the cooling towers by the Secondary Loop of the MNR Heat Transport System. Demineralized light water flows by gravity through the reactor core and grid plate into the plenum, then proceeds to the core outlet pipe, and eventually reaches the HUT. From there, the water is drawn by the primary pump, circulated through the shell of the HEX, and finally returned to the Pool, where it is directed by a diffuser plate located at the Pool floor. The main circulating piping in the Primary Loop consists of schedule 5S stainless-steel pipes with an internal diameter of 10.482 inches. This piping facilitates the flow of coolant from the reactor Pool through the Primary Loop, encompassing the HUT, primary pump, and HEX.

Figure 2.2 provides a schematic layout of the Primary Loop, highlighting its principal components, the positioning of main valves, and the flow path in the forced convection mode (with the primary pump activated). The setup of the valving and piping within the Primary Loop enables the operation of the core in either end of the main reactor Pool. This flexibility is achieved through a second set of Pool outlet and Pool return positions. However, it is important to mention that, in practice,

the core is typically operated in the end of the Pool containing the experimental and irradiation facilities. The valving and piping associated with the operating position of the core are henceforth referred to as the "operational" line, while the second set of outlet/return is termed the "alternate" line.

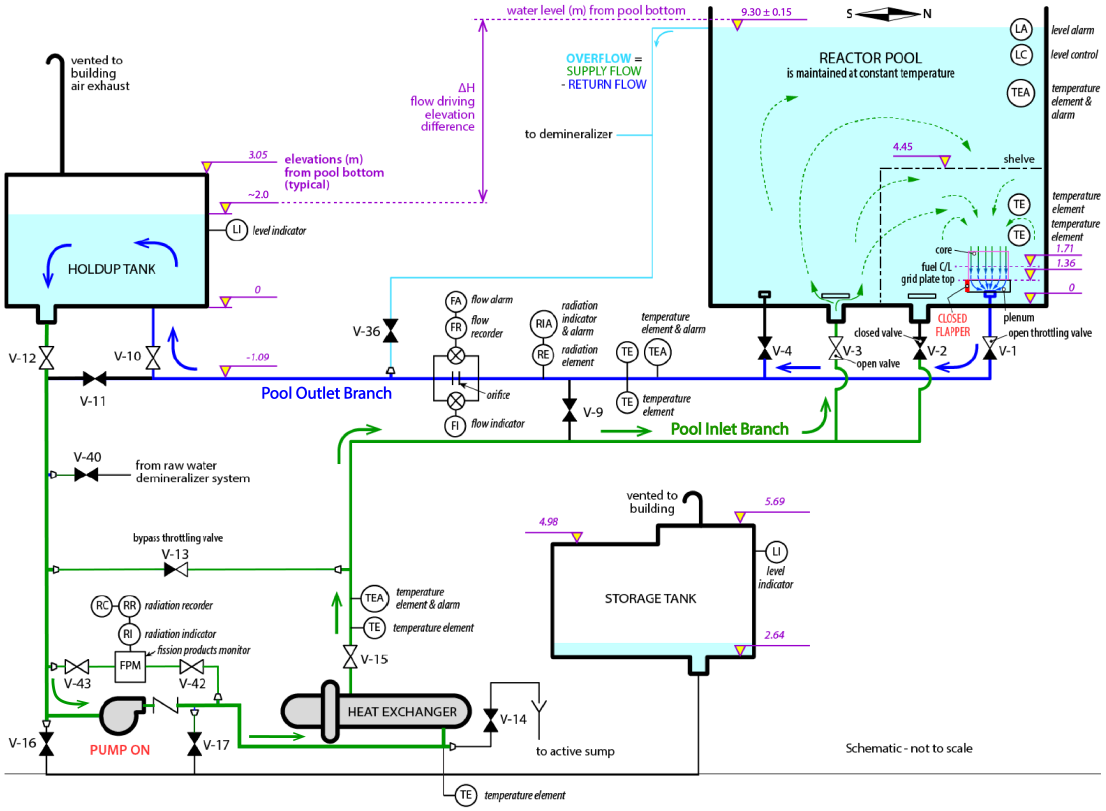

Figure 2.2: McMaster Nuclear Reactor heat transport system. Taken from MNR Facility Specification Thermal-Hydraulics [20].

The operational inlet/outlet line includes a pair of butterfly valves, V-1 and V-3, to regulate the flow through the core and from the HEX to the Pool, respectively. The same function is achieved on the alternate line with valves V2 and V4, which are kept closed to prevent coolant outflow from the unused Pool section. Additionally, a manual valve on a bypass line from the heat exchanger primary outlet to the primary

pump suction header (V-13) is adjusted to maintain the Pool level above the gutters.

For the HEX return to the Pool, two lines with butterfly valves V-2 and V-3 are available. During normal full-power operation, the line located in the Pool opposite to the core is used. Since the core is currently positioned in Pool 1, associated with valve V-1, the HEX return is situated in Pool 2, using the line associated with valve V-3. This setup enhances Pool thermal mixing and temperature uniformity.

Hydraulically, the primary system is divided into two branches: the Pool-outlet branch and the Pool-inlet branch. The Pool-outlet branch extends from the Pool outlet to the HUT inlet, and flow through this branch, which is also the flow through the core, depends on the difference in water level between the Pool and the HUT and the head losses in the connecting pipeline, particularly from valve V-1. Flow rate can be determined by Bernoulli's principle, considering factors like water level variance, fluid properties, pipe geometry, and valve configurations.

On the other hand, the Pool-inlet branch covers the loop from the HUT outlet to the Pool inlet, incorporating the primary pump, heat exchanger, and associated valves. Here, coolant flow is influenced by the pump characteristics and hydraulic loop properties, considering pressure losses in the pipes from the HUT outlet to the Pool inlet, including valves, elbows, pipe walls, and the heat exchanger.

To ensure a constant water level in both tanks, the primary pump draws water from the HUT and sends it back to the Pool, aiming for identical flow rates in both branches. Any slight variance in flow between the Pool-inlet and Pool-outlet branches, leading to gradual fluctuations in the Pool level over time, is countered by adjusting globe valve V-13 to modulate the water flow and maintain a consistent level above the gutters in the Pool.

During standard full-power operation, valves V-10 and V-12, located at the inlet and outlet connections of the HUT, are fully open. They can be closed to isolate the Pool from the HUT when necessary. Valve V-11 remains closed during standard operation and is used to bypass the HUT as required.

A check valve positioned at the primary pump exit prevents water from flowing back in the opposite direction. A recirculation line, equipped with valves V-42, V-43, and a radiation detector, serves the purpose of monitoring radionuclide activity within the primary loop water.

Valve V-15, located immediately after the HEX, provides the means to isolate the component when necessary. Additionally, two lines connected to the storage tank, one accessed before (via V-16) and another after (via V-17) the pump, aid in system inventory management, useful during maintenance activities which require draining of the reactor pool.

While most of the flow produced by the pump is directed to the Pool, there are two extra lines that allow recirculation in the system. One is associated with valve V-13, and the other is linked to valve V-9, which diverts water from the HEX back to the HUT. Valve V-9 is typically kept closed, with occasional openings to raise the water level in the HUT, maintained at a nominal height of 2 meters, providing flexibility in system operations and facilitating precise management of water levels as needed.

Maintaining stable conditions during reactor operation involves ensuring a controlled surface flow from the west to the east gutter facilitated by the demineralizer system, with the water level in the Pool kept just above the gutter. This requires the volume of water in the Pool to remain constant. During low-power operation,

achieving this involves bringing the Pool level to the point of overflow at the east gutter before reactor startup. Any increase in the water level due to heating of the Pool water occurs gradually and can be easily rectified by draining some water to the HUT when necessary. Conversely, maintaining steady conditions during high-power operation is more challenging, requiring careful balancing of the water pumped to the Pool with the amount flowing by gravity through the core to the HUT. The Pool bypass valve, denoted as V-13, plays a crucial role in fine-tuning water flow dynamics to meet the demands of high-power reactor operation.

The reactor pool that houses the core is a 10-meter-high reinforced concrete structure that provides structural integrity and biological shielding. It is divided into north and south sections, which are also known as pool 1 and pool 2 (see Figure 2). Pool 1 houses the core and has multiple beam tubes connected to its wall. Pool 2 is larger, and it contains the diffuser where the water coming from the HEX flows back to the pool. This pool is mainly used to store irradiated components and spent fuel. An aluminum gate can be used to separate the two pools.

This type of pool is common among the different designs of research reactors, and they represent a fundamental component from the safety point of view. The pool provides great thermal inertia, a large inventory of water to cool the core, as well as biological shielding to protect the operators.

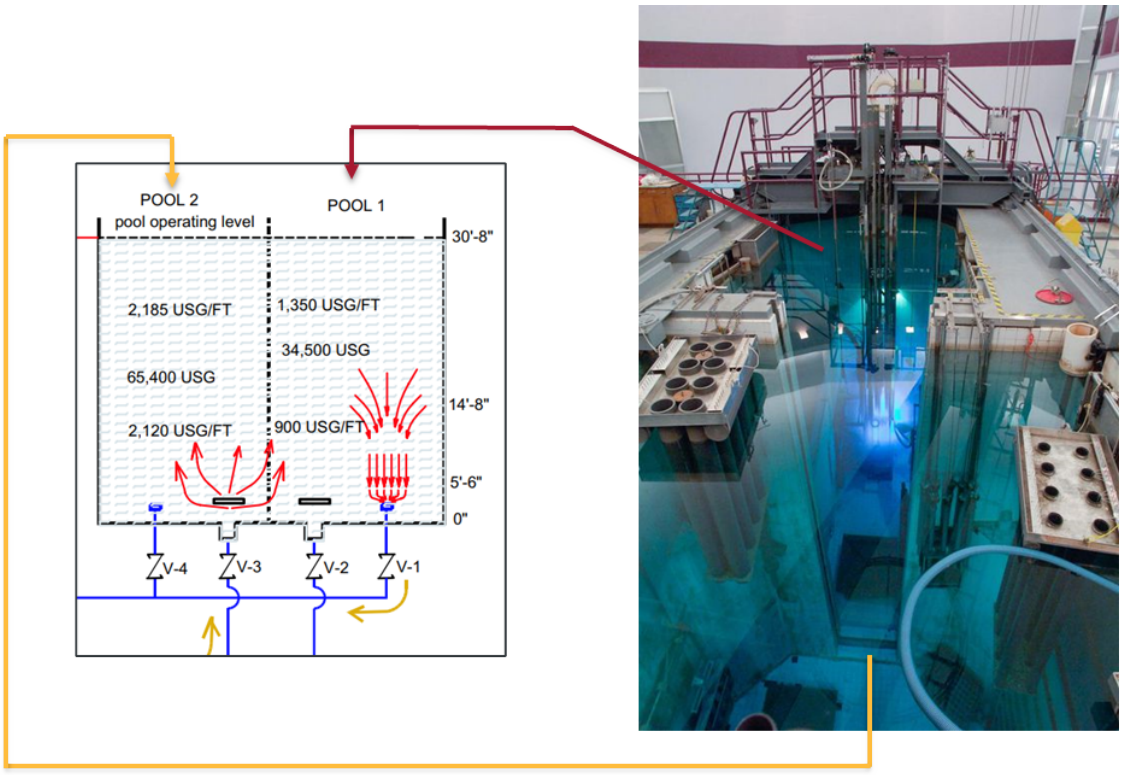

Figure 2.3: MNR pool layout (picture and diagram).

2.2 Loss of Heat Sink Events in the MNR

Loss of heat sink events represents one category from the set of design basis accidents that demand rigorous analysis and mitigation strategies in nuclear reactors [4]. These events involve the loss of heat removal mechanisms, compromising the ability to dissipate the heat produced in the core. This section explores the characteristics, potential consequences, and safety measures associated with loss of heat sink accidents in nuclear reactors.

A loss of heat sink accident is a transient caused by the total or partial decrease

in heat extraction from the primary due to a malfunction of the secondary system. It can be caused by a secondary system failure or due to a bypass of the secondary coolant.

A secondary system failure can occur due to the complete or partial malfunction of components such as pumps, heat exchangers, or cooling towers. For example, if a pump fails, it disrupts the cooling flow in the secondary circuit. This disruption causes the primary temperature to rise. Typically in this kind of event the primary temperature increases steadily as the power remains relatively constant regulated by the automatic control of the reactor [1]. The transient normally ends when the SCRAM signal is triggered by high temperature signal.

Another initiation factor for a loss of heat sink accident can be a secondary coolant bypass, produced by human error. This entails shutting the valve to the cooling towers and opening the bypass to the pool of the towers. Consequently, the power extracted from the heat exchanger is not released to the atmosphere, causing a gradual rise in the outlet temperature of the tower.

The main concern in loss of heat sink accidents is the potential for core overheating. In the most extreme situations, elevated temperatures can lead to fuel melting, release of radioactive materials, and structural damage. The severity of consequences depends on factors such as the duration of the heat sink loss, reactor design, availability of backup cooling systems and the successful activation of the core shutdown system.

This thesis primarily focuses on scenarios involving the loss of the secondary pump, responsible for maintaining flow across the heat exchanger.

[1] This steady power is achieved through the fine control rod, which compensates for the negative reactivity introduced by the rising coolant temperature. If the core temperature reaches the trip set point, the reactor automatically shuts down, and the core begins to be cooled by natural circulation.

Two transients are available for validation. The first occurred in 2020, involving the failure of the secondary pump. The second incident, termed the "Pool Temperature Experiment," was conducted in 2023, entailing the intentional shutdown of the secondary pump to simulate a loss-of-heat-sink scenario. The next section will provide a brief description of each of these events.

2.2.1 Loss of forced circulation in the secondary side in 2020

A failure of the secondary pump occurred at the MNR on September 22, 2022, lasting from 8:45 pm to 10:00 pm, during which the reactor was operating at a stable 3 MW thermal power level. This event did not represent an immediate safety concern and operation was continued until the administrative limit on core inlet temperature was approached. Various reactor parameters, including core inlet and outlet temperatures, primary and secondary temperatures at the heat exchanger inlet and outlet, and primary and secondary coolant flow rates, were recorded and archived in the reactor database.

Figure 2.4 illustrates the progression of temperatures within the core and the heat exchanger (both primary and secondary sides). Before the failure of the secondary pump, the reactor operated steadily at 3 MW power. However, when the secondary flow rate was disrupted due to the pump failure, a notable change occurred: the inlet and outlet temperatures on the primary side of the heat exchanger became identical. This occurrence signaled a lack of heat extraction from the primary system, prompting a gradual rise in primary temperatures.

While the event was identified almost immediately at 8:45 pm, the reactor remained in operation for approximately 75 minutes to complete an isotope production

run. This was allowed as there was sufficient margin at all times during the event. The incident concluded when reactor operators inserted shim rods into the core at 10:00 pm. This action caused the inlet and outlet temperatures of the core to equalize, establishing equilibrium within the primary system.

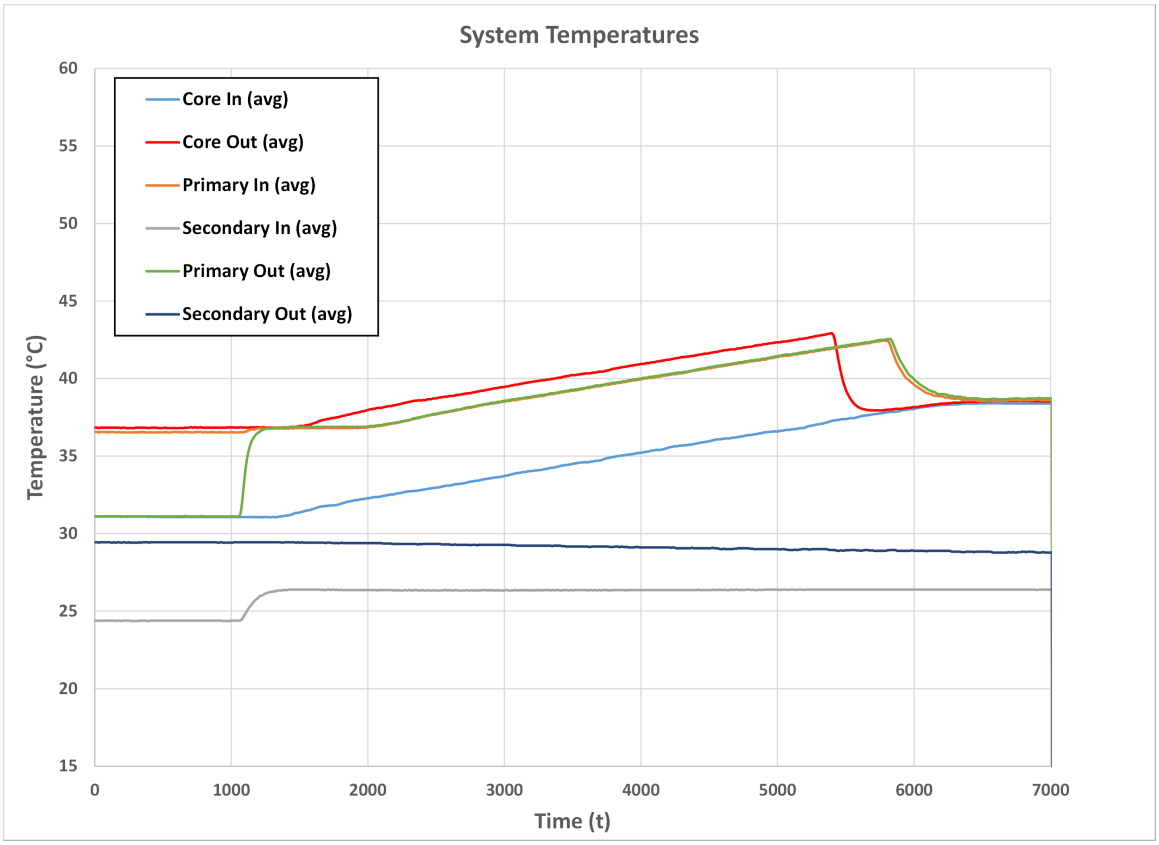

Figure 2.4: Temperature readings during the loss of forced circulation in the secondary side in 2020.

While valuable for preliminary validation, existing reactor instrumentation did not cover all validation quantities. Therefore, an experiment was planned and executed in 2023 to gather this information. This experiment, known as the "Pool Temperature Experiment," will be detailed in the following section.

2.2.2 Pool Temperature Experiment 2023

The "MNR Pool Temperature Experiment," conducted on March 11, 2023, deliberately shut down the secondary heat removal system, particularly the secondary pump, enabling an intentional rise in the primary system temperature. In the context of nuclear behavior and the core sub-moderated design, the elevation in pool temperature produces a decrease in reactivity. Throughout the experiment, the control system remained in automatic mode, compensating for this reactivity change by retracting the regulation rod. One of the goals of this experiment was to determine the reactor temperature feedback coefficient by utilizing the calibration curve of the regulating rod and temperature measurements. This task was performed by the MNR team and is not covered in this thesis. Another major objective of the experiment was to provide experimental data for computer code validation, which is the main goal of this thesis.

This experiment holds importance as it serves as a foundational evaluation for verifying reactor safety. Furthermore, it stands as a critical validation instance for computational models. The experiment scope encompasses the entire plant thermo-hydraulics, intimately interconnected with the core physics through pool temperature and reactivity feedback.

Preceding the experiment initiation, efforts were made to attain the lowest operational pool temperature, approximately 18°C. This was accomplished by running the cooling towers at maximum capacity for a specific duration. The test comprised two cycles involving heating and subsequent cooling of the primary system. The aim of each cycle was to raise the pool temperature close to the maximum permissible limit of 38°C before cooling it back down to 18°C. Figure 2.5 provides an illustrative

depiction of temperature measurements alongside core thermal power fluctuations observed during the experiment.

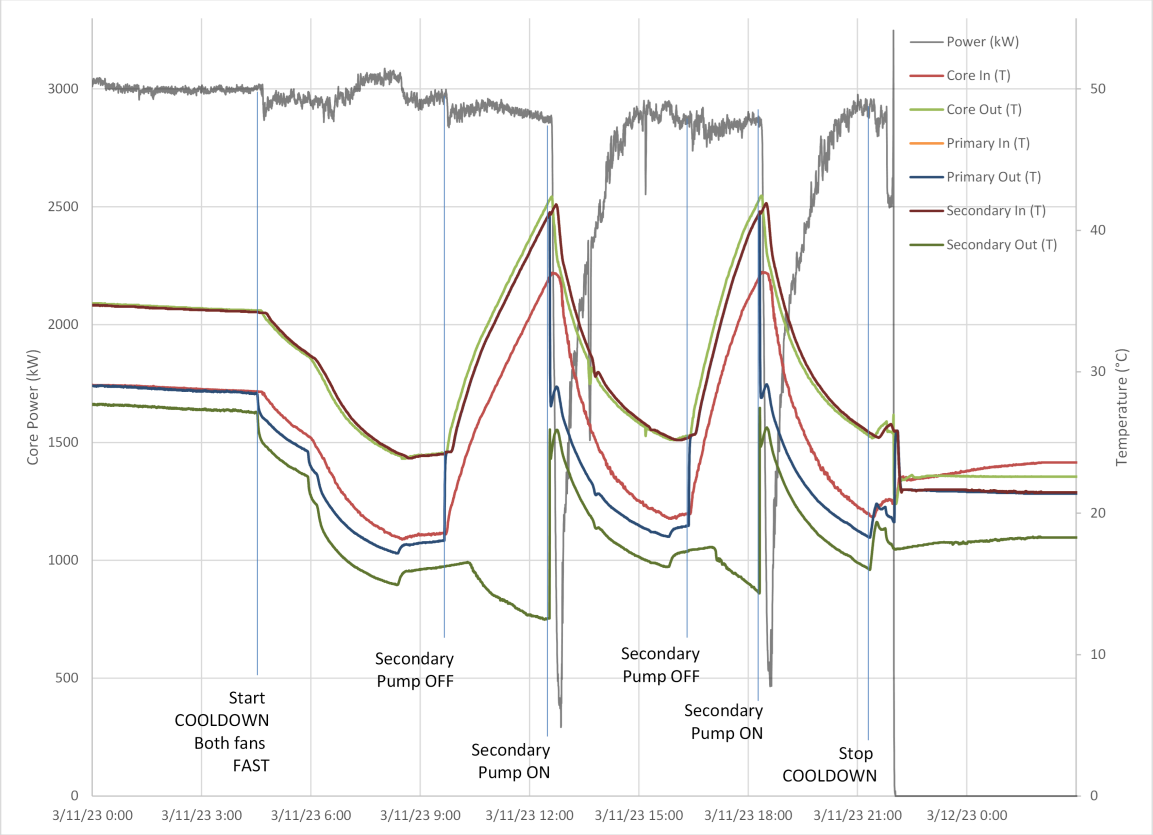

Figure 2.5: Temperature and power readings during the Pool Temperature Experiment.

The sequential use of events like the secondary pump failure in 2020 and the Pool Temperature Experiment in 2023 within the MNR served dual purposes for the RELAP5 model. The secondary pump failure in 2020 initially provided the foundational data necessary for developing and refining the RELAP5 model. The insights gained from this incident aided in adjusting the model parameters, nodalization, and initial conditions to accurately simulate and replicate real-time reactor behavior during such critical events. On the other hand, the Pool Temperature Experiment in 2023 was

a crucial test case for assessing the predictive capabilities of the fine-tuned RELAP5 model. This experiment, designed to mimic a heat sink loss event due to the secondary pump failure, served as a validation instance. It allowed for an evaluation of the model predictive capacity and its ability to simulate and anticipate reactor responses under conditions resembling those observed in the 2020 incident.

2.2.3 Comparison between LOHS events in the MNR

It's important to analyze the distinct temperature behaviors observed during the loss of heat sink events in the MNR. These occurrences, despite seemingly similar due to the shutdown of the secondary pump, exhibited distinct temperature evolution patterns within the primary system.

In an ideal scenario where no phase changes occur, and assuming constant thermal properties of water while neglecting heat losses to the environment, the heating rate (expressed as the temperature derivative) remains constant. Consequently, the change in temperature (T) should exhibit a near linear relationship with time (t). However, it is noteworthy that the temperature derivatives observed during two events discussed in this paper reveal intriguing disparities, as depicted in Figure 2.6.

Notably, during the loss of forced circulation in the secondary side event in 2020, the temperature derivative remained relatively constant throughout the event duration. However, in the Pool Temperature Experiment, the derivative displayed an initial sharp ascent followed by a consistent temperature decrease after about an hour and a half, indicating a non-linear temperature evolution within the primary system over time.

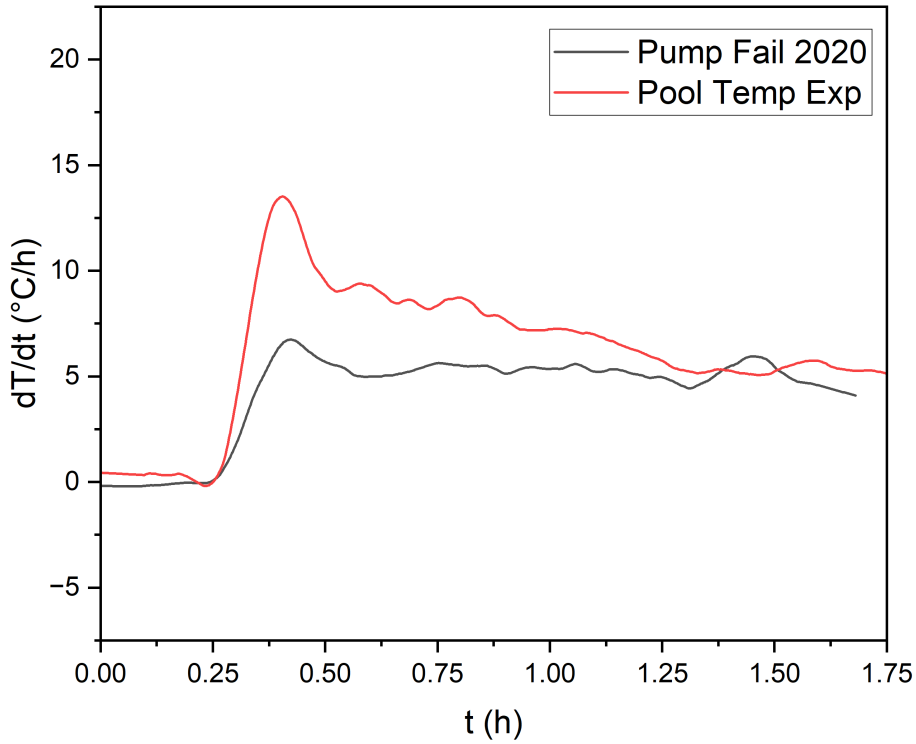

Figure 2.6: Derivative of the core inlet temperature over time.

This discrepancy in temperature behavior between the two events, despite a seemingly identical cause—the secondary pump shutdown—can be traced back to the differing initial conditions preceding the events. In the 2020 incident, the reactor had been in a prolonged steady state before the pump failure, implying a relatively uniform pool temperature at the start of the event. On the other hand, before the "Pool Temperature Experiment" in 2023, the pool had undergone an extended cooling period to attain its lowest temperature. This cooling phase potentially induced thermal stratification within the pool.

The presence of thermal stratification, stemming from the cooling transient before

the 2023 experiment, likely altered the heating phenomenon initially. Consequently, the temperature rise exhibited a nonlinear behavior at the experiment onset, followed by a transition to a linear heating ramp over time—a pattern more consistent with the ideal scenario.

In essence, these distinctions in temperature behavior underscore the critical influence of initial conditions, particularly the occurrence of thermal stratification induced by a prior cooling transient, on the heating patterns observed during events mimicking heat sink loss in the MNR. This analysis highlights the significance of comprehensively understanding the reactor state prior to and during transient events for accurate predictive modeling and operational assessments.

2.3 Instrumentation in the MNR

The McMaster Nuclear Reactor is outfitted with flow and temperature sensors throughout both the Primary and Secondary Loops. Within the Primary Loop, an orifice flowmeter is positioned on the piping section connecting the reactor Pool and the Hold-up tank. Temperature readings are obtained using Resistance Temperature Detectors (RTDs) at the inlet and outlet of the reactor core, as well as at the inlet and outlet of the heat exchanger on the primary side. Real-time data from these sensors is displayed in the reactor control room and simultaneously archived digitally. Furthermore, the flow and temperature data are utilized to compute the thermal power, which is then presented in real-time within the control room.

In the Secondary Loop, similar instrumentation is employed, including an orifice flowmeter and RTDs at the inlet and outlet of the heat exchanger on the secondary side.

Additional instrumentation within the reactor comprises absorber rods position monitoring, radiation detectors positioned downstream of the Hold-up tank, and monitoring of flow and temperature within the water demineralization system.

2.3.1 Available measurements for validation

For the validation against the Loss of Forced Circulation in the secondary side in 2020, operational measurements are available from the day of the event, captured by the orifice flowmeters and the RTDs in both the Primary and Secondary Loops. The list of measured parameters for comparison includes:

- Primary Flow (orifice flowmeter)
- Secondary Flow (orifice flowmeter)
- Core inlet temperature (RTD)
- Core outlet temperature (RTD)
- Heat exchanger inlet temperature on the primary side (RTD)
- Heat exchanger outlet temperature on the primary side (RTD)
- Heat exchanger inlet temperature on the secondary side (RTD)
- Heat exchanger outlet temperature on the secondary side (RTD)

For the Pool Temperature Experiment, two additional sensors were installed in the reactor to complement the existing operational instrumentation. An ultrasonic flowmeter was added to the primary piping, and an array of 6 thermocouples (TCs) was installed above the core. The ultrasonic flow sensor was intended to provide

an independent, low-uncertainty measurement of the primary flow. The additional temperature instrumentation served a dual purpose: firstly, to offer an independent measurement of core inlet temperature, and secondly, to provide data for assessing potential temperature variations across the core inlet, thus measuring the uniformity of the inlet temperature. These two extra sensors provide two additional parameters for validation purposes. Therefore, for the Pool Temperature Experiment validation, the list of measured parameters remains the same as the one presented above, and it also includes the following two items:

- Primary Flow (Ultrasonic Flowmeter)
- Core inlet temperature (TCs)

Figure 2.7 illustrates the placement of the specified sensors within the Primary Loop, which includes the ultrasonic flowmeter denoted as "AMAG CROSSLOW" installed in the piping from the reactor pool to the hold-up tank, as well as the array of TCs positioned above the core labeled as "TCs Rake".

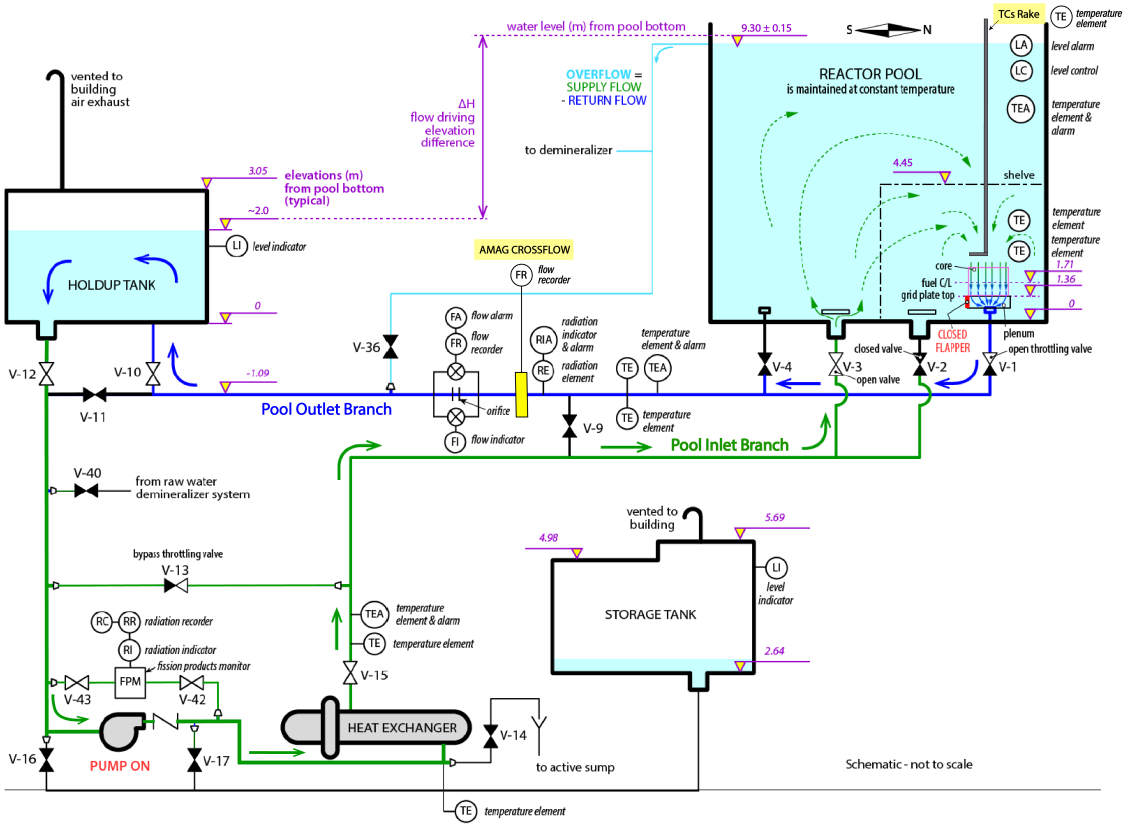

Figure 2.7: Schematic of the Primary Heat Transport System including the position of the flow and temperature sensors.

2.3.2 Uncertainty of measurements in the MNR

The uncertainties of the measurements in the MNR are summarized in Table 2.1.

Parameter	**Uncertainty**	**Type**	**Note**
Primary Flow (ultrasonic)	3.9%	Random	Provided by manufacturer
Primary Flow (orifice)	4.3%	Systematic	Relative to ultrasonic flowmeter
Secondary Flow (orifice)	-	-	To be determined
RTD Temperature	0.1°C	Random	Calibration acceptance limit
TC Temperature	<1%	Random	Relative to reference RTD
Reactor Power	4.6%	Random	Error propagation

Table 2.1: Uncertainties of the reactor measurements.

- The random uncertainty associated with the ultrasonic flowmeter, provided by the manufacturer (AMAG), is estimated at 3.9%.
- A comparison between the average readings of the orifice flowmeter and the ultrasonic flowmeter reveals a systematic discrepancy, with the orifice meter consistently indicating lower values by approximately 4.3%. However, no information was found on the random uncertainty of this instrument.
- Uncertainties in system temperatures measured with the RTDs are determined by a calibration check against a reference thermistor, with an acceptance limit of 0.1°C.
- For thermocouple (TC) measurements, uncertainties are determined through comparative measurements against a previously calibrated reference RTD.
- The uncertainty associated with total core power is calculated using linear error propagation of random uncertainties in total core flow and core inlet and outlet RTD measurements, assuming a nominal temperature difference across the core of 5.7°C.

Uncertainties in reactor measurements play an important part in the validation of computer codes. Specifically, data collected from the reactor may be used directly in the simulation through inputs related to boundary or initial conditions, and also may affect the comparison of simulated outputs to reactor responses through the uncertainty in the measured responses. The most significant source of uncertainty in loss of heat sink events is expected to be the 4.6% uncertainty in thermal power (indicated in table 2.1). This value was calculated through error propagation based on uncertainties in primary flow and core inlet and outlet temperatures. For instance, when the reactor nominal power is set at 3 MW, this uncertainty suggests that true power output may range from 2.86 MW to 3.14 MW. Such variability can lead to substantial changes in core ΔT and heating rates during a loss of heat sink event. Specifically, higher power levels increase the system heating rate, while lower levels decrease it. In the simulations, the reactor power is used directly as an input and hence affects the simulated steady-state and heat-up transients.

Similarly, uncertainties in flow rates can impact core and heat exchanger temperature differences. Higher flow rates result in lower core and heat exchanger temperature gradients. Furthermore, uncertainties in flows and temperatures play a significant role in defining the model initial conditions, thus influencing steady-state and transient simulation outcomes.

Finally, the measured responses of the reactor (e.g., inlet and outlet temperature transients) contain some uncertainty and hence the assessment of the accuracy in the simulation of these quantities must consider the impact of these uncertainties.

It is essential to evaluate the simulation results presented in this thesis with an understanding of the uncertainties in initial and boundary conditions, as they directly

impact the outcomes. Although this thesis does not include uncertainty quantification, incorporating it in future work is recommended for a more comprehensive assessment of model accuracy.

2.4 The RELAP5 code

RELAP (Reactor Excursion and Leak Analysis Program) is a computer code that is widely used in the field of nuclear engineering to simulate and analyze the thermal-hydraulic behavior of nuclear power plants. The code was developed by the Idaho National Engineering and Environmental Laboratory (INEEL) and has been updated and improved since its initial release in the 1970s. For this study, the version RELAP5/SCDAP v4.0 was used [13].

RELAP5 is a best-estimate, 1D thermal-hydraulic network code. It considers various physical phenomena such as 2-phase flow, pressure losses, heat transfer, and nuclear point kinetics, among others. The mathematical equations that describe these phenomena are solved using numerical methods, and the code provides output data that can be used to analyze the system behavior.

The code is designed to be highly flexible and can be applied to a wide range of thermal-hydraulic systems, including pressurized water reactors (PWRs), boiling water reactors (BWRs), material testing reactors (MTRs) and other types of nuclear reactors.

An important feature of RELAP5 is the ability to simulate accident scenarios, such as loss of coolant accidents (LOCAs), loss of flow accidents (LOFA), loss of heat sink accidents (LOHS), reactivity insertion accidents (RIA), and more. The code can predict the behavior of the complete heat transport system during these events and

provide insight about the progression of the accident.

2.4.1 Problem statement and nodalization

To use RELAP5 effectively, the user must first acquire a detailed physical description of the system. The next step involves organizing and defining the initial and boundary conditions. These conditions encompass parameters like temperature, pressure, flow rate, fluid velocity, thermodynamic quality, and various other options. Subsequently, the problem must be nodalized, which entails discretizing the system into small volumes or cells interconnected by junctions. RELAP5 then solves the thermal-hydraulic equations for mass, momentum, and energy balance within these discretized elements.

In RELAP5, the user is required to separately define the hydraulic nodalization where the mass, momentum and energy equations are solved for the fluid and the heat structures, where the heat conduction equation is solved for structural materials.

With all this information in place, the user can proceed to write and execute the input file. For a more in-depth understanding of RELAP5 functionality and the implementation of the input file, users can refer to the comprehensive guidance provided in the user manual [13].

2.4.2 Calculation scope

The first step is to divide the system into discrete volumes called "nodes" or "control volumes". Each node represents a section of the system, such as pipes, junctions, or heat exchangers. The components and their interactions are modeled within these nodes using equations that describe fluid flow, heat transfer, and other relevant physical processes. The code solves a system of partial differential equations that represent

the conservation laws for mass, momentum, energy, and other properties of the fluid within each node.

The transient behavior of the system is simulated over discrete time steps. The time integration process involves updating the solution at each time step based on the calculated values from the previous step. The chosen time step size affects the accuracy and stability of the simulation. Within each time step, an iteration loop is performed to achieve convergence. The code iteratively solves the equations for each node, updating variables such as pressures, temperatures, and flow rates. The iterative process continues until a predefined convergence criterion is met. As the simulation progresses, the code generates a set of output data, including time histories of various parameters like temperatures, pressures, flow rates, and power levels. This data can be visualized and analyzed to understand the system behavior under different conditions.

2.4.3 Hydraulic modelling

In RELAP5, the user needs to define the hydraulic nodalization and the heat structures separately. The hydraulic component solves the mass, momentum and energy balance for the fluid, while the heat conduction through structural materials is solved in the heat structures. The mass and energy conservation equations are solved at the nodes (or volumes) and the momentum conservation equation is solved at the junctions that connect the nodes. The basic building blocks relevant for this study are presented in the following list. Using these building blocks, the user can create fluid networks that represent nuclear reactor systems.

- Single volume: it is the basic building block. It represents a single control

volume or node in the system.

- Single junction: it is used to connect multiple single volume components, allowing fluid to flow between them.
- Pipe: a pipe component represents a section of pipe within the system. It is basically a string of volumes with interior connecting junctions with different options for flow models. It is used to model fluid flow and heat transfer along a specific path.
- Heat Structure component: they are used to model solid structures within the system that can transfer or generate heat, such as reactor fuel elements, cladding, or structural components.

In RELAP5, the boundary conditions of the problem are implemented by using time-dependent building blocks, also known as time-dependent components. These are needed wherever flow can enter or leave a hydrodynamic system. They can be defined as conditions in the flow, velocity, pressure, temperature and quality that are constant over time. The type of time-dependent components used for this specific study are listed below.

- Time-dependent volume: it is used wherever flow can enter or leave a hydrodynamic system. It defines pressure and temperature of fluid (and include fraction of liquid, vapor, or gas if necessary).
- Time-dependent junction: it is used to set the flow rate or flow velocities of the fluid entering or leaving a system. It must be always associated with a time dependent volume.

2.4.4 Heat transfer models

In RELAP5, various heat transfer models are employed to simulate the transfer of thermal energy between different components and fluids within a system. The most relevant models for this study are presented below.

- Conduction: Conduction heat transfer is modeled using Fourier's law, which relates the heat flux through a material to the temperature gradient. In RELAP5, conduction is used to simulate heat transfer within solid structures, such as fuel rods, cladding, and other components. It is important for capturing temperature distributions and changes in solid materials.

- Convection: Convective heat transfer accounts for the transfer of thermal energy between a fluid and a solid surface due to fluid motion. RELAP5 uses correlations and empirical relationships to model convective heat transfer coefficients, which depend on factors like flow velocity, fluid properties, and geometry. Convection is crucial for simulating heat exchange between the fluid and structural components, such as coolant channels.

For more information on how RELAP5 works and how the input file is implemented, the user manual can be consulted.

Chapter 3

Theory

Here is a brief overview of the basic theory necessary to understand the physical phenomenology involving the thermo-hydraulic analysis of the MNR reactor using the RELAP5 code. It is suggested to refer to specific literature on fluid mechanics [23] and heat and mass transfer [17] for a more detailed development of these topics. Moreover, the RELAP5 user manual can be consulted to look at the specific implementation and numerical solution of the conservation equations [13].

RELAP5 is a one-dimensional code that models and simulate two-phase non-homogeneous fluids under non-equilibrium conditions. The code internally solves a system of 8 equations with 8 dependent variables within a control volume in a fluid.

The set of variables that RELAP5 calculates is:

- Pressure (P)
- Phasic specific internal energies (U_f, U_g)
- Vapor volume fraction or void fraction (α_g),

- Phasic velocities (v_g, v_f)
- Non-condensable quality (X_N)
- Boron density (ρ_B)

And the set of equations formulated internally in the code is:

- Conservation of mass (or continuity equation) for each phase (2 equations in total)
- Conservation of momentum for each phase (2 equations in total)
- Conservation of energy for each phase (2 equations in total)

This results in a system of 6 equations with 6 unknowns. Additionally, the following 2 equations can be added to complete the 8x8 system:

- Non-condensable transport equation
- Boron transport equation

This system of equations is solved with respect to the independent variables: time (t) and distance (x). The code also incorporates equations of state and various constitutive relationships.

This theory section will focus on the main system of 6 equations with 6 unknowns, derived from the conservation of mass, momentum, and energy for each phase in a two-phase fluid. In the following subsections the RELAP5 implementation of the conservation equations will be presented.

3.1 Conservation of Mass

The RELAP5 implementation of the mass energy conservation equations for each phase separately of a 2-phase fluid are presented below, where the subscript f reefers to the liquid and g to the vapor. These equations are averaged in a cross section.

$$\frac{\partial}{\partial t}(\alpha_g \rho_g) + \frac{1}{A}\frac{\partial}{\partial x}(\alpha_g \rho_g v_g A) = \Gamma_g \tag{3.1.1}$$

$$\frac{\partial}{\partial t}(\alpha_f \rho_f) + \frac{1}{A}\frac{\partial}{\partial x}(\alpha_f \rho_f v_f A) = \Gamma_f \tag{3.1.2}$$

The terms Γ_g and Γ_f correspond to volumetric mass generation rate of the vapor and liquid respectively. These two parameters are linked and satisfy the expression:

$$\Gamma_g = -\Gamma_f \tag{3.1.3}$$

These equations describe the conservation of mass in each phase, stating that the rate of change of mass within a control volume, plus the net mass flux across its boundaries, must be equal to the generation rate.

3.2 Conservation of Momentum

The RELAP5 implementation of the momentum conservation equations for each of the 2 phases is presented below.

$$\begin{aligned}\alpha_g\rho_g A\frac{\partial v_g}{\partial t}+\frac{1}{2}\alpha_g\rho_g A\frac{\partial v_g^2}{\partial x}=&-\alpha_g A\frac{\partial P}{\partial x}+\alpha_g\rho_g B_x A-\left(\alpha_g\rho_g A\right)FWG\left(v_g\right)\\&+\Gamma_g A\left(v_{gI}-v_g\right)-\left(\alpha_g\rho_g A\right)FIG\left(v_g-v_f\right)\\&-C\alpha_g\alpha_f\rho_m A\left[\frac{\partial\left(v_g-v_f\right)}{\partial t}+v_f\frac{\partial v_g}{\partial x}-v_g\frac{\partial v_f}{\partial x}\right]\end{aligned}\tag{3.2.1}$$

$$\begin{aligned}\alpha_f\rho_f A\frac{\partial v_f}{\partial t}+\frac{1}{2}\alpha_f\rho_f A\frac{\partial v_f^2}{\partial x}=&-\alpha_f A\frac{\partial P}{\partial x}+\alpha_f\rho_f B_x A-\left(\alpha_f\rho_f A\right)FWF\left(v_f\right)\\&-\Gamma_g A\left(v_{fI}-v_f\right)-\left(\alpha_f\rho_f A\right)FIF\left(v_f-v_g\right)\\&-C\alpha_f\alpha_g\rho_m A\left[\frac{\partial\left(v_f-v_g\right)}{\partial t}+v_g\frac{\partial v_f}{\partial x}-v_f\frac{\partial v_g}{\partial x}\right]\end{aligned}\tag{3.2.2}$$

Where,

- $\alpha_f\rho_f A\frac{\partial v_f}{\partial t}+\frac{1}{2}\alpha_f\rho_f A\frac{\partial v_f^2}{\partial x}$: This term represents the transport of momentum.
- $-\alpha_f A\frac{\partial P}{\partial x}$: This term represents the pressure gradient, which is the change in pressure per unit distance in a given direction.
- $\alpha_f\rho_f B_x A$: This term represents the body force per unit volume due to gravity.
- $\left(\alpha_f\rho_f A\right)FWF\left(v_f\right)$: This term represents the friction with the walls.
- $\Gamma_f A\left(v_{fI}-v_f\right)$: This term represents the momentum transfer due to interface mass transfer.
- $\left(\alpha_f\rho_f A\right)FIF\left(v_f-v_g\right)$: This term represents the interface frictional drag.
- $C\alpha_f\alpha_g\rho_m A\left[\frac{\partial\left(v_f-v_g\right)}{\partial t}+v_g\frac{\partial v_f}{\partial x}-v_f\frac{\partial v_g}{\partial x}\right]$: This term represents the force due to virtual mass.

3.3 Conservation of Energy

The RELAP5 implementation of the energy conservation equations for each of the 2 phases is presented below. These equations describe the conservation of energy, considering changes in energy within a control volume due to heat transfer, work done by pressure forces, work done by viscous forces, work done by body forces, and heat generation.

$$\begin{aligned}\frac{\partial}{\partial t}\left(\alpha_g \rho_g U_g\right) + \frac{1}{A}\frac{\partial}{\partial x}\left(\alpha_g \rho_g U_g V_g A\right) = -P\frac{\partial \alpha_g}{\partial t} - \frac{P}{A}\frac{\partial}{\partial x}\left(\alpha_g V_g A\right) \\ +Q_{wg} + Q_{ig} + \Gamma_{ig} h_g^* + \Gamma_w h_g' + DISS_g\end{aligned} \tag{3.3.1}$$

$$\begin{aligned}\frac{\partial}{\partial t}\left(\alpha_f \rho_f U_f\right) + \frac{1}{A}\frac{\partial}{\partial x}\left(\alpha_f \rho_f U_f v_f A\right) = -P\frac{\partial \alpha_f}{\partial t} - \frac{P}{A}\frac{\partial}{\partial x}\left(\alpha_f v_f A\right) \\ +Q_{wf} + Q_{if} - \Gamma_{ig} h_f^* - \Gamma_w h_f' + DISS_f\end{aligned} \tag{3.3.2}$$

Where,

- $\frac{\partial}{\partial t}\left(\alpha_f \rho_f U_f\right) + \frac{1}{A}\frac{\partial}{\partial x}\left(\alpha_f \rho_f U_f v_f A\right)$: This term represents the transport of energy.
- $-P\frac{\partial \alpha_f}{\partial t} - \frac{P}{A}\frac{\partial}{\partial x}\left(\alpha_f v_f A\right)$: This term represents the work due to phase change.
- Q_{wf}: This term represents the heat transfer with the structures.
- Q_{if}: This term represents the interfacial heat transfer.
- $\Gamma_{ig} h_f^*$: This term represents the heat transfer due to condensation in the interface.
- $\Gamma_w h_f'$: This term represents the heat transfer due to condensation in the surrounding of the structures.
- $DISS_f$: This term represents the viscous dissipation.

RELAP5 solves these equations for fluid in two phases; however, in the problem addressed in this research, the fluid remains in a subcooled phase at all times. Therefore, the equations are simplified for single-phase fluid.

3.4 Heat transfer

The heat structures within RELAP5 facilitate the computation of heat transfer across solid boundaries within hydrodynamic volumes. These structures are employed in modeling the fuel plates within the reactor core, as well as in the tubes of the heat exchanger. Thermal calculations are conducted assuming one-dimensional heat conduction within a specified geometry, which may take the form of rectangular, cylindrical, or spherical configurations.

Subsequently, the integral form of the heat transfer equation is presented.

$$\iiint_V \rho(T,\bar{x})\frac{\partial T}{\partial t}(\bar{x},t)dV = \iiint_S k(T,\bar{x})\bar{\nabla}T(\bar{x},t) \bullet d\bar{s} + \iiint_V S(\bar{x},t)dV \quad (3.4.1)$$

Where,

- k is the thermal conductivity
- s is the surface area
- S is the internal heat source
- t is the time
- T is the temperature

- V is the volume
- x is the axial coordinate
- ρ is the volumetric heat capacity

The boundary condition options are presented in the Table 3.1 presented below. These can be imposed through a connection to a hydrodynamic volume or can be imposed as input.

Boundary condition options:		
Connection to hydrodynamic volume	$-k\frac{\partial T}{\partial z} = h_{\text{vol}}\ (T - T_{\text{vol}}\ )$	
Conditions imposed by input	$-k\frac{\partial T}{\partial x} = 0$	Adiabatic
	$-\mathrm{k}\frac{\partial \mathrm{T}}{\partial \mathrm{x}} = \mathrm{q}_{\text{table}}(\mathrm{t})$	Heat flux defined in table
	$-\mathrm{k}\frac{\partial \mathrm{T}}{\partial \mathrm{x}} = \mathrm{h}_{\text{table}}\,(\mathrm{T} - \mathrm{T}_{\text{table}})$	Convection with heat transfer coefficient and external temperature tabulated
	$\mathrm{T} = \mathrm{T}_{\text{table}}(\mathrm{t})$	Boundary temperature

Table 3.1: Boundary condition options for the heat transfer problem in RELAP5.

Chapter 4

Model Development

4.1 RELAP5 model of the MNR

A comprehensive thermal-hydraulic model of the McMaster Nuclear Reactor (MNR) was developed using the RELAP5 code, incorporating all major components of the heat transport system. This intricate model includes the reactor pool, reactor core, Hold-Up Tank (HUT), primary pump, heat exchanger, secondary pump, valves, and interconnected piping.

The initial phase of this endeavor involved an in-depth examination of prior attempts at modelling the MNR, primarily founded on the work of Wm. J. Garland and his model within the CATHENA code [14]. Previous endeavors aimed to transition the CATHENA model into RELAP5, yet pertinent documentation and substantial knowledge regarding this model have diminished over time. Hence, this study focused on exhaustively researching the input file and comprehending the model.

During this phase, model details were improved to ensure alignment with confirmed reactor specifications. This involved rectifying any discrepancies between the

model representation and the reference specifications, relying on information sourced from official MNR documentation [1][9][20][2].

Additionally, the core configuration was updated to meet current specifications. The original core model from CATHENA was based on a 1997 setup that featured highly enriched fuels, assemblies consisting of 10 and 18 plates, and some slightly enriched fuel assemblies. Therefore, a thorough effort was made to bring the core configuration up to date. This involved modifying assembly geometries, fluid pathways, and the power distribution within the fuel plates.

Neutronic calculations were conducted using the MGRAC code [22], enabling an estimation of the power profile for the current core configuration. Upon completion of meticulous revision and enhancement efforts, a robust model emerged, capable of simulating a wide array of events while maintaining stability and accuracy in reflecting the current core configuration.

4.2 Reactor nodalization

The nodalization of the MNR model is presented in Figure 4.1. The reactor pool is represented by two vertical pipe components with 21 nodes each, interconnected laterally through cross-flow junctions simulating mixing. Pipe 100 denotes pool 1, housing the reactor core, while pipe 200 represents pool 2, accommodating the diffuser that receives water from the heat exchanger. Both components interface with time-dependent volumes emulating the containment environment air, maintained at 20°C and atmospheric pressure. The 16th volume of Pipe 100 connects laterally to a single volume that models the inlet plenum of the core. This plenum then divides into two pipe-type components that constitute the core: representing the average fuel assembly

(pipe 106) and the bypass flow (pipe 066) – a discussion on these components will be detailed in the "Core Model" section.

The outlet plenum (snglvol 110) collects water from all core assemblies and the unheated bypass flow. This volume interfaces with the flapper system, allowing core cooling through natural circulation under low power conditions. The flapper volume (snglvol 112) connects to the 19^{th} volume of pipe 100, forming a closed loop for natural circulation. Subsequently, the flapper links to the bellows and then to the exit piping, connecting pool 1 to the hold-up tank.

Between these tanks, a coarse flow control valve labeled valve 1 (or valve 119 in the nodalization) regulates the core flow based on its generated power. This valve is crucial in estimating cooling flow, accounting for significant pressure losses along the piping from Pool 1 to the Hold-Up Tank.

Regarding the Hold-Up Tank (HUT), it mirrors the reactor pool modelling approach. It comprises seven vertical pipes connected laterally through cross-flow junctions (pipes 122, 222, 322, 422, 522, 622 and 722). Pipe 122 represents the tank inlet section (from the tank bottom), while pipe 722 leads to the outlet section directing water from the tank bottom to the rest of the primary loop. Subsequently, a series of pipes link the HUT to the primary pump (pump 132) that flows water through the heat exchanger, and back to the reactor pool through the diffuser located at the base of pipe 200 (the diffuser component is not modelled).

The secondary heat transport system model is relatively simplistic. It is composed of two time-dependent volumes (tmdpvol 250 and 226) that regulates temperature and pressure at the heat exchanger inlet and outlet and a time-dependent junction (tmdpjun 249) that modulates the flow rate. This simple secondary loop model

primarily serves to remove heat from the primary system, without offering detailed information about the secondary fluid conditions.

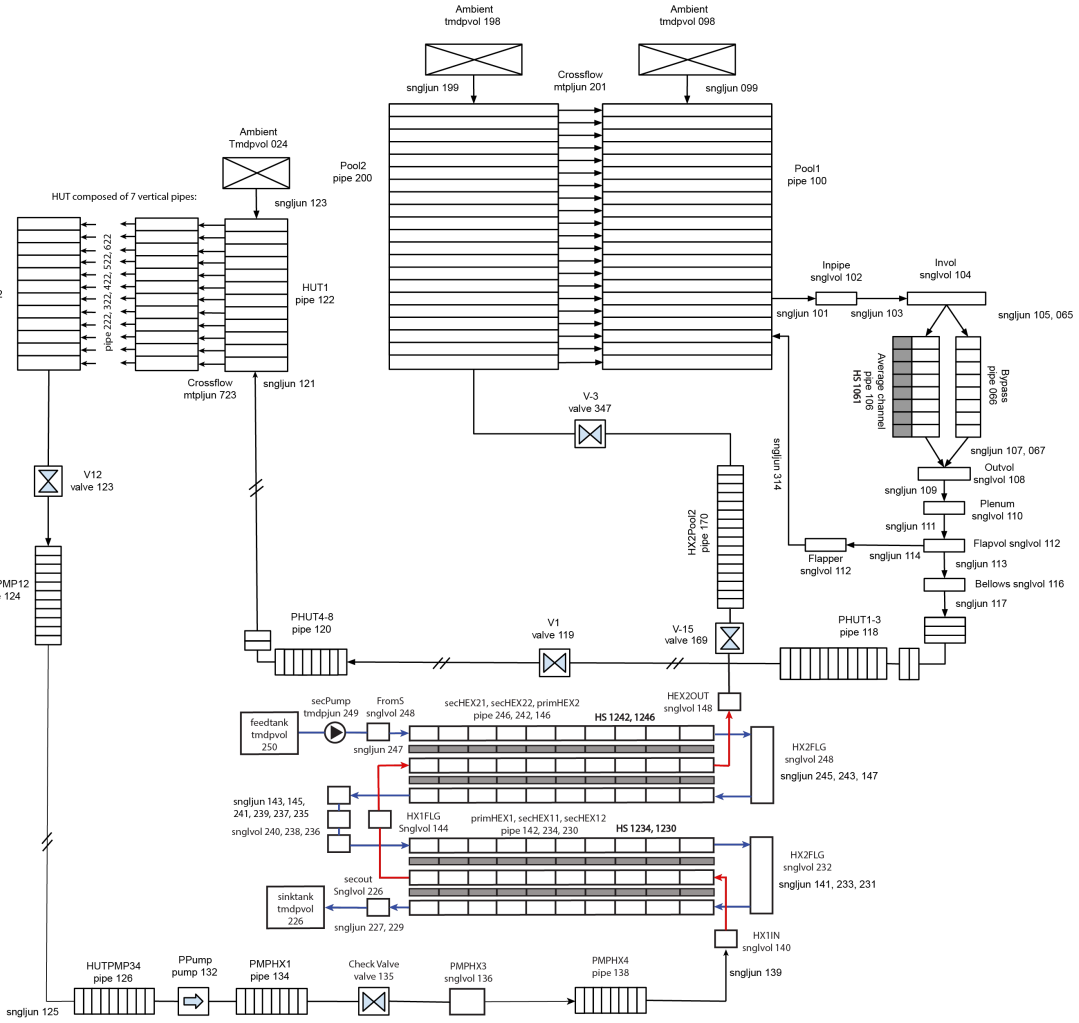

Figure 4.1: Nodalization of the MNR RELAP5 model.

4.3 Reactor Pool

The information presented in this section is primarily sourced from Reference [20]. The Reactor Pool is a reinforced concrete structure filled with light water. Its approximate dimensions are 15.0 x 7.6 x 9.8 meters, and it is designed to fulfill multiple functions such as core cooling, neutron moderation, and providing adequate biological shielding during normal operation at core power levels up to 5 MW. The Pool contains approximately 378,000 liters (about 100,000 US gallons) of water and is divided into two sections. The north end, referred to as Pool 1, is typically the location of the reactor core and includes wall penetrations for neutron beam experiments. The larger section, known as Pool 2, is primarily utilized for equipment storage and spent fuel. Figure 4.2 depicts the layout of the Pool. The physical separation between these sections can be achieved by installing a full-height aluminum gate. This watertight gate, when positioned in the designated bulkhead opening, facilitates the independent draining of each Pool section.

As the largest component of the primary coolant system, the Pool serves as a crucial heat reservoir. In the event of a reactor failure to operate without forced cooling, the extensive thermal inertia and heat capacity of the Pool enable natural convection cooling for an extended duration.

The temperature of the Pool is influenced by the conditions of the Secondary Loop, which functions as the heat sink. Various factors, including flow in the Secondary Loop, cooling tower fan settings, and external ambient temperature, determine the Pool temperature. Typically, the Pool temperature is maintained within the range of 20-32°C.

Table 4.1 summarizes important nominal parameters and their range of variation.

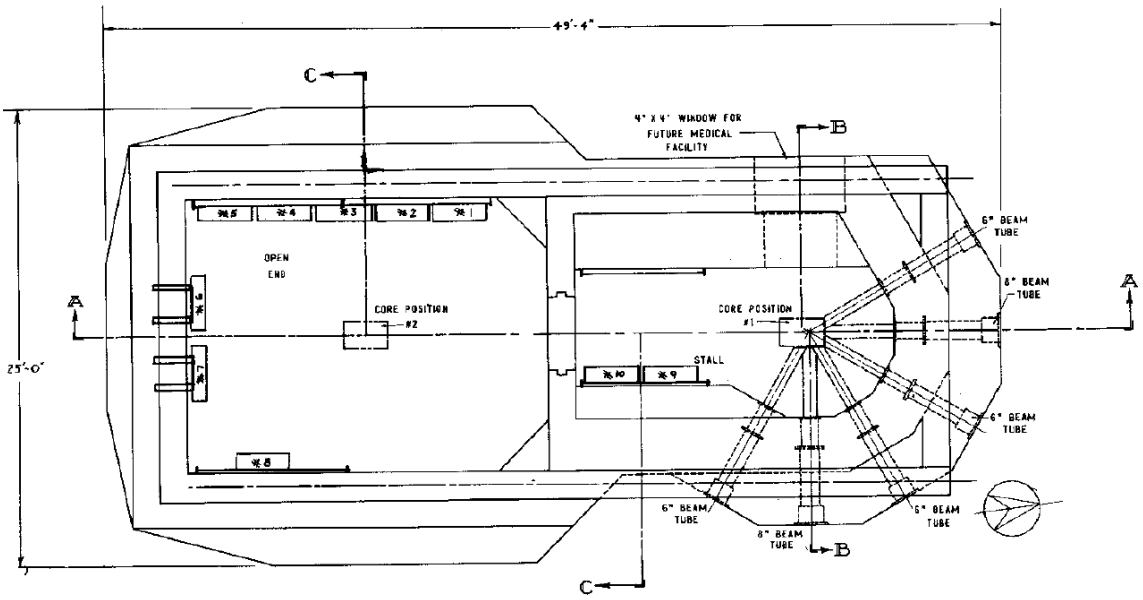

Figure 4.2: Top view of the Pool with dimensions and positions of structures. Taken from MNR Safety Analysis Report [1]

Parameter	**Nominal value**	**Range of variation**	**Unit**
Water level	9.30	± 0.15	(m)
Volume POOL 1	133.7	± 2.6	(m^3)
Volume POOL 2	253.9	± 4.2	(m^3)
Total Pool volume	378.1	± 6.8	(m^3)
Operating temperature	26	± 6	(°C)

Table 4.1: MNR Pool operational parameters.

Hydraulic model

In the RELAP5 nodalization, Pool 1 and Pool 2 are modelled as distinct vertical pipes interconnected through cross-flow lateral junctions as shown in Figure 4.3. This modelling approach allows for the simulation of mass, momentum and energy transfer

between the pools, enabling the representation of the mixing process. It's important to note, however, that RELAP does not solve 3D conservation equations, meaning that the 3D mixing process in the pool is not modelled. Instead, lateral junctions are included as a rough approximation of lateral flow. Furthermore, it should be noted that the Reynolds numbers for the pool flows are very low, reaching the limit at which RELAP can be applied.

Each vertical pipe was discretized into 21 volumes. The first volume of both vertical pipes (top of the pool) is linked through single junctions to two time-dependent volumes that emulate the containment environment. These two volumes, containing air, are maintained at atmospheric pressure and 20°C. No heat structures were incorporated to simulate heat transfer between the pool surface and the ambient air in the containment. Consequently, processes like pool evaporation are not considered in this model.

The 21st volume of the pipe 200 (the bottom of Pool 2) is connected to a pipe originating from the heat exchanger outlet, representing the inlet of the pool. In a similar vein, the 16th volume of the pipe 100 is connected via a cross-flow junction to the core inlet plenum, representing the outlet of the pool.

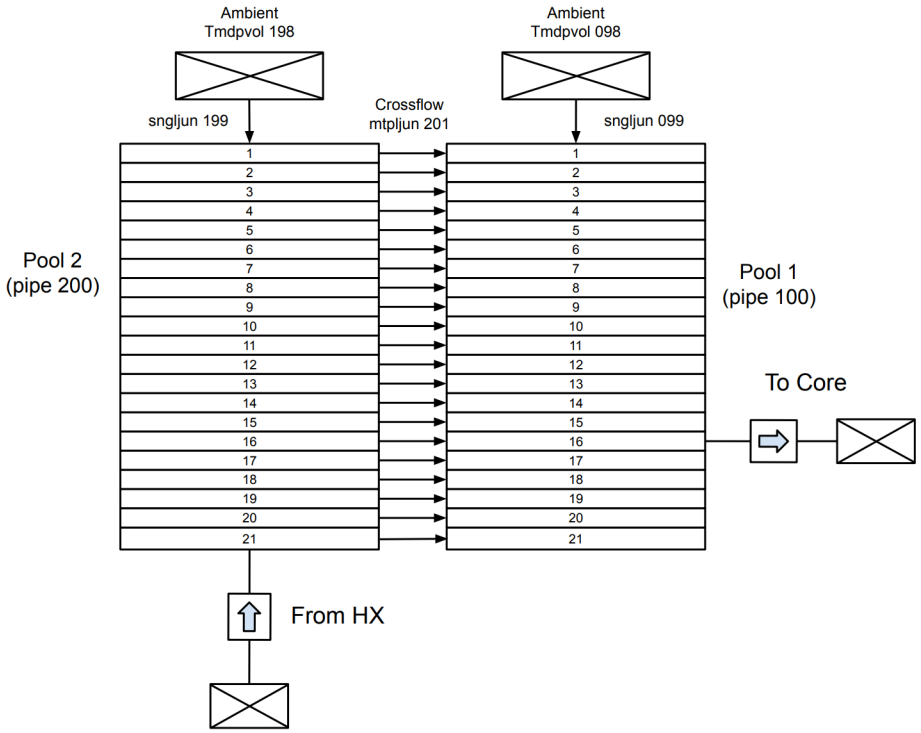

Figure 4.3: Pool nodalization with two vertical pipes interconnected through cross-flow lateral junctions.

The total length of pipes 100 and 200 is 9.30 meters (or 30.5 feet). Table 4.2 indicates the axial position of the 21 nodes comprising the pool nodalization. The node position reported in the table corresponds to the center of each node. The 16^{th} volume of Pool 1, which connects to the core inlet plenum, is located at a height of 1.97 meters measured from the bottom.

As part of the nodalization construction, the initial pressure and temperature of the 21 volumes must be specified. The temperature condition depends on the case being simulated. Generally, a homogeneous temperature profile is assumed based on reactor operational conditions (i.e. fully mixed pool), but non-homogeneous temperature profiles can also be used (i.e. stratified initial condition), as will be shown later

in this thesis. On the other hand, the initial pressure in each volume is a simpler factor to predict. To obtain these values, the static pressure at the axial position of each node was calculated using a density of 996 kg/m^3 (taking the density of water at 30°C as a reference [23]). Table 4.2 also displays the static pressure values used for each pool node.

Node #	**Axial position (node-center) (m)**	**Static Pressure (Pa)**
Pool surface	9.30	1.01E+05
1	9.16	1.03E+05
2	8.75	1.07E+05
3	8.24	1.12E+05
4	7.74	1.17E+05
5	7.24	1.22E+05
6	6.74	1.26E+05
7	6.24	1.31E+05
8	5.73	1.36E+05
9	5.23	1.41E+05
10	4.73	1.46E+05
11	4.23	1.51E+05
12	3.73	1.56E+05
13	3.23	1.61E+05
14	2.72	1.66E+05
15	2.32	1.69E+05
16	1.97	1.73E+05
17	1.67	1.76E+05
18	1.38	1.79E+05
19	0.98	1.83E+05
20	0.59	1.86E+05
21	0.20	1.90E+05
Pool bottom	0.00	1.92E+05

Table 4.2: Axial position and static pressure of the pool nodes.

The cross-sectional area (or flow area) of each pipe was extracted from the information illustrated in Figure 4.4 (which is referenced in [20]). The pool cross section presents an axial variation due to the presence of two shelf structures in the pool. The shelf at Pool 1 extends up to 4.45 meters while the shelf in Pool 2 reaches 5.33 meters from the bottom. Below the shelf, the equivalent cross-sectional area of pipe 100 is $11.3m^2$, while for pipe 200, this area is $26.9m^2$. Above the shelf, the cross-sectional area of pipes 100 and 200 is $17.2m^2$ and $27.9m^2$, respectively.

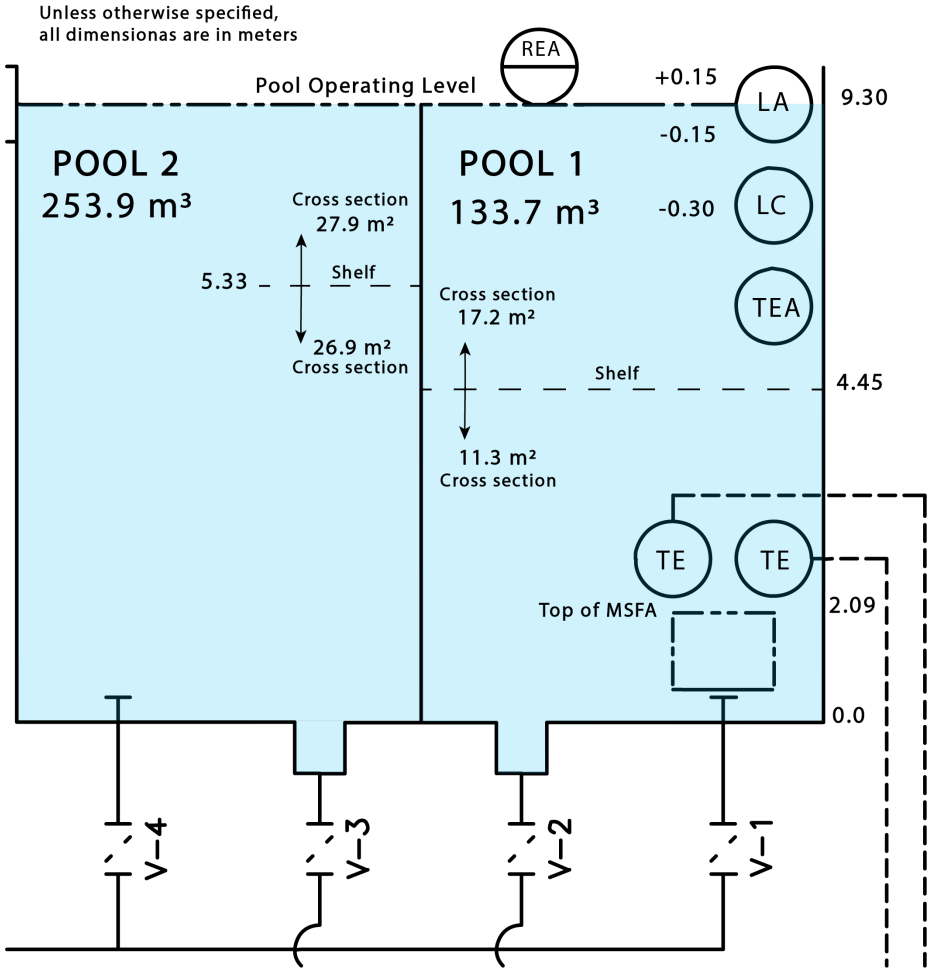

Figure 4.4: Cross section of the Pool with dimensions.

Thermal model

To account for heat transfer with the environment, the concrete walls surrounding the pool water were modelled as heat structures. The nominal thickness of these walls is 1 meter, as presented in official MNR diagrams detailing the pool concrete structure. The thermal model for the pool walls is a slab model with 10 equidistant nodes. On the left wall, heat transfer occurs through convection with the pool water, while on the right wall, free convection with environmental air at 20°C is considered. The heat transfer coefficient h was sourced from [17], with a chosen value of $25 W/Km^2$. The thermal model is visually depicted in Figure 4.5.

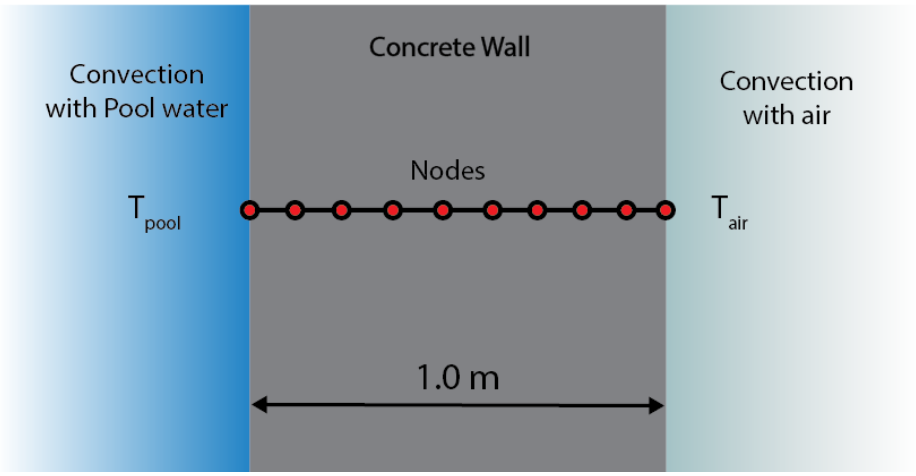

Figure 4.5: Slab thermal model used in the heat structures of the Pool wall.

The thermal properties of concrete used for the model were extracted from [17] and are presented in table 4.3. The thermal conductivity and heat capacity are considered constant with temperature.

Concrete thermal properties		
Temperature	Thermal Conductivity [W/(m.K)]	Heat Capacity [J/(kg.K)]
273.15	1.4	880
2000.15	1.4	880

Table 4.3: Thermal properties of concrete.

4.4 Reactor core

A brief description of the core thermal-hydraulics will be provided in the this section. Detailed information of the geometry and technical specifications of the core components is provided in [1] (McMaster Nuclear Reactor: Reactor Specifications technical report).

The reactor core consists of a grid plate, fuel, control and irradiation assemblies. A typical core plan is shown in Figure 4.6[1]. The grid plate is a 12.5 cm (5 in) aluminum block. Fifty-four large holes accept core components, which may be arranged in different configurations as research needs dictate. Forty small grid plate holes provide additional bypass coolant flow paths. Typically, 24 bypass are left open, while 16 are plugged. Both the larger (assembly) holes and the smaller (bypass) holes can be completely blocked by grid plate plugs[2]. The grid plate is attached to a plenum (an aluminum box structure) which directs flow through a bellows mechanism to the core outlet pipe.

[1]The Central Irradiation Facility (CIF) in position 5C can be replaced with a MSFA.

[2]Grid plugs are used to block flow through assembly holes in vacant core positions such as not to divert flow from fuel or sample positions. Similarly, smaller bypass hole plugs are used to close these flow paths when not needed for cooling. In MNR a set number of bypass holes are opened to achieve cooling for the fueled outer plates of control fuel assemblies.

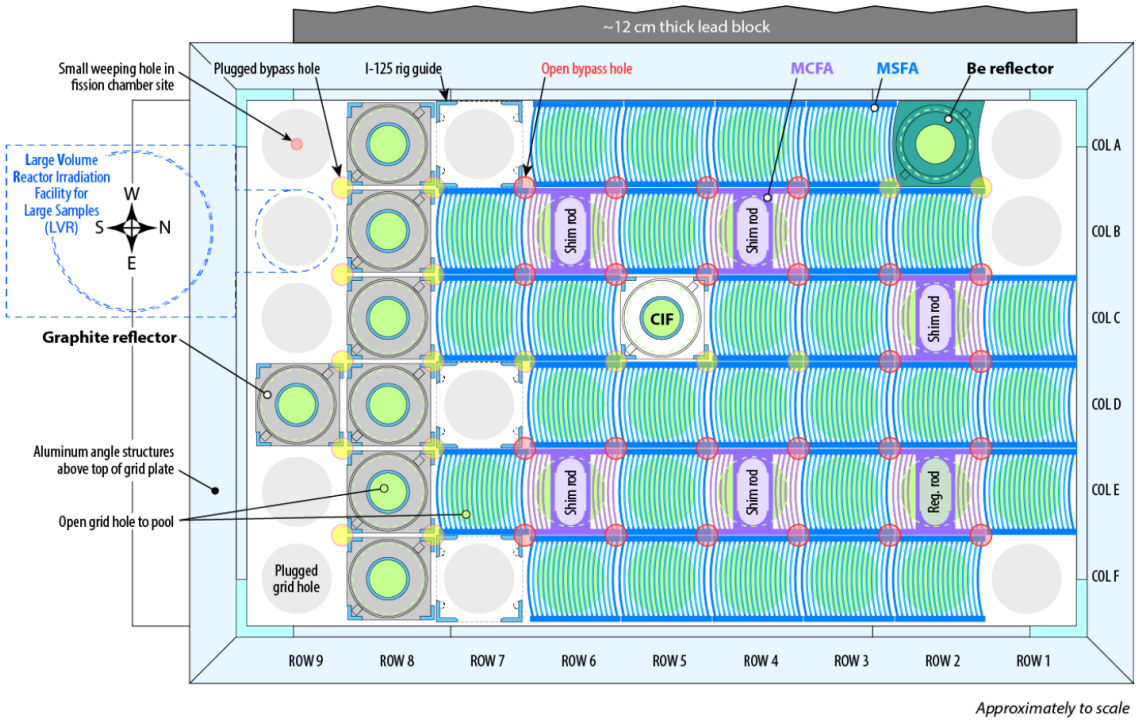

Figure 4.6: Typical Core Layout. Taken from MNR Safe Operating Envelope [2].

Hydrodynamically, the core is composed of a series of parallel flow paths, through loadable components and bypass holes, ultimately through the core grid plate into the plenum. All primary paths have the common boundary conditions (i.e., water in the reactor pool and water in the reactor plenum at an essentially constant pressure). Thermally, the core is the source of heat, generated by the fission reaction. The majority of the heat is deposited within the fuel material inside the fuel plates.

The nominal core inlet temperature has a range of 20-32°C, consistent with the Pool temperature mentioned earlier. Conversely, the core outlet temperature is linked with the inlet temperature and is dependent on the thermal power generated in the core and the coolant flow rate. For a nominal thermal power of 3MW and a flow rate of 2000 USGPM, the temperature increase across the core is approximately 5-6°C.

Consequently, the outlet temperatures can be anticipated to fall within the range of 25-39°C.

The following subsections will provide a concise overview of the core assemblies, encompassing the MNR Standard Fuel assemblies (MSFA), the MNR Control Assemblies (MCA), and the Graphite and Beryllium reflectors. Additionally, a brief description of the core bypass flow will be included. This information offers valuable insights into the development of the core model.

4.4.1 MNR Standard Fuel Assembly (MSFA)

The MNR Standard Fuel Assembly is composed of curved fuel plates enclosed by side plates and top and bottom end fittings, resulting in a rectangular configuration. The MSFA comprises a total of 18 curved plates, with 16 of them containing U3Si2-Al type fuel, while the remaining two plates (the outer ones) do not contain any fuel and are referred to as "dummy" plates. Typically, the MNR core can accommodate between 28 to 32 MSFAs, depending on operational and production requirements. In thermohydraulic and neutronic modelling, it is assumed that the plates are straight to simplify the geometry.

A single MNR Standard Fuel Assembly (MSFA) and a typical core loading configuration are shown in Figure 4.7. These graphics have been created directly from the MNR OSCAR-5 model[3] [10]. The geometry specifications used for the RELAP5 model are summarized in Table 4.4. Figure 4.8 offers an axial view of a typical MSFA, and Figure 4.9 shows an schematic of the cross section of the MSFA also indicating

[3]OSCAR-5 is the fifth release of the OSCAR platform developed by Necsa RRT (South Africa). The MNR OSCAR-5 model has been developed as a fuel management operational support tool and currently uses the neutronics codes MGRAC (nodal diffusion), MCNP6, and Serpent.

geometry information.

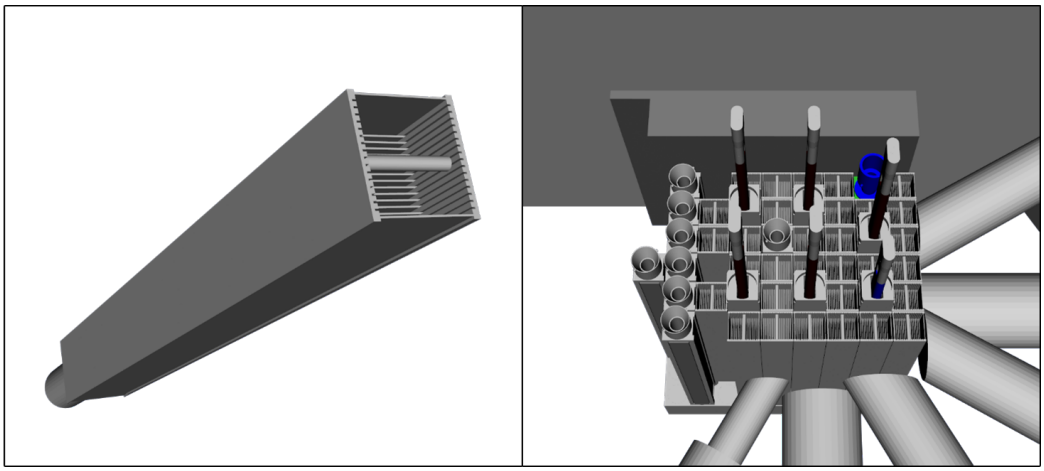

Figure 4.7: Perspective of an MSFA (left) and a typical core configuration (right). Schematic provided by MNR analysis team.

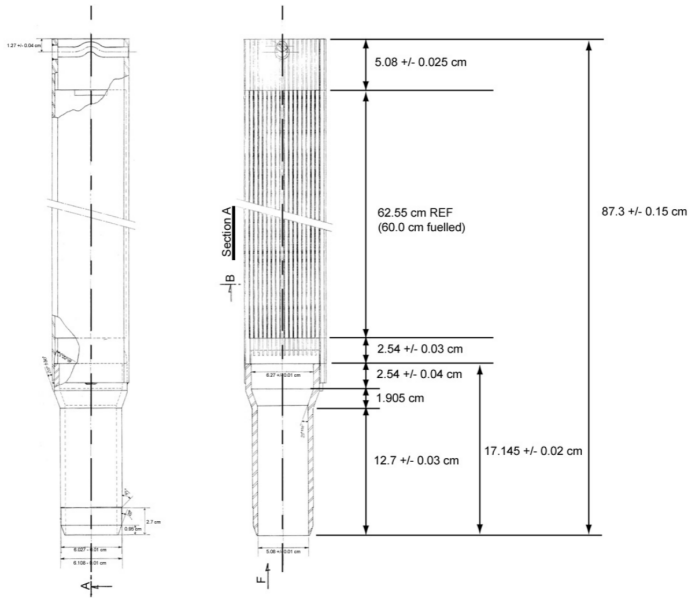

Figure 4.8: Axial view of the MSFA. Taken from MNR Reactor Specification technical report [9].

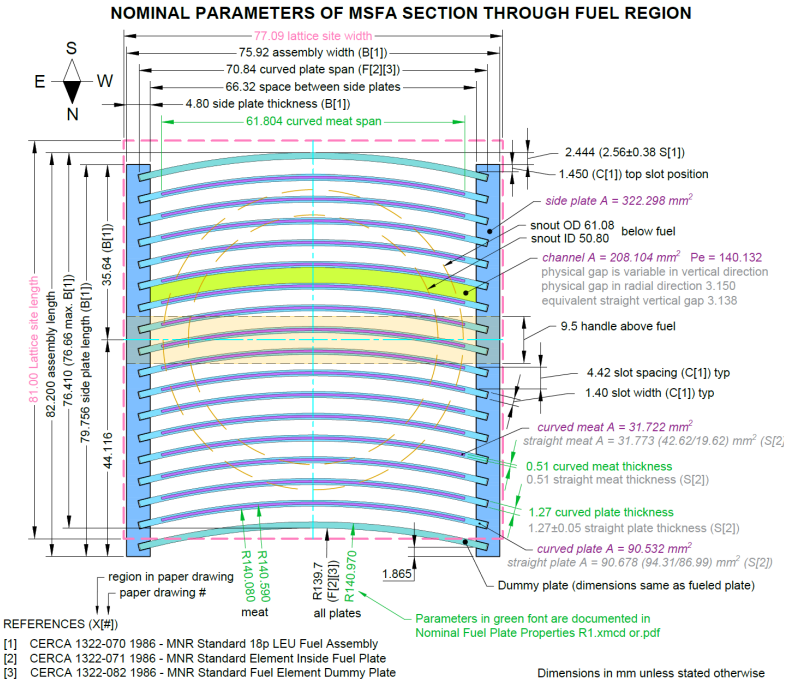

Figure 4.9: Cross section of the MSFA with dimensions. Taken from MNR Safe Operating Envelope [2].

Parameter	Value
Total number of plates	18
Number of active plates (U3Si2-Al)	16
Height of fuel plate (mm)	625.5
Height of fuel meat (nominal) (mm)	600.0
Span between side plates (width) (mm)	66.32
Span of fuel meat (nominal, before curving) (mm)	62.3
Thickness of fuel meat (mm)	0.51
Thickness of cladding (mm)	0.38
Thickness of coolant (equivalent straight gap) (mm)	3.138
Number of coolant channels	17
Flow area of 1 channel (cm^2)	2.081
Flow area of 1 assembly (17 channels) (cm^2)	1132.086
Hydraulic diameter (mm)	5.94

Table 4.4: Geometric parameters of the MSFA for constructing the core model.

4.4.2 MNR Control Assembly (MCA)

Within the MNR core, there are six control fuel assemblies housing a single regulating absorber rod and five shim-safety absorber rods. These assemblies share the same outer dimensions and bottom end fittings (snouts) as the standard fuel assemblies. The MNR control fuel assembly comprises nine fuelled plates without any dummy plates, along with a central aluminum guide for the absorber rod. Figure 4.10 and Figure 4.11 show the geometry and dimensions of this component.

The MNR control fuel assembly differs from the standard fuel assembly in several aspects. It is taller and includes an aluminum shock absorber seat as part of the top end fitting, which connects to a stainless steel shock absorber tube. The outer fuel plates in the control fuel assembly match the outer dimensions of dummy plates in the standard fuel assembly and have the same meat dimensions as the inner fuel plates. If not explicitly stated, the specifications remain the same as those for the MNR standard fuel assembly.

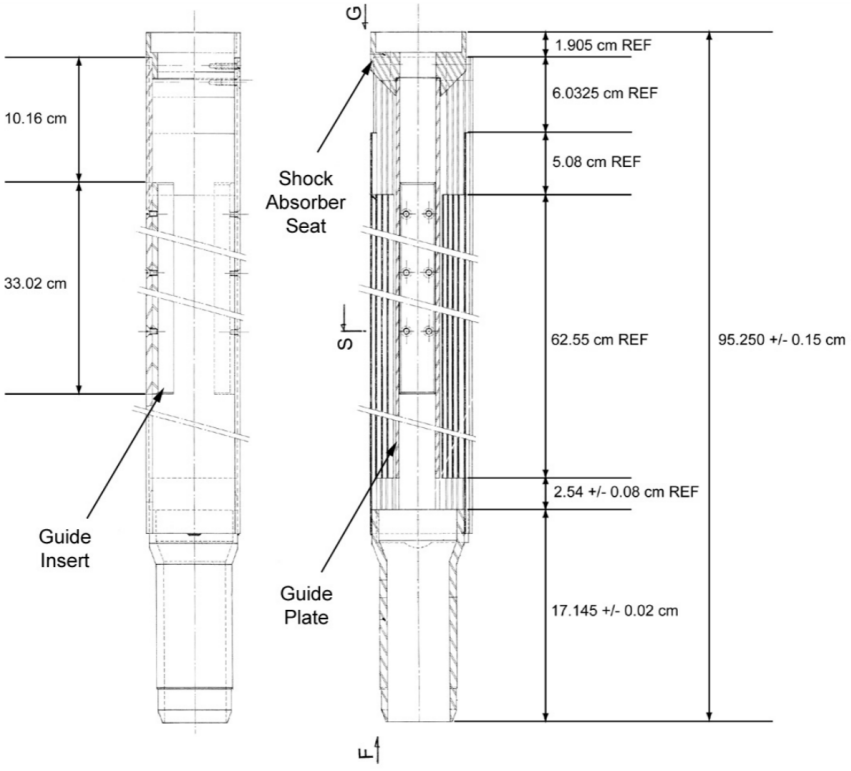

Figure 4.10: Axial view of the MCA. Taken from MNR Reactor Specification technical report [9].

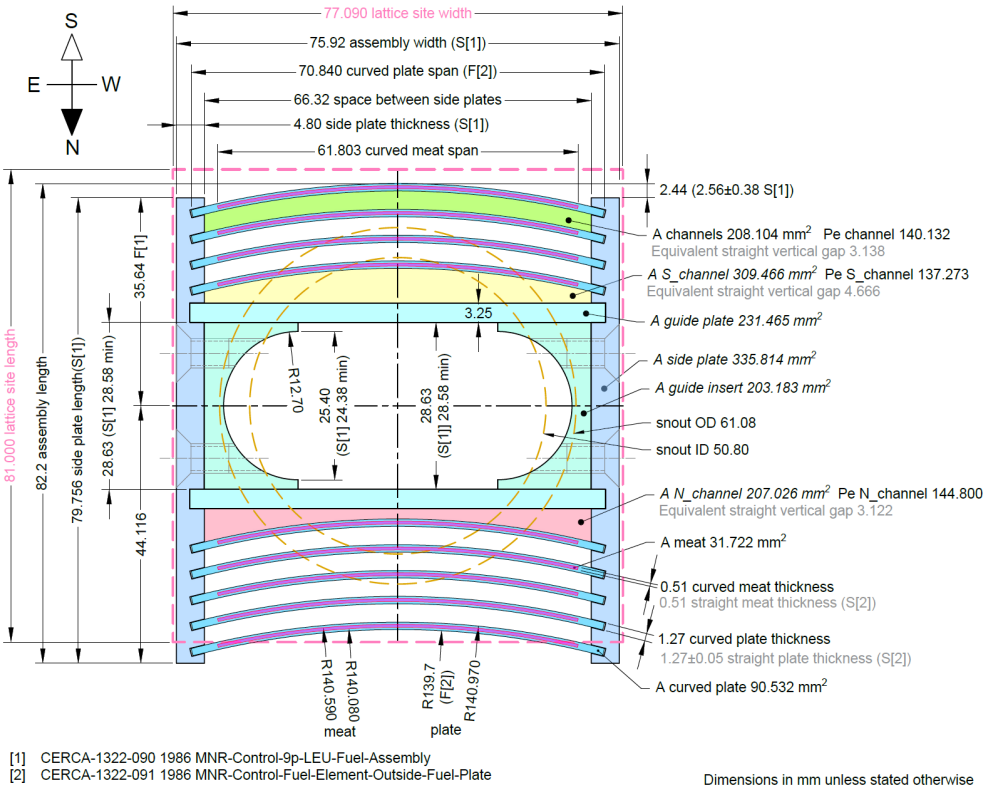

Figure 4.11: Cross section of the MCA with dimensions. Taken from MNR Safe Operating Envelope [2].

4.4.3 MNR Graphite Reflector Assembly

The MNR core includes graphite reflector assemblies positioned on the grid plate, akin to standard and control fuel assemblies. Each graphite reflector assembly consists of a graphite block with a central hole, a cage frame made up of four aluminum angle pieces, upper and lower cage blocks, top and bottom end fittings, and a central aluminum tube with a sample hole. Figure 4.12 shows a schematic of the graphite assembly including dimensions and main characteristics.

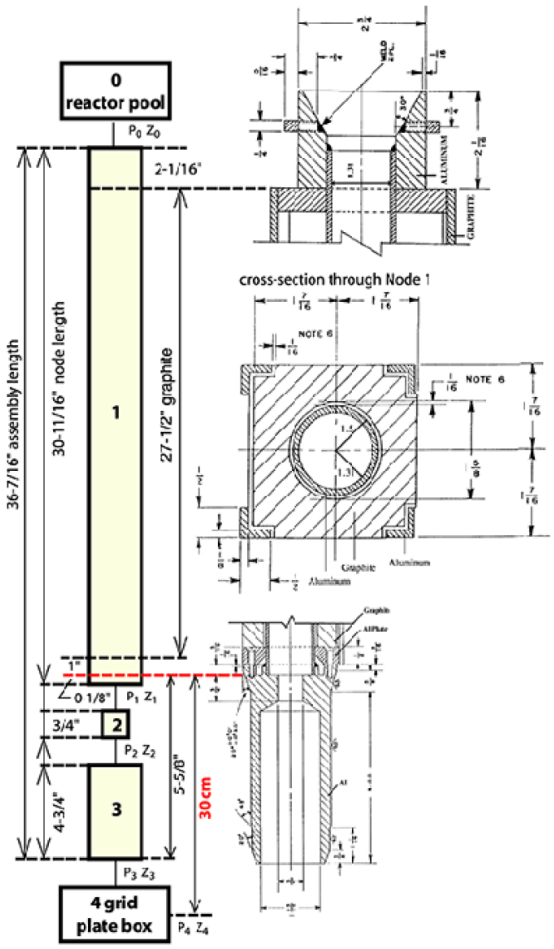

Figure 4.12: Schematic of the MNR graphite reflector assembly. Taken from MNR Safe Operating Envelope [2].

4.4.4 MNR Beryllium Reflector Assembly

Within the MNR core, a single beryllium reflector assembly serves as part of the start-up source configuration and can also function as a potential sample irradiation site. Its design is akin to the graphite reflector assemblies, featuring a central sample hole. However, notable differences lie in the top and bottom end fittings, as well as the absence of any support angle or irradiation cage. Figure 4.13 shows a schematic

of this component.

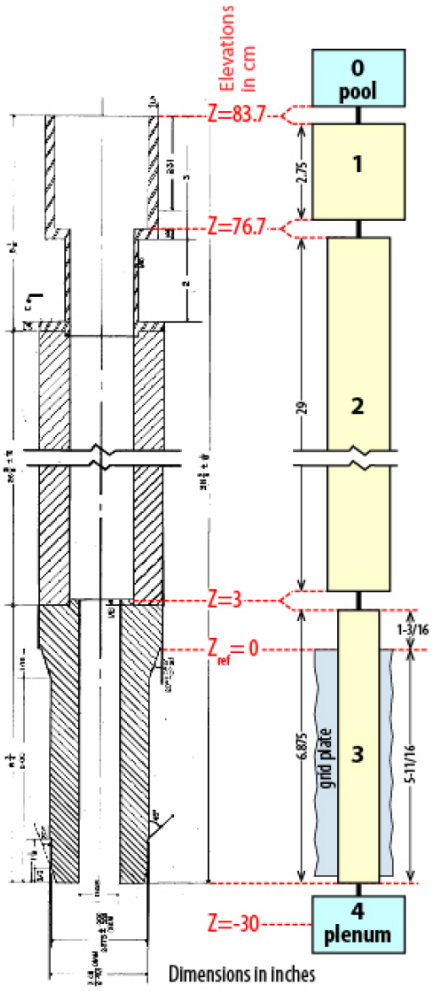

Figure 4.13: Schematic of the MNR beryllium reflector assembly. Taken from MNR Safe Operating Envelope [2].

4.4.5 Bypass holes

The complex and variable paths of pool water to the entrances of open holes are schematically illustrated in Figure 4.14. All, or a portion, of the pool water passing through the open bypass hole must flow through the interspaces between the loaded

assemblies before reaching the entrance of the hole. The reactor core is not housed within a box with side walls, therefore pool water not only flows into the bypass from the top of the core but also from the sides. Figure 4.6 shows typical locations of open bypass holes (highlighted by red, semi-transparent shading) in MNR cores. Four holes are normally open around each of the 6 MCFAs in order to enhance cooling of their outermost plates which are fuelled.

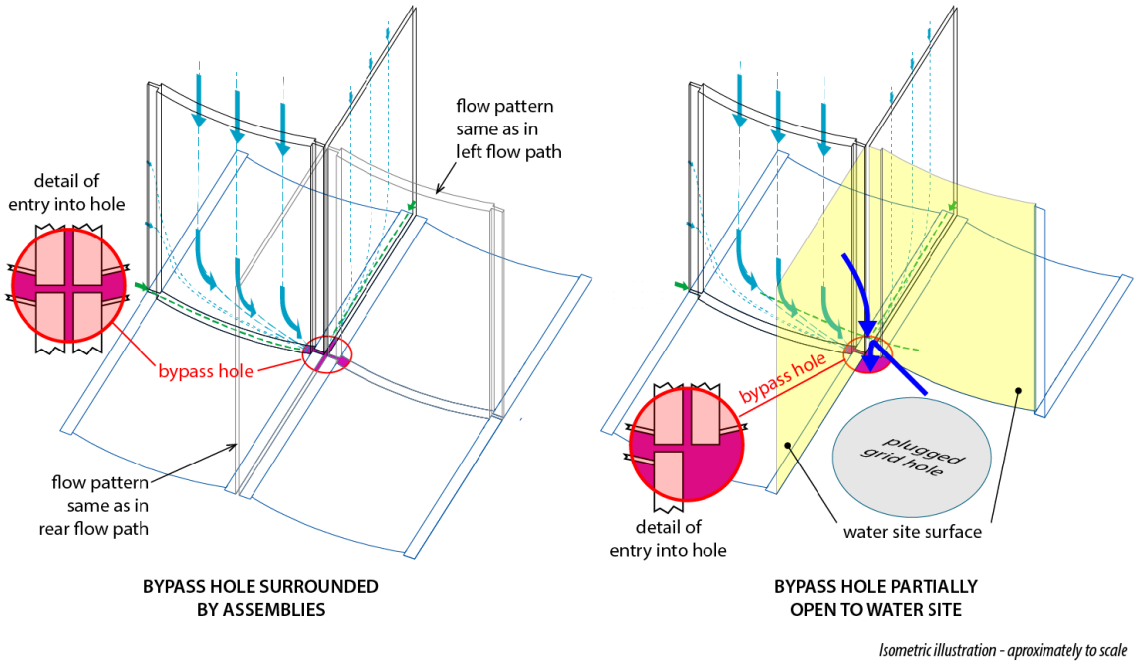

Figure 4.14: Upstream flow paths to open bypass hole. Taken from MNR Safe Operating Envelope [2].

Core hydraulic model

The hydraulic core model implemented in the RELAP5 nodalization comprises two pipe components simulating the average assembly (encompassing standard fuel assemblies and control assemblies) and the bypass flow through reflector assemblies and bypass holes (see Figure 4.16). It is considered that the flow that circulates

through the reflectors and the bypass holes is not heated. These pipe representations incorporate geometric data for channels, including water flow area, active length, minor head losses at the inlet and outlet, and friction losses. Longitudinally divided into eight sections, these pipes undergo thermal transfer calculations within each section, following a power distribution on the plates provided by neutronic calculations with the MGRAC code [22].

The core configuration selected for the core model was Core 62P (illustrated in Figure 4.15). This configuration was used during the 2020 Secondary Loss event in the MNR. This same configuration was utilized for simulating the Pool Temperature Experiment, even though this was slightly different in reality, since the CIF was located in position 5C on the day of the experiment (replacing one MSFA). This approximation was made to simplify the model development process. As the model solely accounts for the average channel, it averages thermal-hydraulic parameters across the entire core, encompassing factors such as total flow area, length, and power deposition. Consequently, any discrepancies arising from the placement of either a MSFA or a CIF in position 5C are effectively minimized.

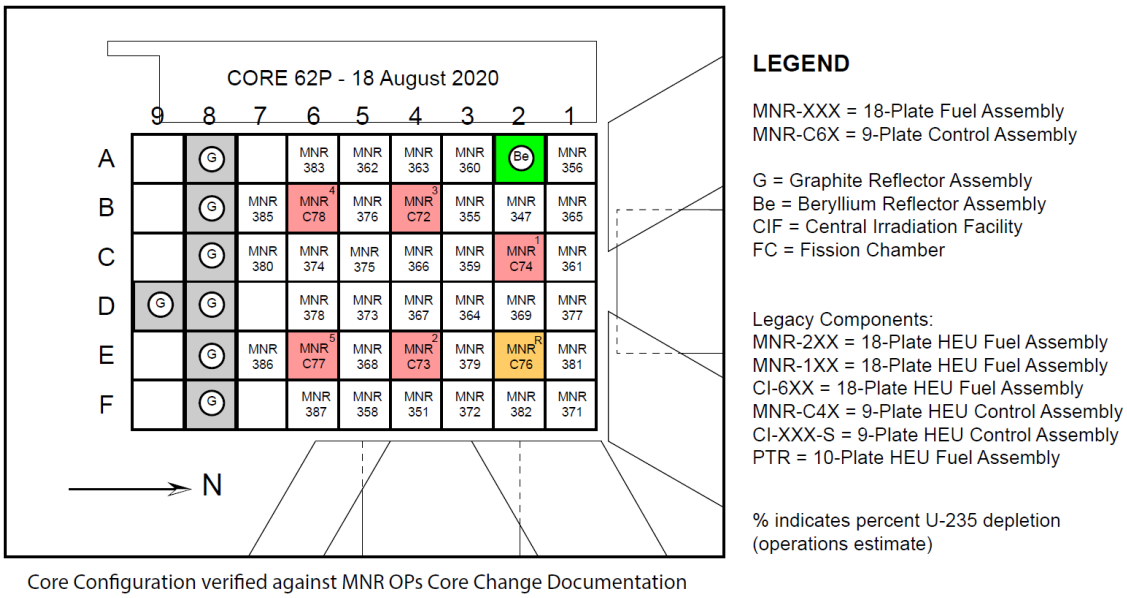

Figure 4.15: Core configuration 62P.

This choice is supported by the fact that validation between the RELAP5 model and experimental data from the MNR primarily focused on bulk core inlet and outlet temperatures. However, if a more detailed analysis of core thermal-hydraulics is necessary (such as examining temperature distribution in the plates, the hottest plate temperature, margin to boiling in the hottest channel, margin to CHF, etc.) a higher resolution model should be employed. This entails modelling the assemblies in greater detail and distinguishing the hottest channel in the core.

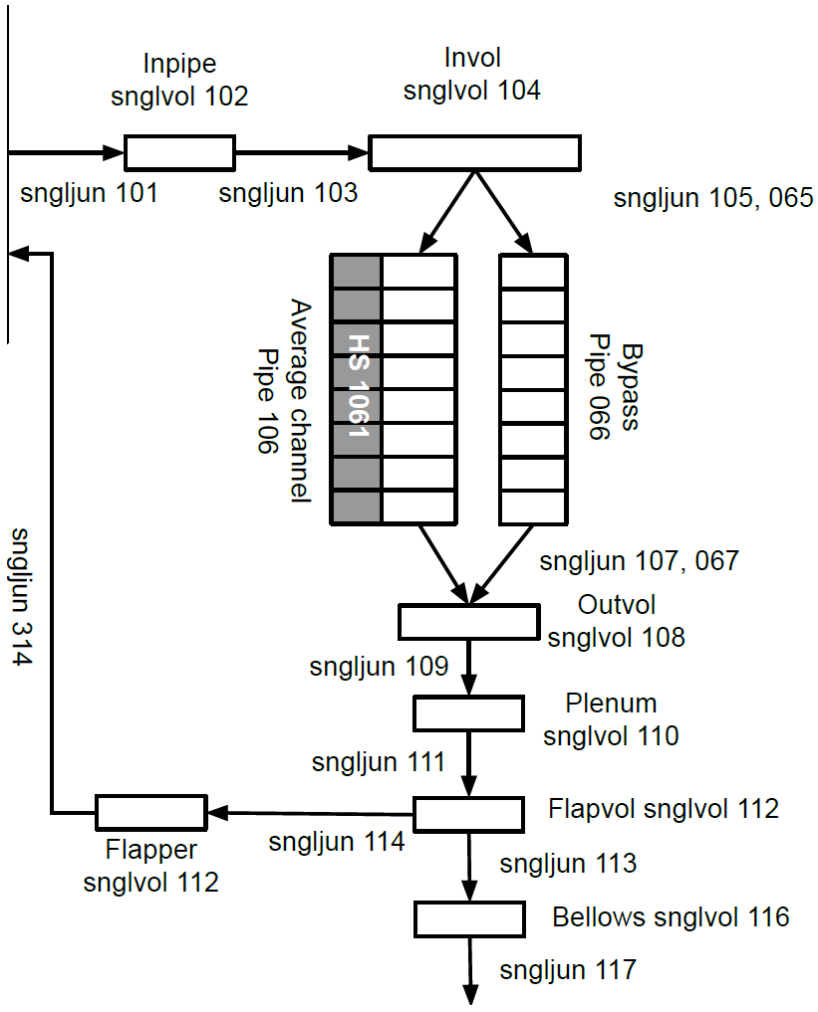

Figure 4.16: Core nodalization.

The core configuration 62P comprises 32 MSFAs, 6 MCAs, 7 Graphite reflectors, 1 Beryllium reflector and 24 open bypass holes. For the average channel, the flow area of all the 32 MSFAs and the 6 MCAs was added up and implemented in a pipe component. The length of this pipe is equivalent to the active length of the core. This means that frictional pressure losses in the unfueled clad section are not considered.

The flow area for the average channel model was calculated accounted for the flow area of all of the 32 MSFAs and 6 MCAs. The calculation follows the following

expression:

$$A_{avg\_channel} = 32 \cdot A_{MSFA} + 6 \cdot A_{MCA} \tag{4.4.1}$$

The average channel hydraulic diameter was calculated based on the flow area and wetted perimeter of the 32 MSFAs and the 6 MCAs.

$$D_{avg\_channel} = 4 \cdot \frac{32 \cdot A_{MSFA} + 6 \cdot A_{MCA}}{32 \cdot P_{MSFA} + 6 \cdot P_{MCA}} \tag{4.4.2}$$

The flow area and wetted perimeter calculations for the MSFA (A_{MSFA}, P_{MSFA}) and the MCA (P_{MCA}, P_{MCA}) were performed following the data from Figures 4.9 and 4.11.

The flow area for the bypass pipe component was calculated combining the flow area of all the graphite reflector assemblies (7), Beryllium assembly (1) and open bypass holes (24). The flow across these assemblies is considered as not heated.

$$A_{bypass} = 7 \cdot A_{Graphite} + A_{Beryllium} + 24 \cdot A_{hole} \tag{4.4.3}$$

The hydraulic diameter was calculated in a similar way, according to the next expression:

$$D_{bypass} = 4 \cdot \frac{7 \cdot A_{Graphite} + A_{Beryllium} + 24 \cdot A_{hole}}{7 \cdot P_{Graphite} + P_{Beryllium} + 24 \cdot P_{hole}} \tag{4.4.4}$$

The following table 4.5 summarizes the main hydraulic parameters that describe the simplified core model. The wall roughness considered for both the average channel and bypass corresponds to the reference value for steel pipes extracted from [23].

Parameter	**Average Channel**	**Bypass**
Flow area (cm^2)	1250.4	138.8
Length (m)	0.6	0.6
Wall roughness (m)	4.60E-05	4.60E-05
Hydraulic diameter (mm)	5.968	24.38

Table 4.5: Averaged hydraulic parameters for the core model.

Core thermal model

The average power and the axial power distribution in the plate were obtained from a full-core steady-state neutronics snap-shot calculation using the nodal-diffusion neutronics code MGRAC [22]. This MGRAC snap-shot calculation was performed with the MNR OSCAR-5 model for cycle 62P at the beginning of the Loss of Secondary event (2020). The core loading for this snap-shot calculation was shown in Figure 4.15. The MGRAC power distribution data is produced on the nodal mesh of the model. For MNR the radial nodal mesh is the extent of a full fuel assembly and the axial mesh divides the total active height of the fuel into eight equidistant axial nodes, which are 7.50 cm high each. Output is in the form of the total power per assembly and an axial average power distribution over the nodal axial mesh. The MGRAC calculation was for a total core power of 3 MW (thermal). The core power distribution associated with this calculation is given in Table 4.6 and shown in Figure 4.17 and 4.18.

	Node boundary (cm)	**Relative power distribution [-]**	**Core power (MW)**
Node 1	7.5	0.098	0.29
Node 2	15	0.128	0.38
Node 3	22.5	0.153	0.46
Node 4	30	0.161	0.48
Node 5	37.5	0.155	0.47
Node 6	45	0.133	0.40
Node 7	52.5	0.101	0.30
Node 8	60	0.072	0.22
Total	**-**	**1**	**3.00**

Table 4.6: Relative and absolute axial power distribution.

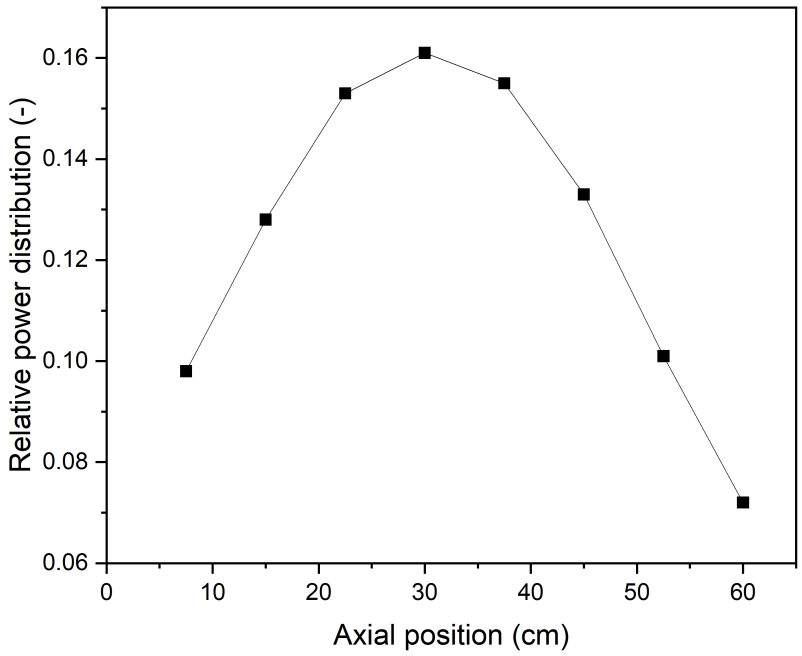

Figure 4.17: Core power distribution.

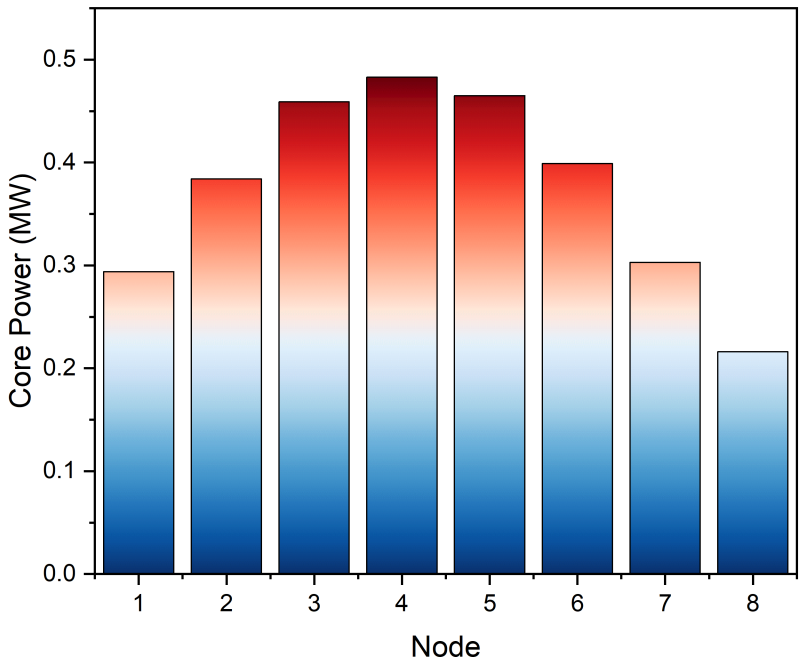

Figure 4.18: Core power per axial node.

The thermal model for the core heat structures, integrated with the hydraulic model, adopts a one-dimensional slab representation for the plate meat and cladding (as depicted in Figure 4.19). Discretized into five nodes in the x-direction the model enforces forced convection at the cladding wall with coolant flow directed downward in the y-direction. Applying symmetry conditions at the meat center (zero heat flux), the model accounts for one side of the cladding and half of the meat, facilitating heat transfer from the plate to the cladding via conduction and subsequent removal by convection through coolant flow. In RELAP5, an axial discretization of 8 nodes was chosen to align one-to-one with the neutronic mesh utilized in the MGRAC code. Constant power density within each axial node across the plate width is assumed. Heat transfer is one-dimensional convective from the cladding surface to the coolant.

The temperature calculation along the cladding and meat follows a one-dimensional

heat conduction concept through a material medium, considering the heat generation term in the meat. Convection cooling of the plate uses the Dittus-Boelter correlation [11], the default option to estimate the Nusselt number based on Reynolds and Prandtl numbers. Subsequently, the code employs this parameter to calculate the cladding wall temperature.

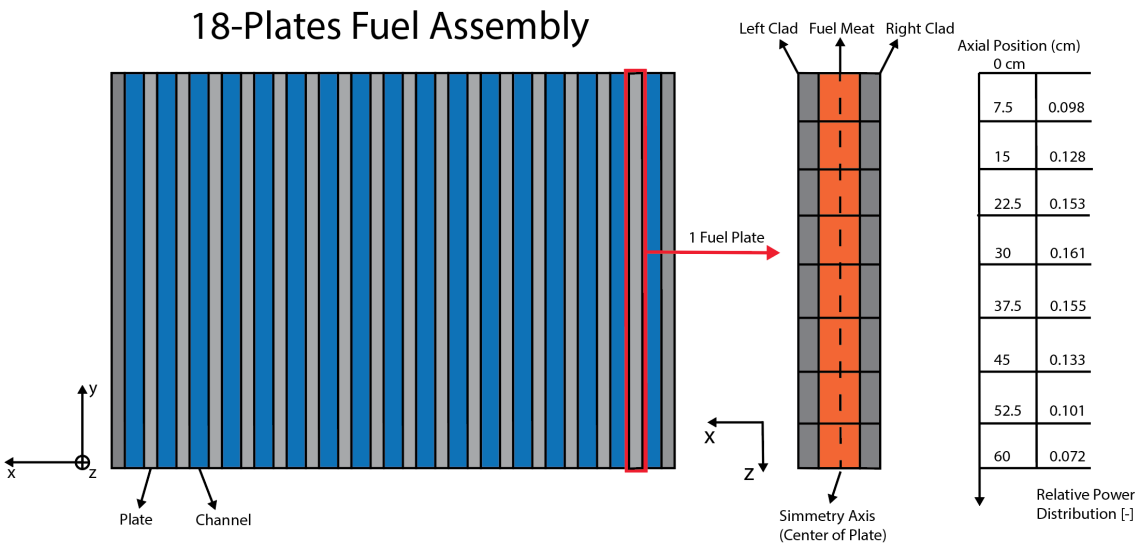

Figure 4.19: Slab thermal model used in the heat structures of the core.

The following tables 4.7 and 4.8 indicate the thermal properties assumed for the fuel plate materials. These properties are available in the MNR Safety Analysis Report [1]. The thermal conductivity is assumed constant while the heat capacity changes with temperature.

Fuel-Meat (Uranium Silicide)		
Temperature	Thermal Conductivity [W/(m.K)]	Heat Capacity [J/(kg.K)]
273.15	73.0	2.367E6
1873.15	73.0	3.273E6

Table 4.7: Thermal properties of the fuel meat.

Cladding (Aluminum)		
Temperature	Thermal Conductivity [W/(m.K)]	Heat Capacity [J/(kg.K)]
273.15	123.0	2.4084E6
1873.15	123.0	3.153E6

Table 4.8: Thermal properties of the cladding.

4.5 Primary piping and valves

The entire primary loop is composed of stainless-steel pipes of 10.482" internal diameter. This pipe allows the coolant to flow from the reactor Pool through the Primary Loop, passing through the HUT, the primary pump, and the HEX. Table 4.9 shows the main characteristics of the primary piping, including geometric and material specifications. Table values are taken from the MNR technical report [20].

Property	**Value**
Nominal OD	10.75”
Nominal ID	10.482”
Schedule	5S
Wall thickness	0.134”
Pipe material	Stainless Steel
Wall roughness	46E-6m (Reference value for stainless steel pipe)

Table 4.9: Primary piping information.

Piping sections and lengths were obtained from official blueprints from the MNR, and the primary heat transport system loop was built following these specifications. The list of drawings consulted for the model development is presented below:

- AMF-89-23-B-3500, “Pool Structure Embedments, McMaster University”, Rev. B, 4/26/1957.
- AMF-89-23-E-3501, “McMaster university Reactor Pool”, Rev. B, 9/5/1957.
- AMF-89-23-E-3503, “McMaster University Reactor Pool – Ceramic Tile Details”, Rev. A, 9/3/1957.
- AMF-89-23-D-6150, “Intake Connection Assembly”, Rev. A, 7/31/1957.
- AMF-89-4-D-6656, “Pool Sump”, 10/10/1956.
- AMF-89-22-D-6220, “Sump Cover Plate”, 10/10/1956.
- AMF-89-4-D-6695, “Gate Guide”, Rev. B, 4/2/1957.

- AMF-89-22-E-6160, "Plenum and Bellows Assy", Rev. A, 3/30/1957.
- AMF-89-22-D-6161, "Bellows Assembly", Rev. A, 5/11/1957.
- AMF-89-22-D-6162, "Plenum", Rev. B, 9/26/1957.
- AMF-89-22-D-6188, "Bellows", 10/10/1956.
- AMF-89-23-E-5000, "McMaster University Piping Arrangement Plans & Sections (B-C-D)", Rev. J, 6/5/1958.
- AMF-89-23-E-5002, "McMaster University Piping Arrangement Section E-E & Details", Rev. C, 9/4/1957.
- WRS, "Nuclear Research Building Research Building Extension, McMaster University, Hamilton, Ontario", Sheet 2, Rev. 15 Nov 1957, Drawing, William R. Souter and Associates, Architectural Drawing.
- WRS, "Nuclear Research Building Research Building Extension, McMaster University, Hamilton, Ontario", Sheet 11 – Detail Sections, Rev. 15 Nov 1957, Drawing, William R. Souter and Associates, Architectural Drawing.
- W. H. Fleming, "McMaster Nuclear Reactor Heat Exchanger", Engineering Drawing, 16 Nov 1960.

Hydraulic model

The primary piping network is modelled using pipe and valve components. The piping nodalization was constructed according to the dimensions reported in the MNR diagrams. Here, a demonstrative example of how the nodalization of the primary

piping was constructed is presented. The nodalization of all pipe sections will not be detailed to avoid making this section overly extensive.

In Figure 4.20, an example of a pipe section after valve V-1 is shown, which is used to regulate the flow through the core. This valve is open 40% during normal operation at 3MW of power, resulting in a flow rate through the core of 2000 GPM. This valve is modelled in the RELAP nodalization as a valve component, with the opening percentage set at 40%, which is associated with a specific resistance coefficient K_1.

Following this valve, there is a straight pipe section with a length of 1.143 meters (the number 4 assigned to this pipe section is part of a system numbering process to maintain order and traceability of the primary system modelling). This section is modelled as a hydrodynamic pipe component with the indicated length and internal diameter of 0.254 meters.

Next is an 84-degree elbow, which is modelled as a localized pressure drop represented by a resistance coefficient K_2, taken from [23]. After this elbow, there is a pipe section of 3.835 meters, where various factors causing pressure losses are accounted for and added to the model. First, there is a Tee connection to the line controlled by valve 4 (which is closed), then there is a thermowell containing temperature sensors measuring the core outlet temperature, and finally, there is a flow sensor of the plate-orifice type measuring the flow through the core. These three sources of localized pressure loss are modelled with resistance coefficients K_3, K_4 and K_5 applied to the corresponding junctions. These coefficients also were taken from [23].

Similarly, the modelling of the rest of the primary system continues, following the methodology detailed above.

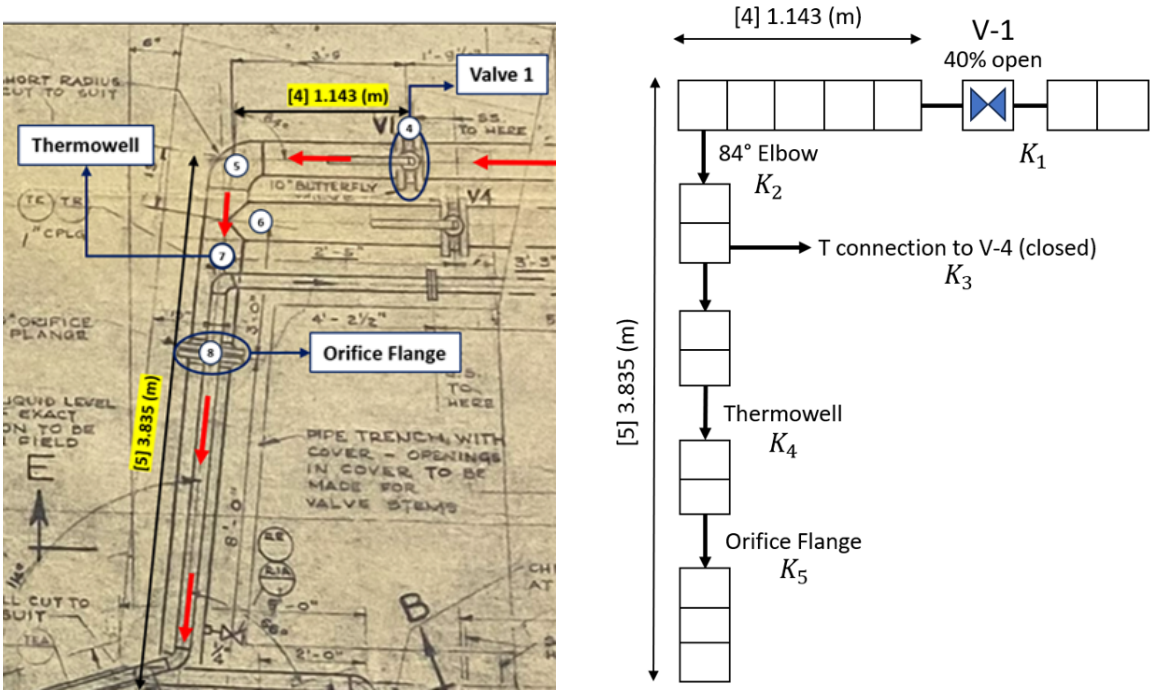

(a) Piping diagram.

(b) RELAP5 nodalization.

Figure 4.20: Example of how the piping system is nodalized in the RELAP5 model.

Thermal model

Heat losses within the piping system are modelled using a radial thermal approach. This method involves assigning heat structures to each section of piping, characterizing the stainless steel walls that separate the primary coolant from the surrounding containment air[4]. The thermal model comprises a radial stainless steel structure with 5 equidistant radial nodes and boundary conditions set to account for forced convection with the primary coolant on the left and natural convection with air on the right (illustrated in Figure 4.21). The containment air is maintained at a constant

[4]Some sections of the MNR piping are buried or surrounded by concrete structures. These cases were not considered in the thermal model. All the piping sections were considered as surrounded by air.

temperature of 20°C.

The heat transfer coefficient between the piping wall and the containment air is selected as $25 W/Km^2$, as referenced from [17].

Thermal properties assigned to the steel piping structures were extracted from [19] and are summarized in Table 4.10. Figure 4.21 provides a visual representation of the implemented thermal model for assessing heat losses within the piping system.

Stainless Steel (type 304)		
Temperature	Thermal Conductivity [W/(m.K)]	Heat Capacity [J/(kg.K)]
100.0	9.734	1.935E6
1000.0	24.296	4.566E6

Table 4.10: Thermal properties of Stainless Steel (type 304).

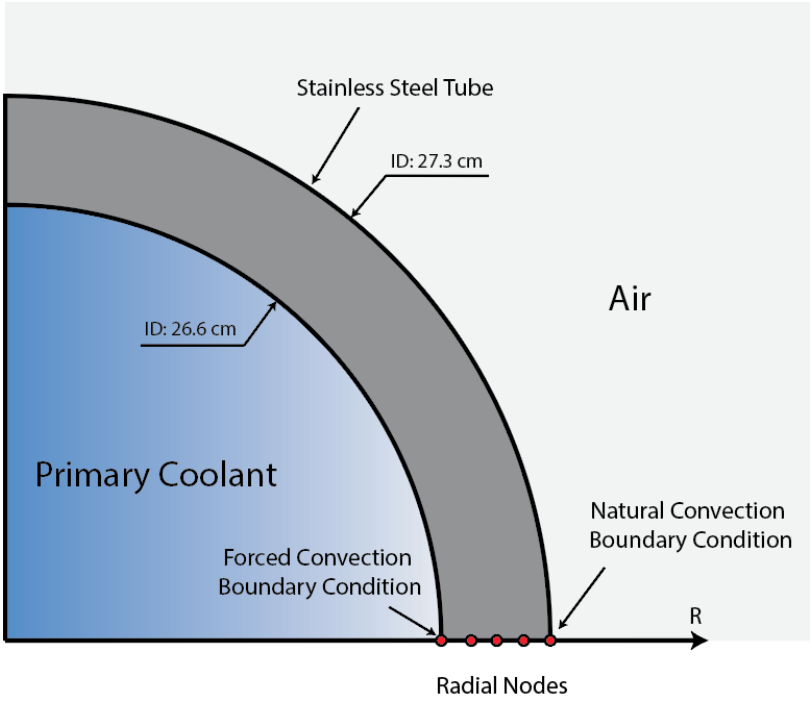

Figure 4.21: Radial thermal model used in the heat structures of the piping.

4.6 Hold-up tank

The Hold-up Tank (HUT) is an open-top U-shaped concrete enclosure with a total capacity of 125,000 liters (equivalent to 33,000 US gallons). Its primary function is to induce a time delay (typically around 10 minutes) in the circulation of primary water coming from the core. This deliberate delay, which actually depends on the flow rate, facilitates the decay of short-lived activity within the water, predominantly from N-16, consequently diminishing radiation fields in both the pump room and on the pool surface. Under standard operational conditions, the tank sustains a water level hovering at approximately 2 meters (or 6.5 feet). Figure 4.22 shows a top view of this component. For modelling purposes, the HUT was partitioned into seven sections, each identified on the drawing by a number enclosed in a circle.

The holdup tank and the pool are strategically positioned at elevations ensuring that, without hydraulic head, their water levels remain consistently about two meters (7-8 feet) above the core. This design ensures operational reliability and safety compliance, even in scenarios where hydraulic head is lacking.

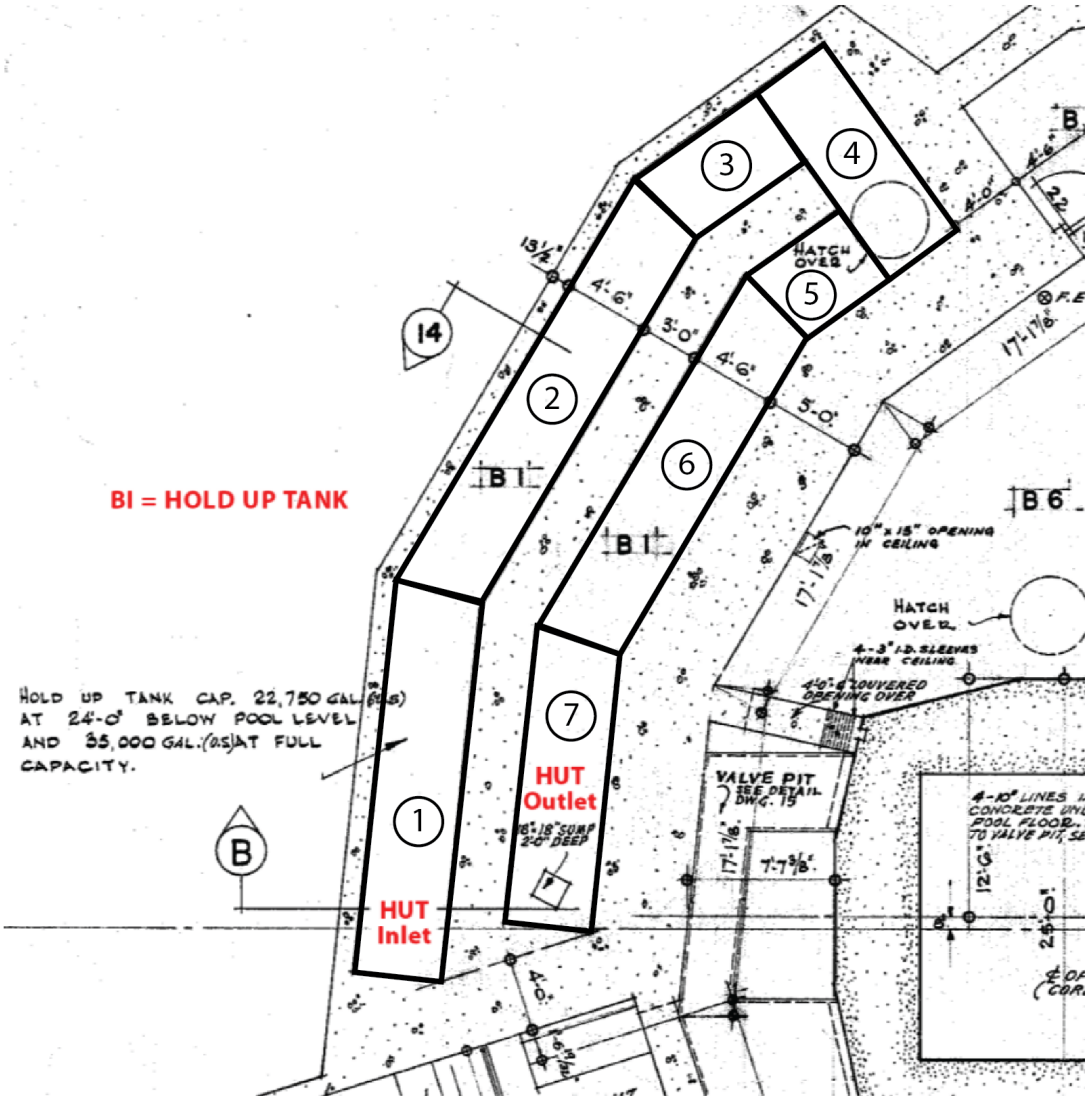

Figure 4.22: Top view of the HUT "U" shaped geometry.

Hydraulic model

The hydraulic model of this component consists of seven vertical pipes: pipes 122, 222, 322, 422, 522, 622, and 722. These pipes are discretized into 10 volumes and they are interconnected laterally with cross-flow junctions (using mtpljun components).

Each pipe corresponds to one of the HUT sections illustrated in Figure 4.22. For example, pipe 122 corresponds to HUT section number 1, pipe 222 corresponds to section number 2, and so forth. The dimensions of the flow area and total volume of each pipe were selected according to the dimensions presented in the drawings.

The total height of all seven pipes is 3 meters. The bottom seven volumes, from the base upwards, are filled with liquid water, reaching a level of 2 meters. The remaining three volume at the top of the pipes contain air, spanning a length of 1 meter. At the top of the first pipe (pipe 122), there is a connection to a time-dependent volume that simulates the air within the containment. This configuration establishes atmospheric pressure at the surface of the HUT water.

Figure 4.23 displays a top and lateral view of the nodalization. The inlet of the HUT is defined at the bottom volume of pipe 122, while the outlet is positioned at the bottom of pipe 722.

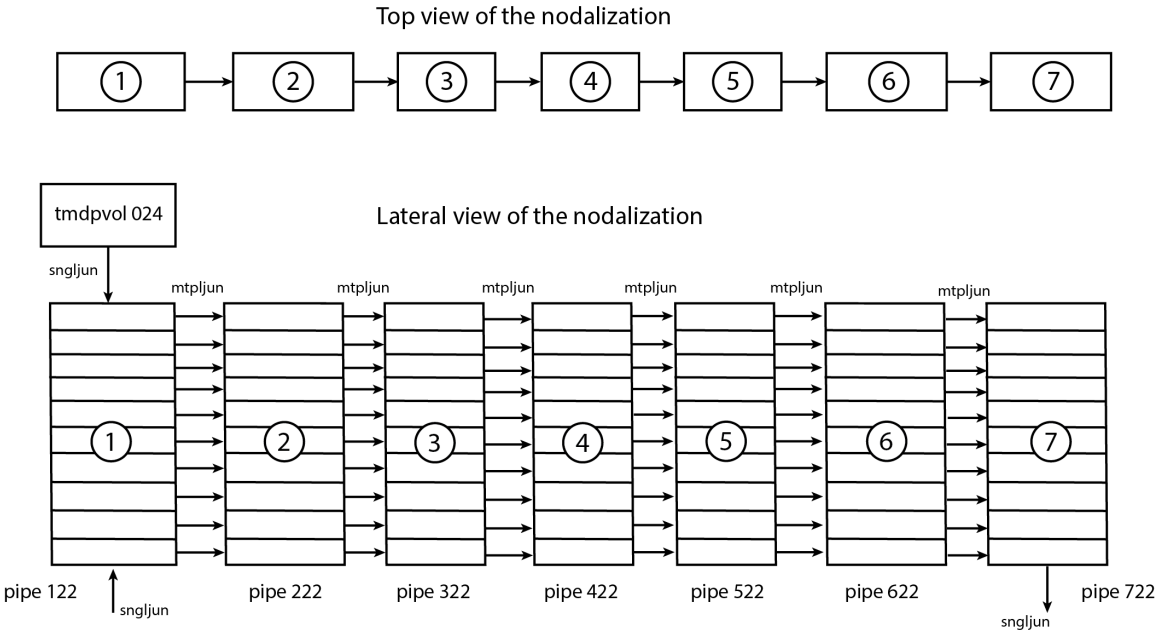

Figure 4.23: Representation of the HUT nodalization.

It's worth mentioning that, akin to the Pool model, the lateral crossflow junctions offer a crude approximation to the lateral flow in the HUT. The RELAP code does not solve the 3D conservation equations and this is a clear limitation of the model. For this reason, this HUT model primarily focuses on simulating the significant thermal inertia provided by the HUT to the primary system, rather than accurately predicting the coolant flow delay. Sensitivity studies were conducted to assess the change in the coolant flow delay as a function of the number of vertical pipes that make up the HUT model. The results of this sensitivity study are presented later in the "Sensitivity Analysis" section of the "Results and Discussion" chapter.

Thermal model

The wall thickness of the hold-up tank is detailed in Figure 4.24. The outer-facing wall has a thickness of 13 1/2 inches (34.3 cm), while the concrete partition dividing the tank into sections measures 3 feet (91.4 cm). On the inner side of the containment, the wall is 5 feet (1.524 m) thick.

The heat structure for the HUT is similar to the one used for the reactor pool. For simplicity, the HUT wall was considered to have a uniform thickness of 1 meter thick concrete slab with 10 equidistant nodes. The boundary condition on the left surface is convection with the primary water, while on the right surface is free convection with containment air at 20°. The graphical representation of this model can be consulted in Figure 4.5.

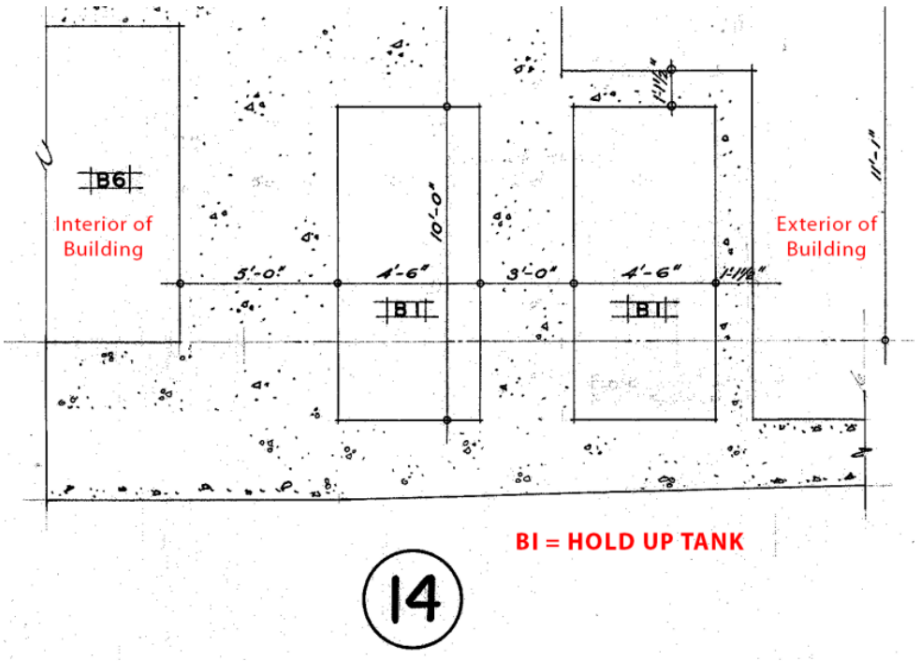

Figure 4.24: Cross section of the HUT showing concrete wall thickness.

4.7 Primary pump

The circulation of primary water is driven by a centrifugal pump, powered by a 550V three-phase, 50 HP electric motor. The pump inlet is connected to the Holdup Tank outlet, drawing water from that system. The water is then pumped through the shell of each heat exchanger before being directed back to the Pool. A check valve installed at the pump outlet ensures that back-flow is effectively prevented, maintaining the intended direction of the water circulation.

The hydrodinamic pump model was created following the technical data consulted in [20]. Table 4.11 shows the main parameters used in the pump input section.

Parameter	**Value**	**Unit**
Flow area	0.0507	m^2
Length	1.521	m
Rated pump velocity	186.9	rad/s
Rated flow	0.1451	m^3/s
Rated head	24.689	m
Rated torque	234.56	$N.m$
Moment of inertia	0.001	$kg.m^2$

Table 4.11: Parameters used for the primary pump model.

4.8 Heat exchanger

The MNR heat exchangers were manufactured by Foster Wheeler Limited of St. Catherines, Ontario. These units consist of two-loop, low-pressure, and low-temperature coolers, arranged in series. Each unit comprises 686 welded 304 stainless steel tubes, each 14 feet long and 18 gauge in thickness. These tubes are mechanically expanded into 1-inch steel tube sheets. The baffles within the heat exchangers are arranged in a staggered and overlapping pattern to optimize thermal efficiency. Primary system water circulates through the shell of the heat exchanger, while secondary water flows through the tube side, facilitating effective heat transfer between the two fluid streams. Design specifications of this integral component are presented in Table 4.12.

The data presented in tables are sourced from the Eddy Current Inspection Report, McMaster Research Reactor Heat Exchangers, dated July 2018.

Design Specifications of the Heat Exchanger (2 identical units in series)	
Heat exchanger type	Water to water, fixed tube sheet type, straight tubes.
Nozzle sizes	10”
Number of Tubes (total, two units)	1372
Tube ID	2.54 cm
Tube Length	4.267 m
Pressure rating of flange	150 psi
Shell side coolant (Primary Loop)	Demineralized water
Shell side nominal flow rate	2200 USGPM
Shell side nominal inlet temperature	115.7°F (46.5°C)
Shell side nominal outlet temperature	100°F (37.8°C)
Shell side maximum pressure drop	10 psi
Shell side design pressure	75 psi
Tube side coolant (Secondary Loop)	Raw water
Tube side nominal flow rate	2300 USGPM
Tube side nominal inlet temperature	87°F (30.5°C)
Tube side nominal outlet temperature	102°F (38.9°C)
Tube side maximum pressure drop	12 psi
Tube side design pressure	75 psi

Table 4.12: Design specifications of the heat exchanger.

Figure 4.25 and Figure 4.26 provide visual representations of the MNR heat exchanger, offering a detailed look at its physical structure. Meanwhile, Figure 4.27 and Figure 4.28 present schematic depictions, showcasing the design layout of the heat exchanger and illustrating the flow paths within both the primary and secondary systems.

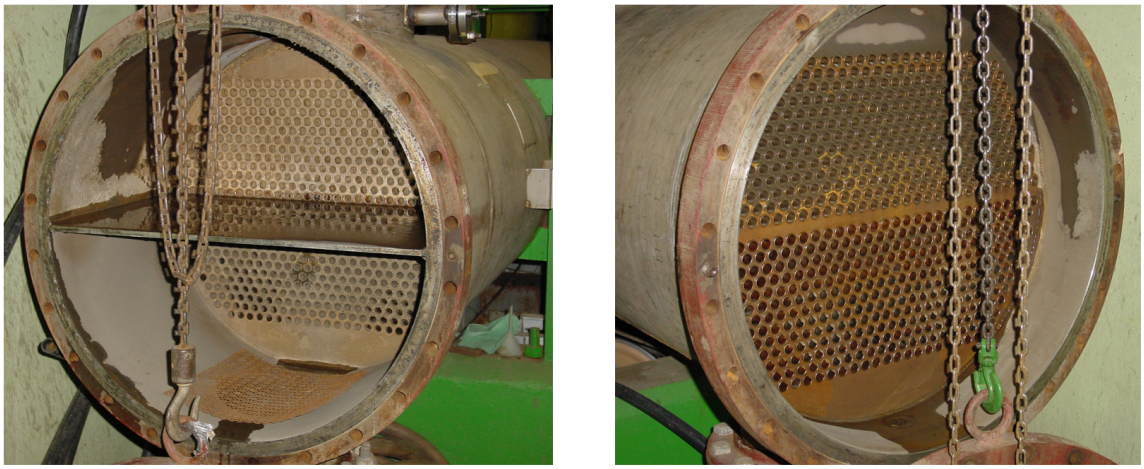

Figure 4.25: Pictures showing the heat exchanger sides.

Figure 4.26: Picture of the two heat exchangers assembled in series.

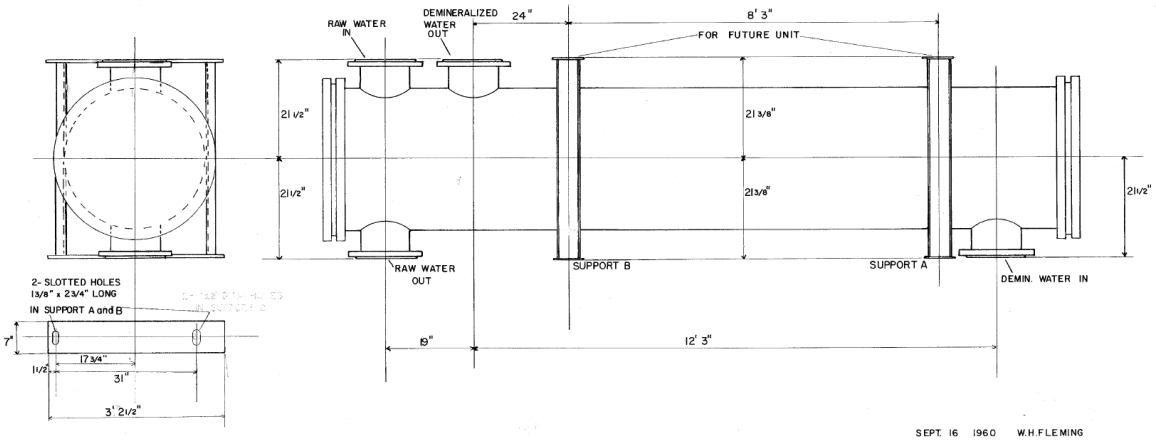

Figure 4.27: Schematic showing the design of the heat exchanger.

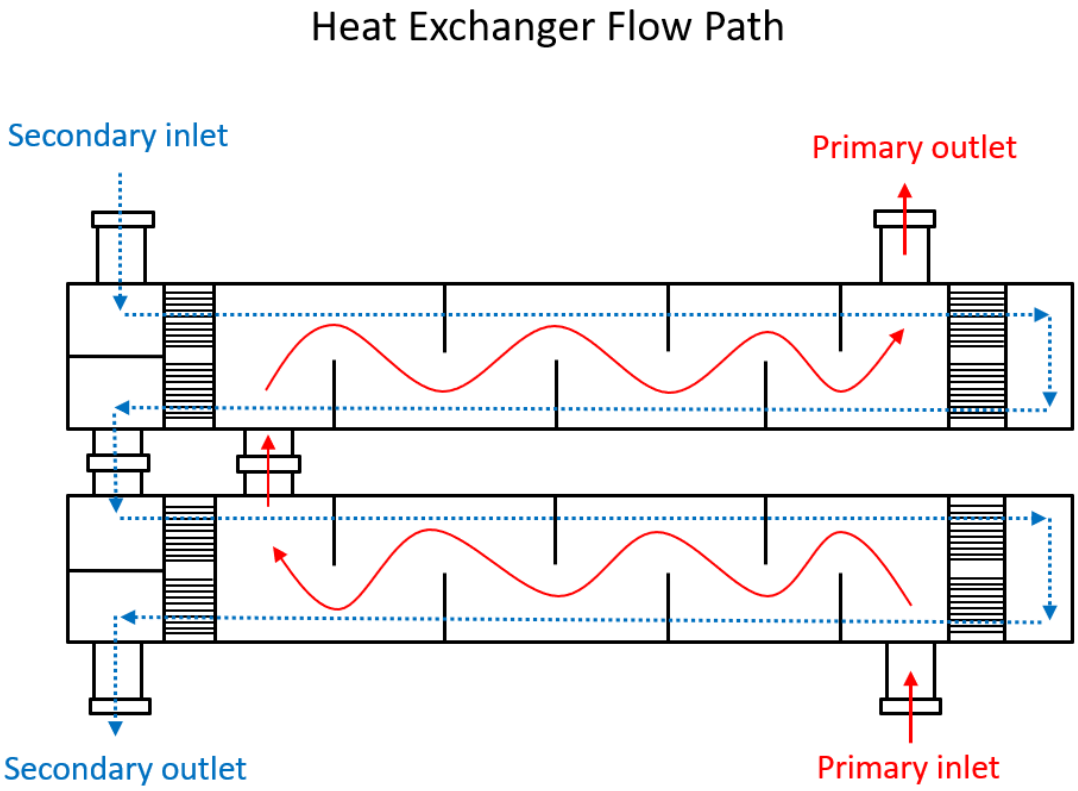

Figure 4.28: Illustration showing the primary and secondary flow paths within the 2 heat exchangers in series.

Hydraulic model

This component is modelled through a network of pipes incorporating associated heat structures as shown in Figure 4.29. In this schematic nodalization, the primary fluid path is delineated by red arrows, while the secondary fluid path is illustrated in blue. The model represents the shell structure within each heat exchanger as a single pipe connected to flanges depicted by single volumes. Each shell pipe transfers heat with two pipes representing the tube side of the heat exchanger. It should be noted that pressure losses stemming from fluid interaction with internal baffles are not accounted for in this model.

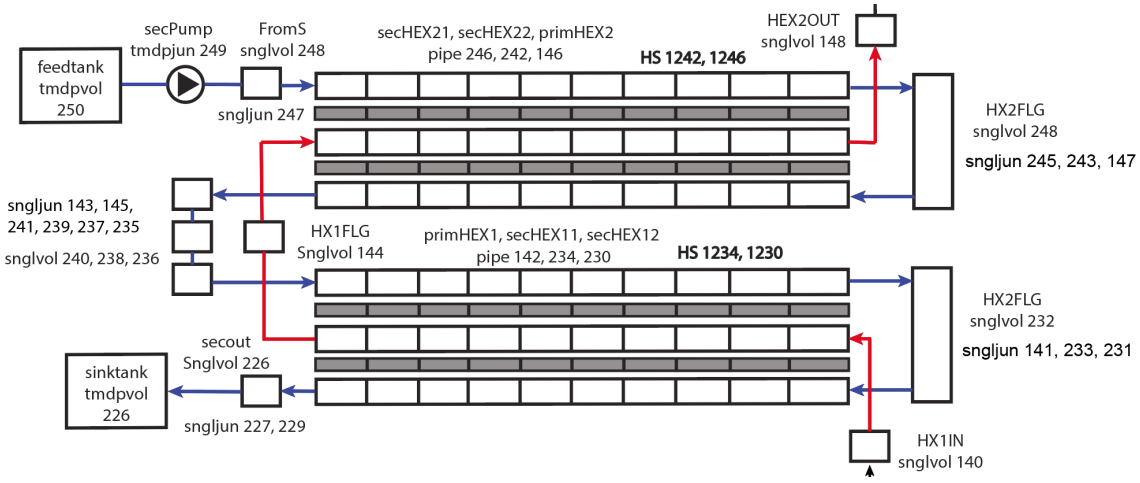

Figure 4.29: Nodalization of the MNR Heat Exchanger.

Thermal model

The thermal model is depicted as a 1D radial system of the heat exchanger tubes. The steel tubes are discretized into 5 radial nodes, wherein a forced convection condition is applied—secondary coolant on the inner side and primary coolant on the outer side. Figure 4.30 illustrates the thermal model used for the Heat Exchanger tubes.

The thermal model contemplate a fouling factor to account for the dirt film that may build up on the heat exchanger tube surfaces[5]. This thermal resistance varies over time and it's significantly reduced every time the heat exchanger tubes are cleaned during maintenance. Since no information about fouling factors or heat exchanger maintenance frequency was found, the fouling factor was chosen as outlined below.

The value of the fouling factor was chosen to align the inlet and outlet temperatures of the heat exchanger and the flow rate on the secondary side with the experimental measurements of these parameters obtained during reactor operation. A different fouling factor value was selected for each of the scenarios chosen in this thesis to validate the RELAP5 model (Secondary loss 2020 and Pool Temperature Experiment 2023). Specifically, for the Secondary Loss Event in 2020, a value of 0.28 was chosen for the inner surface of the tubes[6]. Meanwhile, for the Pool Temperature Experiment, a value of 0.26 was selected for the inner surface of the tubes[7].

[5]In normal heat exchanger operations, surfaces are prone to fouling from fluid impurities, rust formation, or chemical reactions with the wall material. This fouling leads to the accumulation of a film or scale on the surface, substantially increasing heat transfer resistance between the fluids. To account for this effect, thermal models incorporate an additional thermal resistance, known as the fouling factor (Rf). The value of Rf depends on factors such as operating temperature, fluid velocity, and the duration of the heat exchanger service.

[6]The fouling factor was only applied to the interior surface for simplicity, but could also be applied to the exterior surface.

[7]The Pool Temperature Experiment in 2023 yielded a lower fouling value compared to the Secondary Loss event in 2020. This difference can be attributed to the yearly cleaning of the HEX.

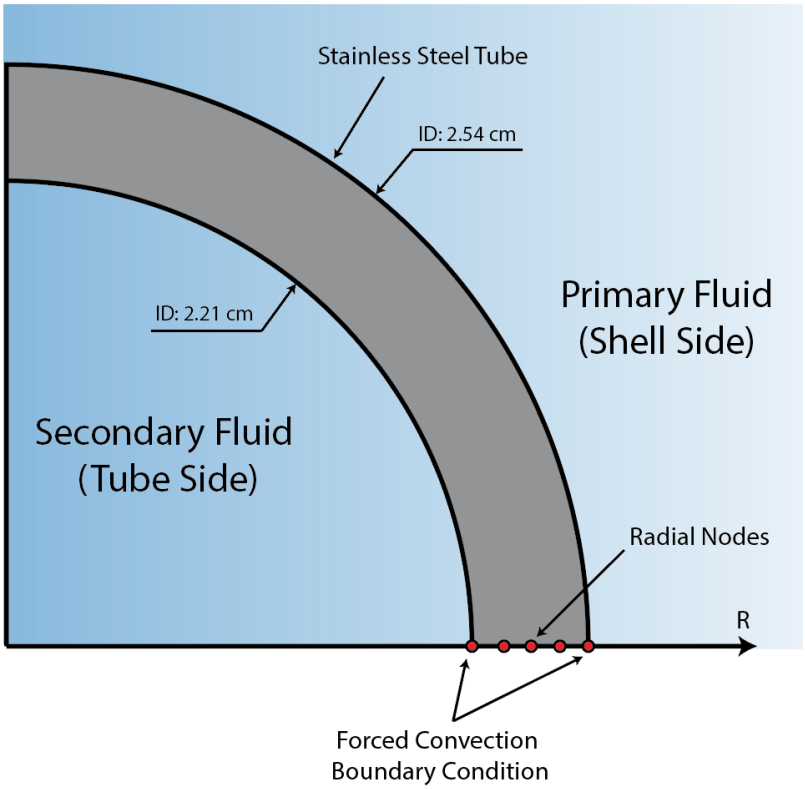

Figure 4.30: Radial thermal model used in the heat structures of the Heat Exchanger tubes.

4.9 Secondary Heat Transport System

The secondary cooling system is responsible for transferring heat from the primary side of the heat exchanger to the atmosphere via the cooling towers. The secondary side of the heat exchanger comprises a bank of tubes within each of the two tanks, utilizing a two-pass system in each tank. In the secondary loop, city water is employed with pH control and algae inhibitors to ensure optimal performance.

To dissipate 3 MW of power from the primary side of the heat exchanger (current reactor power), the required secondary flow is around 138.8 liters per second (2200

USGPM). Typically, the nominal secondary inlet (cold) water temperature varies around 21-30°C, while the oulet temperature can be in the range of 26-35°C.

The cooling towers, located outside the Reactor Building, facilitate the cooling process of secondary water by dissipating heat to the atmosphere. Water is pumped from the hot side of the secondary heat exchanger outlet to the distribution trays at the top of the tower through a closed loop of steel pipe. The heated water then flows by gravity over the PVC fill of each tower into the tower basin. After the cooling process, the secondary water re-enters the heat exchanger inlet through gravity flow.

As mentioned in the "Reactor Nodalization" section, the secondary system is modelled with simplicity, featuring two time-dependent volumes (tmdpvol 250 and 226) regulating temperature and pressure at the inlet and outlet of the heat exchanger. The secondary pump (tmdpjun 249) manages the flow rate of the secondary coolant. This concise description focuses solely on the secondary system role in heat removal from the primary system.

Chapter 5

Results and Discussion

5.1 Simulation of the loss of forced circulation in the secondary side in 2020

The RELAP5 model was employed to simulate the 2020 secondary pump failure event. The analysis on this section will cover both the pre-event steady state and the subsequent transient period.

For this simulation it was assumed that the temperature across the primary system, including the reactor pool and the HUT, was initially uniform. The initial temperature of the primary system was set to 31.0°C.

The initial conditions of the secondary system were set in accordance to reactor measurements. Then the fouling factor of the HEX was iterated until the heat extraction from the secondary system matched the core generation rate. The heat exchanger inlet and outlet temperatures were set to 24.4°C and 29.4°C, while the flow fixed at 135.3 kg/s.

After setting up the secondary system parameters, the simulation was executed, and temperature and flow data for the primary system was recorded.

5.1.1 Steady-State before the pump trip

An initial comparison was conducted between the simulation results and the steady-state measurements gathered from the MNR moments before the secondary pump trip. The RELAP5 simulation was run for 1000 seconds to provide adequate time for the code to stabilize and converge to a steady state.

This validation step serves as a key reference point to evaluate the accuracy and reliability of the RELAP5 simulation in replicating the reactor behavior under steady operating conditions. In the following subsections a short analysis of the various results is presented.

Core temperatures

Simulation results and measurements of core temperatures are shown in Figure 5.1. MNR measurements show that the core inlet temperature hovered around 31.1°C, while the outlet temperature measured 36.8°C, resulting in a core temperature increase of approximately 5.7°C. On the other hand, the simulation exhibited an inlet temperature of 31.0°C and an outlet temperature of 36.9°C, indicating a temperature rise of 5.9°C. The error in the core temperature change is around 3.5%. In general, the results demonstrate good agreement with the measured data.

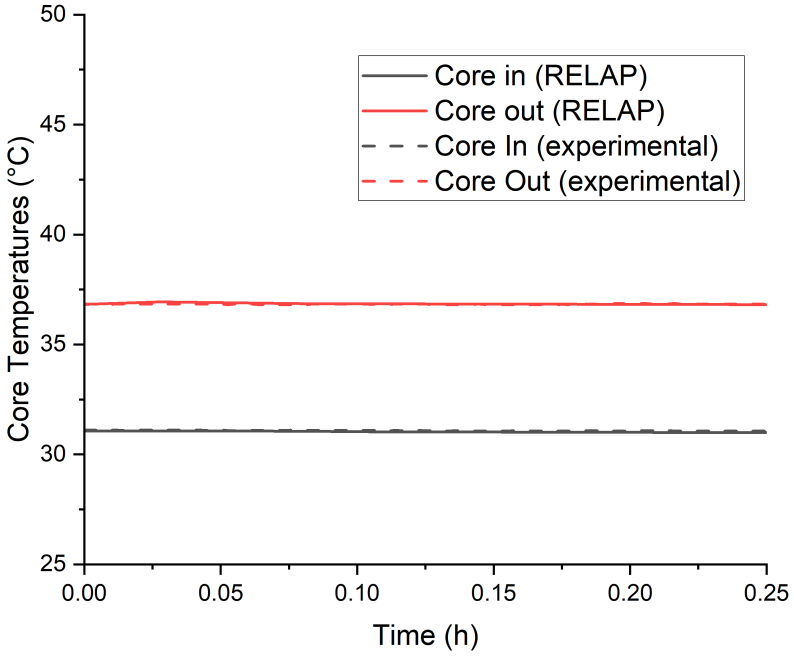

Figure 5.1: Steady State core inlet and outlet temperatures (Loss of secondary, 2020).

Heat exchanger temperatures

According to the plant recorded data, the primary coolant enters the heat exchanger at 36.5°C and exits at 31.1°C. It's noteworthy that the heat exchanger inlet temperature is slightly lower than the core outlet temperature (by approximately 0.3°C). This variation is due to heat losses within the system.

In the RELAP simulation, the calculated temperatures exhibit an inlet temperature of 36.7°C and an outlet temperature of 30.9°C, showing a good agreement with the plant measurements. Results are illustrated in Figure 5.2.

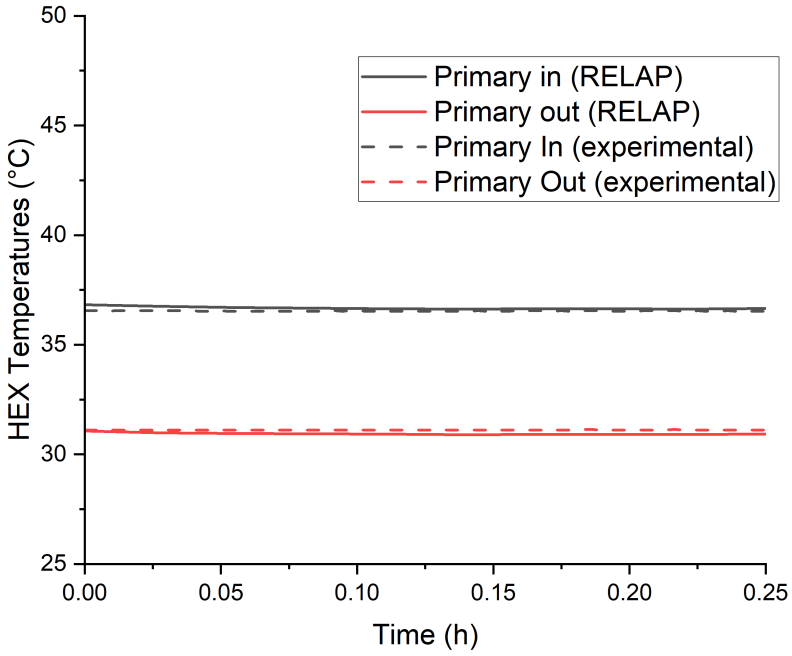

Figure 5.2: Steady State HEX inlet and outlet temperatures (Loss of secondary, 2020).

Primary and secondary coolant flow

The primary flow rate was computed and compared with the recorded values (see Figure 5.3). The average value of the measured primary flow is 123.5 kg/s, while the simulation yields 123.0 kg/s. This translates into a deviation of 0.4%. The flow rate for the secondary was set at 135.0 kg/s as a boundary condition. This value was taken as the average of the experimental data during the steady state operation.

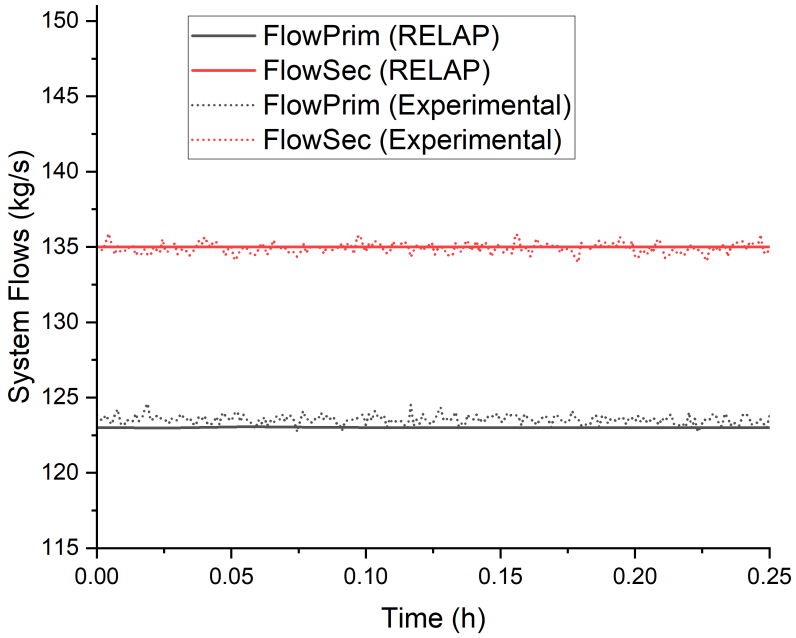

Figure 5.3: Steady State primary and secondary flow (Loss of secondary, 2020).

Below is a summary table comparing the RELAP5 results with the reactor measurements obtained during the steady-state operation preceding the secondary pump failure (Table 5.1).

Steady state operation previous the secondary pump failure			
Parameter	**MNR**	**RELAP5**	**|Error|**
Temperature at core inlet (°C)	31.1 ± 0.1	31.0	0.3%
Temperature at core outlet (°C)	36.8 ± 0.1	36.9	0.3%
Temperature at HEX inlet (primary side) (°C)	36.5 ± 0.1	36.7	0.5%
Temperature at HEX outlet (primary side) (°C)	31.1 ± 0.1	30.9	0.6%
Primary Flow (kg/s)	123.5 ± 0.8*	123.0	0.4%
Secondary Flow (kg/s)	135.0 ± 0.8*	135.0	BC

Table 5.1: Steady-State results and comparison with experimental measurements in the secondary loss simulation. *Note: the window of uncertainty in the orifice flowmeter measurements represents the standard deviation of the data recorded during the steady state period under consideration. The random uncertainty associated with the instrument was not accounted for.

5.1.2 Transient after the secondary pump trip

System Flows

The transient phase of the event is now presented. Figure 5.4 illustrates the comparison between the simulation results and the experimental measurements of the primary and secondary flow rates. The flow in the primary system remains constant and stable, maintaining the same value as in the steady state (123.5 kg/s from the measurements and 123.0 kg/s from the simulations). On the other hand, the flow rate in the secondary system abruptly drops to zero when the pump fails, indicating the onset of the event.

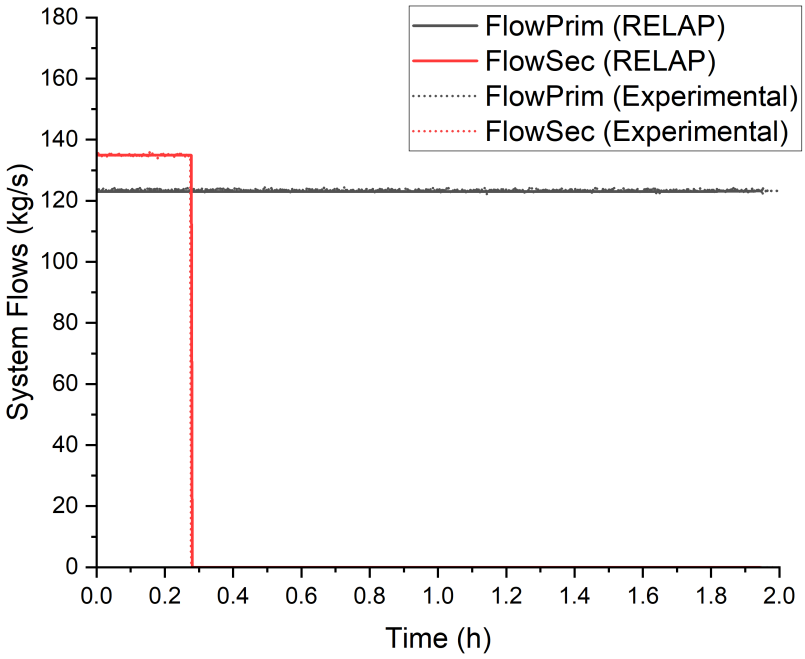

Figure 5.4: Primary and secondary flow over time (Loss of secondary, 2020).

Core temperatures

Figure 5.5 depicts the core inlet and outlet temperature evolution. Right after the secondary pump trip, the core temperatures started to rise. This increase is fairly linear from beginning to end. The heating ramp stops abruptly once the operators shut down the reactor core by inserting the control rods. This shutdown process was simulated by decreasing the core power accordingly. Throughout the event progression, a consistently stable error on the temperature of less than 1% was observed. Both inlet and outlet temperatures match closely with the experimental data.

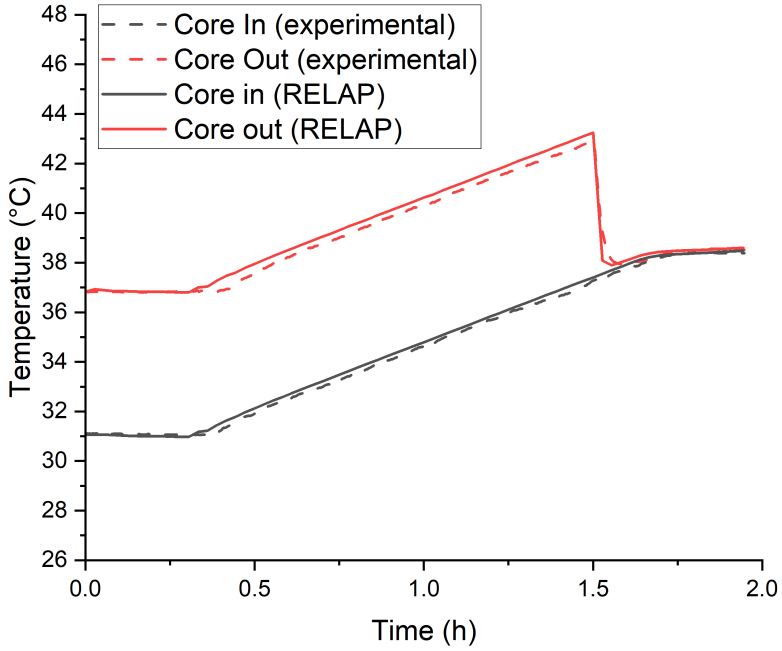

Figure 5.5: Transient core inlet and outlet temperatures (Loss of secondary, 2020).

To analyze in more detail the heating ramp produced by the secondary pump failure, the derivative of the core inlet temperature is calculated and plotted over time. Figure 5.6 illustrates the results of this calculation for the measured data in the reactor and also the simulation results.

It can be seen that the shape of the simulated derivative matches well with the one obtained with the measured values. Even though the derivative of the experimental data does not exhibit a strictly constant behavior over time, it can be assumed to oscillate slightly around a stable value. The RELAP results for this magnitude show a more ideal behavior; the derivative stabilizes quickly and continues to follow an approximately constant value during the heating phase.

The average heating rate from the experimental data is 5.26°C/h, calculated as the average of the derivative in the stable zone (between $t = 0.5h$ and $t = 1.5h$

approximately). RELAP5 predicts a heating rate of 5.25°C/h, just a 0.19% below the experimental value. This result is promising and demonstrates the capability of the RELAP5 model to predict accurately the heating rate during the LOHS event.

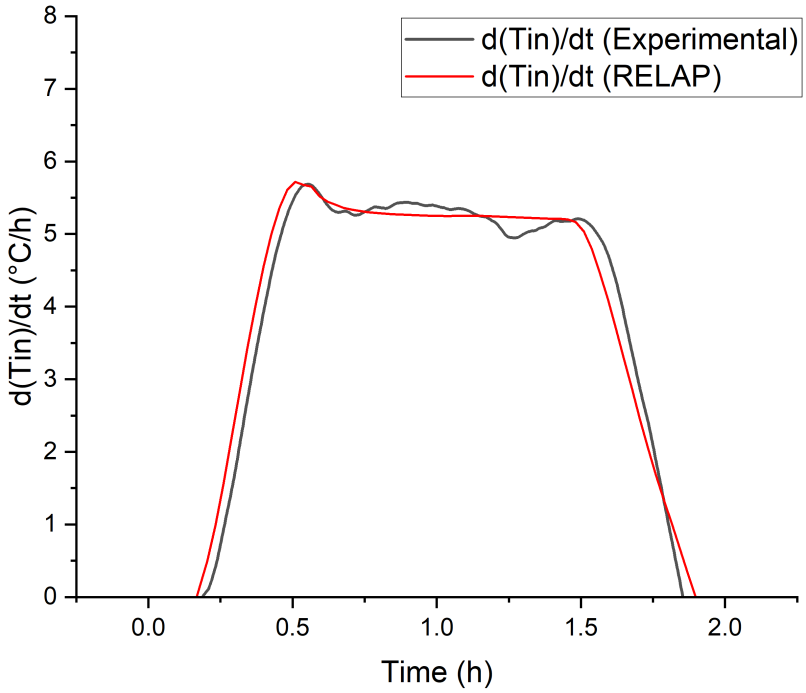

Figure 5.6: Core inlet temperature derivative over time (Loss of secondary, 2020).

HEX temperatures

The results obtained from the HEX exhibit relatively good agreement with the experimental measurements (see Figure 5.7). Upon the secondary pump trip, the temperatures at the inlet and outlet of the HEX converge approximately into the same value since there is no more heat transfer to the secondary system. This event is temporally synchronized in both the simulation and the experimental data. The maximum temperature predicted by RELAP is 42.3°C, while in the actual system, the maximum temperature was 42.4°C at the inlet and 42.5°C at the outlet. This represents

a difference between 0.2% and 0.5%, which is considered a very good estimation.

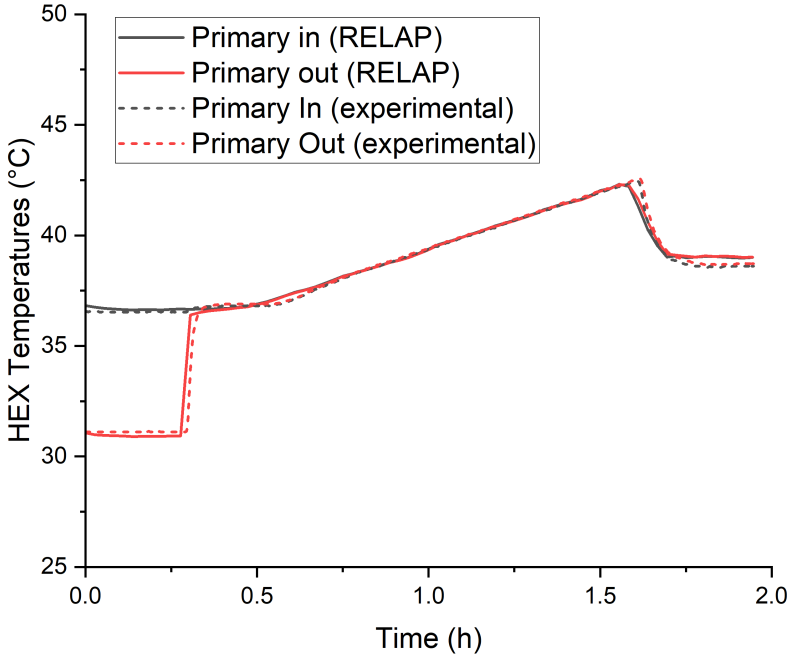

Figure 5.7: Transient HEX inlet and outlet temperatures (Loss of secondary, 2020).

Table 5.2 summarizes some of the results obtained for the transient simulation. This table includes the maximum core temperatures recorded at the culmination of the event (prior to the reactor core shutdown), average heating rate and maximum heat exchanger temperatures.

Transient during the secondary pump trip			
Parameter	**MNR**	**RELAP5**	**|Error|**
Core inlet temperature at SCRAM (°C)	38.4 ± 0.1	38.5	0.3%
Core outlet temperature at SCRAM (°C)	42.9 ± 0.1	43.2	0.7%
Heating rate (°C/h)	5.26 ± 0.14*	5.25	0.19%
Max temp at HEX inlet (primary side) (°C)	42.4 ± 0.1	42.3	0.2%
Max temp at HEX outlet (primary side) (°C)	42.5 ± 0.1	42.3	0.5%

Table 5.2: Transient results and comparison with experimental measurements in the secondary loss simulation. *Note: the window of uncertainty in the heating rate denotes the standard deviation of the temperature derivative during the stable period (from $t = 0.5h$ to $t = 1.5h$).

5.2 Simulation of the Pool Temperature Experiment in 2023

This section presents the results derived from the simulation of the MNR Pool Temperature Experiment which was conducted in March 2023. As mentioned in section 5.2, before initiating the experiment, the primary system underwent a cooling process that led to the thermal stratification of the reactor pool. Unfortunately, temperature measurements at different elevations in the pool were not taken. Consequently, estimating the pool temperature profile before running RELAP simulations becomes imperative. To achieve this, a Computational Fluid Dynamics (CFD) model of the MNR pool was developed and used for simulating the cooling transient. The development of this CFD model was conducted by Dr. Kaltrina Shehu from the Technical University of Munich as part of a research collaboration with McMaster University.

Information regarding the development and testing of the CFD model of the pool is presented in the Appendix A.

The methodology employed for simulating the Pool Temperature Experiment unfolded in two key stages: firstly, the CFD model of the MNR pool was employed to simulate the pool thermal stratification before the start of the experiment. Subsequently, the axial temperature profile of the pool at the end of the cooling stage derived from the CFD simulation was extracted and employed as the initial temperature condition in the RELAP model. This laid the foundation for conducting the RELAP5 simulation of the secondary system loss event.

5.2.1 CFD simulation of the cooling transient before the pool temperature experiment

Boundary conditions for the CFD model were set using temperature measurements at the heat exchanger outlet (primary side) and primary flow measurements. By modeling the inflow of cold water from the pool bottom and outflow from the reactor core, the stratification was simulated. Figure 5.8 illustrates the evolution of the pool inlet temperature over time, extracted from the measurements of the temperature at the outlet of the heat exchanger. It is assumed that there are no heat losses in the piping connecting the outlet of the heat exchanger and the inlet of the pool.

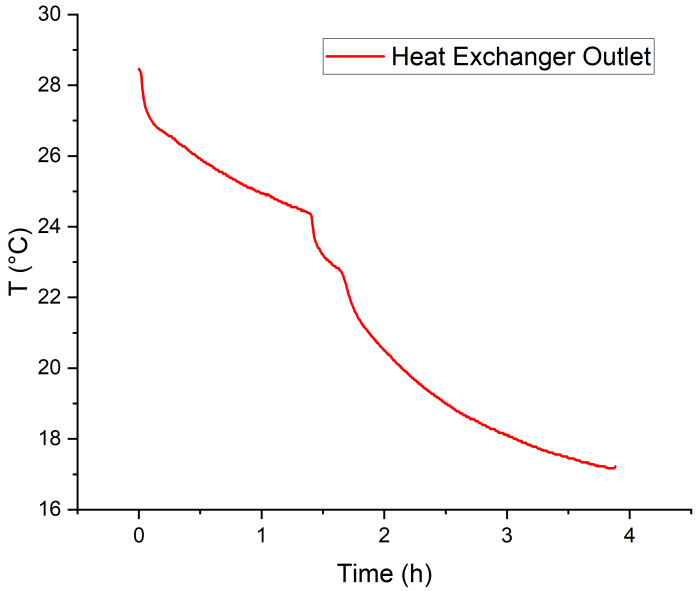

Figure 5.8: Evolution of the outlet Heat Exchanger temperature used as inlet condition for the pool cooling simulation.

Figure 5.9 shows a schematic of the CAD model used to build the pool mesh, and it also includes references to the boundary conditions used in the model. The flow at the inlet of the pool (located at bottom of Pool 2) is exactly the same as the flow at the outlet of the pool (located at core position in Pool 1). The value of said flow is 125.5 l/s based on measurements from the day of the experiment.

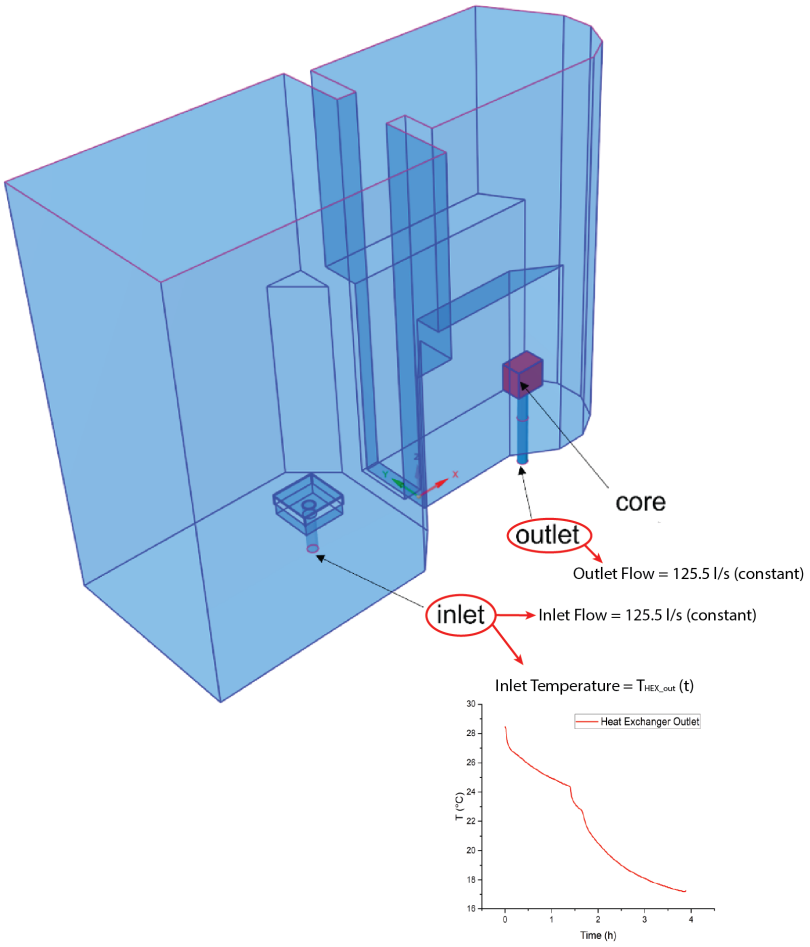

Figure 5.9: CAD model pool used for the CFD simulation. Indications denote the boundary conditions for the model.

The CFD simulation indicates that the introduction of relatively cold water from the heat exchanger triggers a thermal stratification process. As the denser cold water enters from the bottom of the pool, natural circulation isn't initiated due to its higher density compared to the hotter pool water. Consequently, thermal mixing is limited, leading the cold water to settle at the pool bottom and gradually diffuse towards the reactor core, while the surface water remains warm.

Figure 5.10 showcases four snapshots extracted from the CFD simulation, depicting the longitudinal cross-section pool temperature along the core central axis at various time intervals. As the transient unfolds, a stratification layer emerges and ascends within the pool, generating a notable lateral temperature gradient. At the conclusion of the cooling phase, a temperature difference of 7.7°C is observed between the pool bottom and surface. The stratification layer forms at a height around 4.5 and 5.5 meters from the pool bottom.

In Figure 5.11, the temperature profile of the pool is illustrated at the conclusion of the cooling process. This temperature is calculated by averaging the pool temperature across multiple transversal cross-sections at different heights, aligning with the RELAP5 nodalization of the pool (which was shown in Figure 4.3). The axial position of each averaged cross section follows the coordinates presented in Table 4.2. The resulting temperature profile is subsequently exported to the RELAP5 input file, representing the initial temperature condition of the pool before the start of the Pool Temperature Experiment.

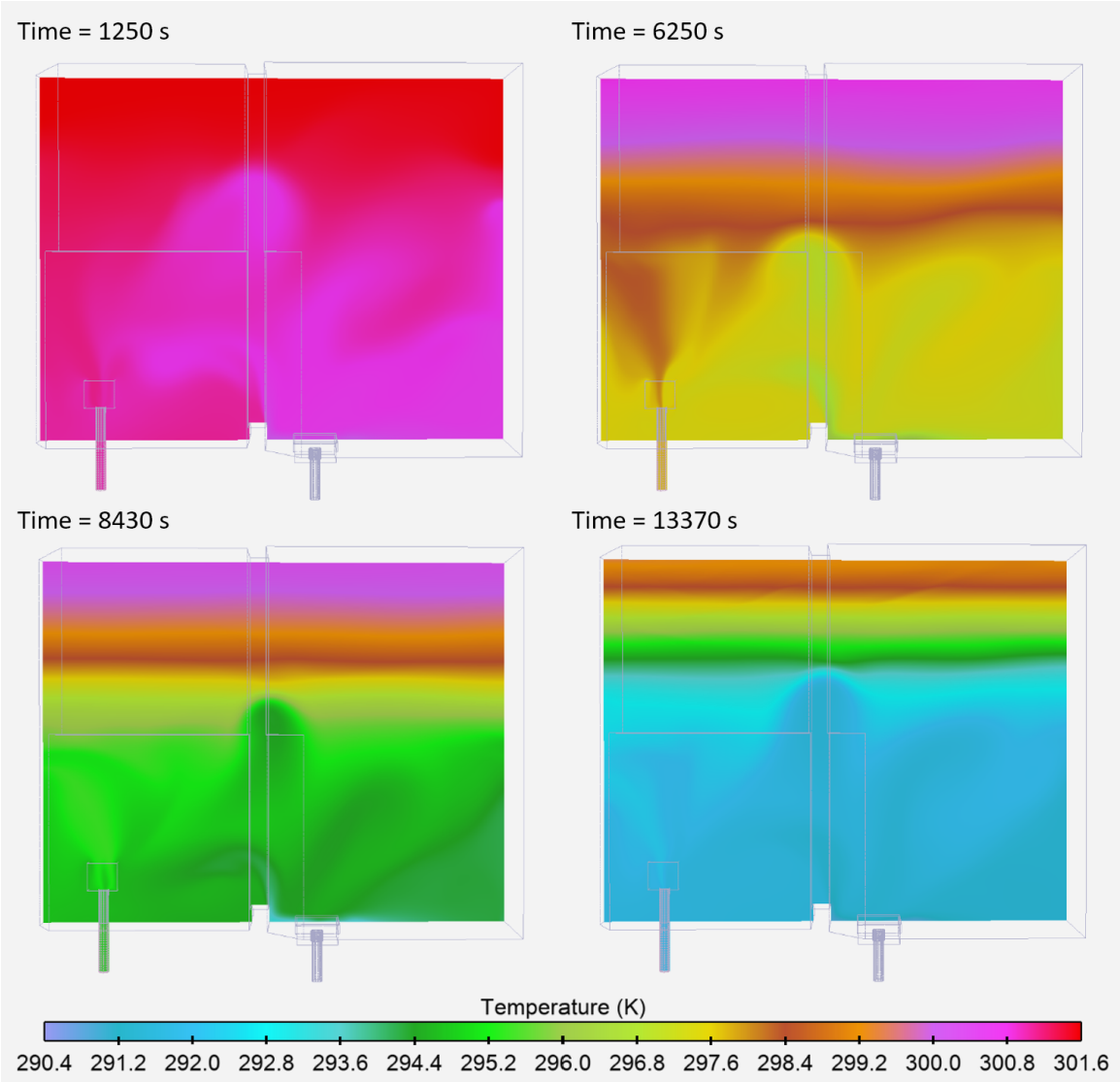

Figure 5.10: Pool temperature results from CFD simulations.

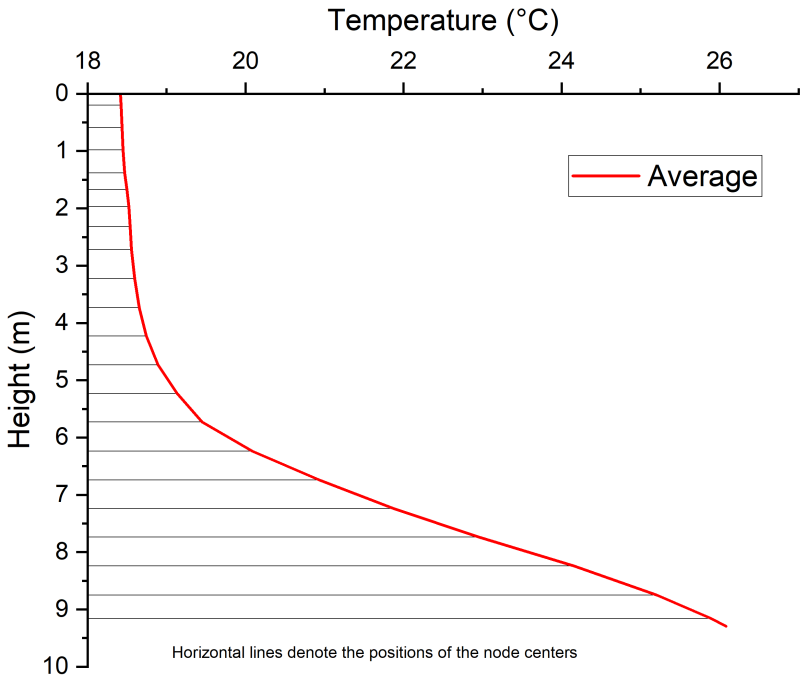

Figure 5.11: Average pool temperature axial profile at the end of the cooling process.

5.2.2 RELAP5 simulation of the pool temperature experiment

Once the CFD-derived pool temperature profile was integrated into the RELAP model as the initial condition, the Pool Temperature Experiment was simulated, with a primary focus on the initial heating phase as both cycles performed in the experiment exhibited similar behavior.

Initially, the system underwent a 1000-second simulation in a steady state to ensure numerical stability before the secondary pump shutdown. This time period was short enough to keep the stratified temperature profile of the pool fairly constant, as illustrated in Figure 5.12. This figure illustrates the temperature profile during

the initial 1000 seconds (approximately 0.27 hours) of simulation.

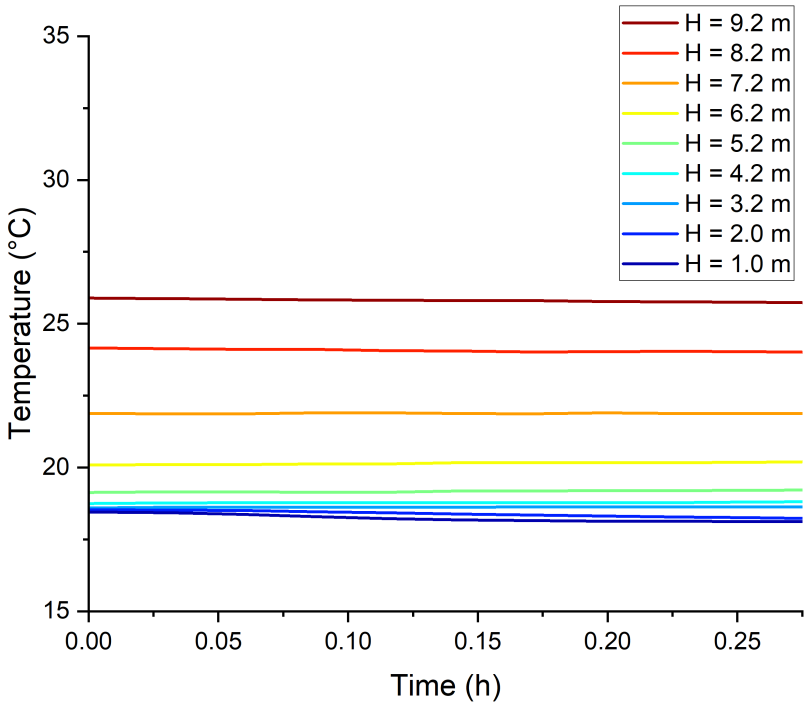

Figure 5.12: Pool temperature profile over the first 1000 seconds (∼0.27 hours) of simulation.

Figure 5.13 displays the evolution of core inlet and outlet temperatures compared to experimental measurements. During the initial steady state conditions, before the experiment, there is a strong agreement between the simulations and the measurements. Maximum error in this stage is around 1%. As the heating phase commenced due to the shutdown of the secondary pump, the primary temperatures began to increase. The first part of the transient (until t=0.75h) the predictions match relatively closely the experimental data. However, after the first hour of the experiment a higher discrepancy was found. This is due to the pool initial stratified temperature which produces a significant effect on the early stages of the heating ramp. Notably, the heating rate during the warming stage, observed after the first hour from the start

of the transient, demonstrates a notable similarity in both cases.

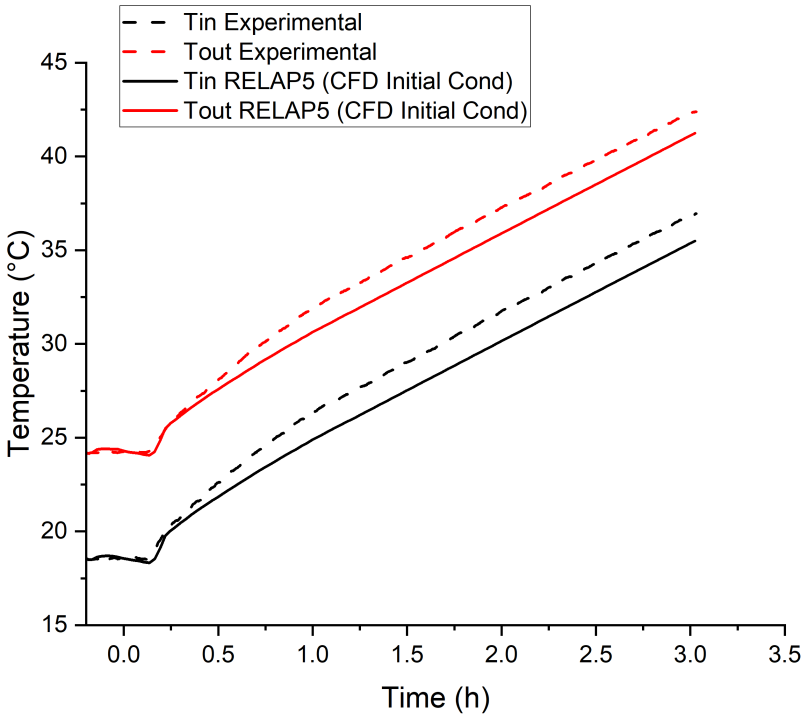

Figure 5.13: Core inlet and outlet temperature over time.

Figure 5.14 illustrates the derivative of the core inlet temperature over time, revealing the non-linear behavior at the experiment onset due to the pool thermal stratification. The derivative initially exhibits a sharp ascent, later transitioning to a stable value where temperature escalation becomes linear. The derivative obtained with RELAP and with the measured data stabilize to a constant value approximately at the same time that is 1.25 hours post-pump failure. However, the heating rate obtained with the reactor measurements exhibit higer values during the stabilization stage, translating into higher temperatures in the pool. This variance might stem from the prediction of the pool stratified temperature profile by the CFD model and the thermal mixing during the heating phase by RELAP5. Firstly, the CFD results

are just an approximation to the real scenario in the reactor. The CFD model was not validated against experimental data, and therefore there is still an unknown uncertainty on the stratified temperature profile of the pool. Secondly, given that pool mixing is inherently three-dimensional, predictions made with a one-dimensional code such as RELAP5 during the heating stage may entail a notable source of error. Furthermore, accurately calculating thermal mixing relies heavily on the nodalization of the pool, accounting for the formation of natural circulation loops.

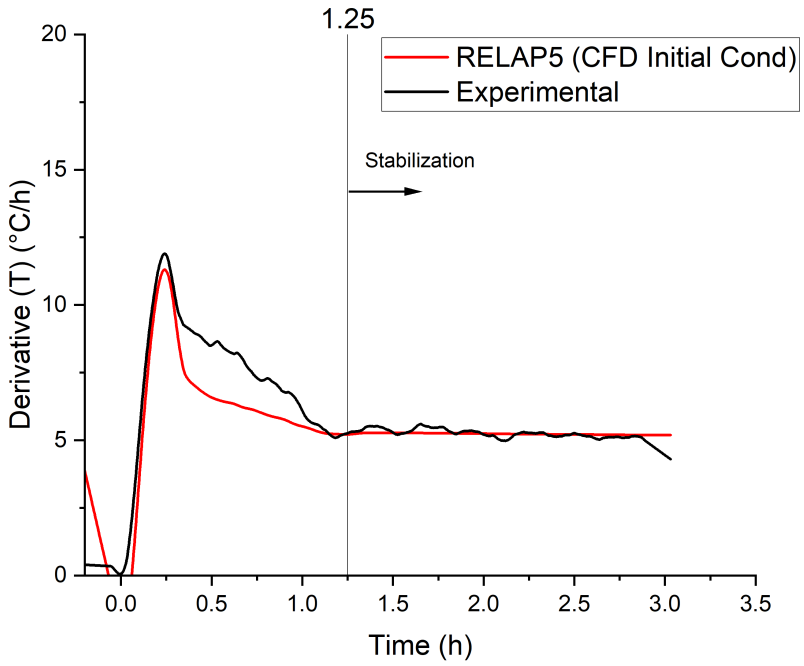

Figure 5.14: Core inlet temperature derivative over time.

Figure 5.15 depicts the temporal evolution of the pool temperature across various height levels, spanning from the bottom to the surface as predicted by CFD. Each line in the graph signifies the average temperature within a specific plane at a certain distance from the bottom. The findings reveal a distinctive non-linear temperature

variation attributed to the stratification present within the pool. Notably, this behavior ceases upon achieving equilibrium. Upon uniformity of the entire pool, the heating rate becomes constant. Consequently, the pool temperature exhibits a linear increase, with the same slope across all heights within the pool.

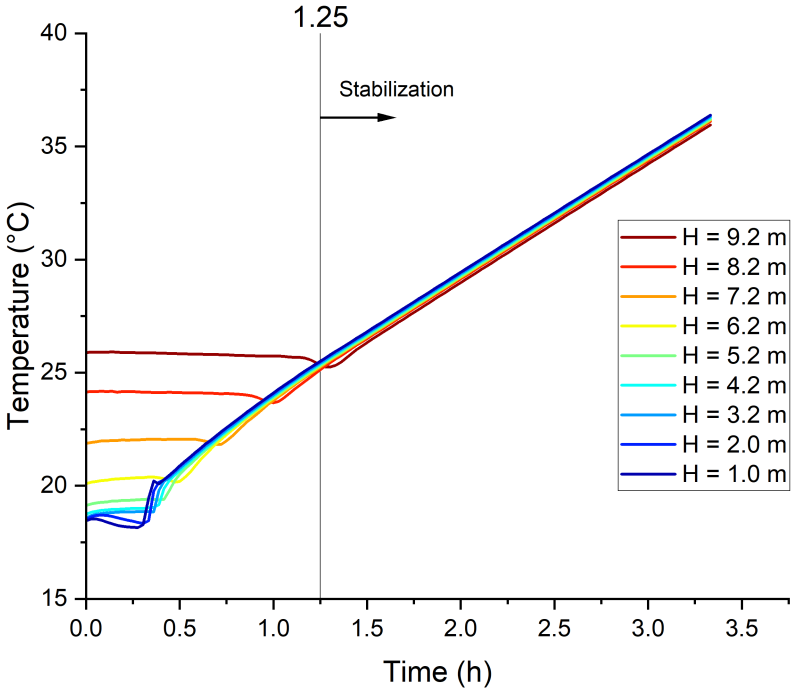

Figure 5.15: Pool temperature across multiple heights from RELAP.

Table 5.3 provides an overview of the maximum temperature values achieved during the heating cycle, the heating slope within the linear phase and the system average flows. RELAP calculated the maximum temperatures at the core inlet and outlet as 35.5°C and 41.2°C, respectively, while experimental measurements reported values of 36.9°C and 42.4°C. This indicates differences of 3.8% and 2.8% respectively. The primary mass flow estimated by RELAP is 125.3 kg/s, compared to 124.8 kg/s obtained with the orifice flowmeter and 130.3 kg/s with the ultrasonic flowmeter. Moreover, RELAP estimation of the temperature derivative within the linear region is 5.24°C/h,

while experimental readings indicate a value of 5.25°C/h. This slight difference of only 0.19% suggests a high level of accuracy in predicting the heating rate.

Pool Temperature Experiment (RELAP with CFD)			
Parameter	**MNR**	**RELAP5**	**|Error|**
Maximum temperature at core inlet (°C)	36.9 ± 0.1	35.5	3.8%
Maximum temperature at core outlet (°C)	42.4 ± 0.1	41.2	2.8%
Heating rate (in linear region) (°C)	5.25 ± 0.14	5.24	0.19%
Primary Flow - orifice flowmeter (kg/s)	124.8 ± 0.8*	125.3	0.4%
Primary Flow - ultrasonic flowmeter (kg/s)	130.3 ± 5.1	125.3	3.8%
Secondary Flow (kg/s)	133.4 ± 0.8*	133.4	BC

Table 5.3: RELAP results and comparison with experimental measurements in the Pool Temperature Experiment simulation. *Note: the window of uncertainty in the orifice flowmeter measurements represents the standard deviation of the data recorded during the first heating cycle of the experiment. The random uncertainty associated with the instrument was not accounted for.

5.3 Sensitivity analysis

Sensitivity analyses were conducted to assess the impact of the pool temperature profile on simulation outcomes. Two scenarios were evaluated: a simulation with a uniform initial pool temperature and another replicating the pool cooling transient simulated by RELAP. Furthermore, a sensitivity analysis investigated the impact of the pool nodalization on simulation results, exploring the feasibility of employing 1, 2, or 4 vertical pipes to represent the reactor pool. Additionally, two more sensitivity analyses were performed: one to assess the effect of the HUT nodalization on coolant delay time and another to evaluate the impact of heat losses in the Pool Temperature

Experiment simulation.

5.3.1 Simulation of the Pool Temperature Experiment with Uniform Initial Pool Temperature

To examine the effect of pool stratification on the experiment initial heating rate, a simulation assuming a homogeneously distributed initial pool temperature was conducted. This means that the thermal stratification effects were neglected. This approach aligns with typical safety analyses assumptions, which rely on perfect pool mixing. The initial uniform temperature of the pool was assumed to be 18.5 °C in accordance with the outlet heat exchanger temperature measurements at the beginning of the experiment.

Figures 5.16 and 5.17 display the core temperature evolution and its time derivative. In this scenario, the nonlinear temperature behavior observed in the experimental data was not replicated in the simulation (i.e RELAP prediction was entirely linear). RELAP temperature results significantly underestimated the experimental measurements, indicating an underestimation of coolant temperatures in the core. However, the temperature derivative exhibited a consistent constant value throughout the simulation, closely aligning with experimental measurements within the linear zone (with a mere 0.19% difference). The transition period of 1.25 hours from the nonlinear to linear zone denotes the time required for the pool to achieve an equilibrium uniform temperature due to thermal mixing facilitated by natural circulation during heating.

Table 5.4 summarizes RELAP maximum core inlet and outlet temperatures, alongside the linear heating rate. Notably, RELAP core temperatures are 8.7% (inlet) and

6.8% (outlet) lower than experimental values. This discrepancy holds significance from a safety perspective, signifying an underestimation of core temperatures when assuming a homogeneous pool temperature profile. Consequently, the assumption of homogeneity resulted in a poorer agreement with the measurements.

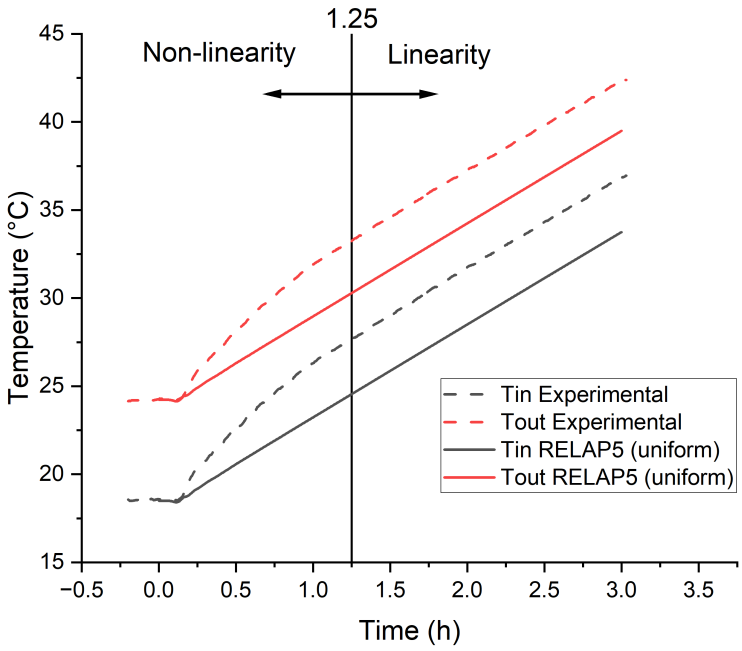

Figure 5.16: Core inlet and outlet temperature over time, with uniform pool temperature as initial condition.

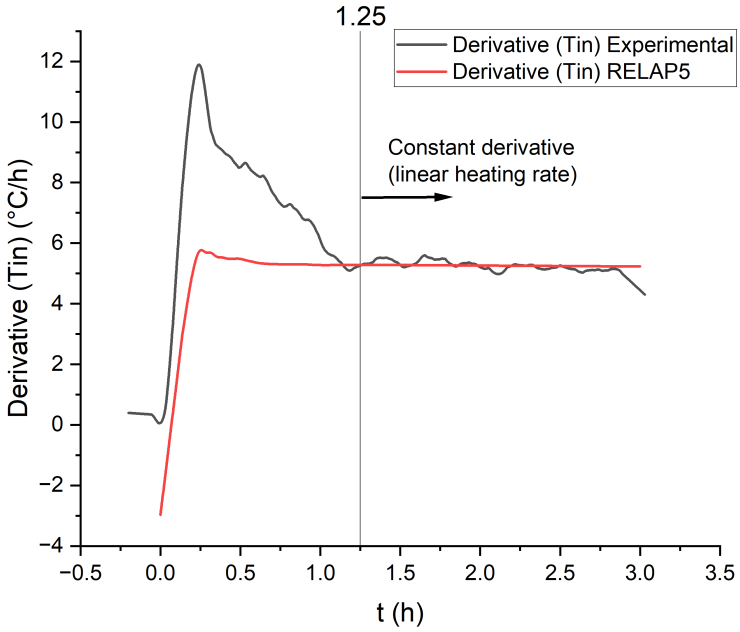

Figure 5.17: Derivative of the core inlet temperature over time, with uniform pool temperature as initial condition.

Pool Temperature Experiment (uniform temperature)			
Parameter	**MNR**	**RELAP5**	**|Error|**
Maximum temperature at core inlet (°C)	36.9 ± 0.1	33.7	8.7%
Maximum temperature at core outlet (°C)	42.4 ± 0.1	39.5	6.8%
Heating rate (in linear region) (°C)	5.25 ± 0.14	5.26	0.19%

Table 5.4: RELAP results and comparison with experimental measurements in the Pool Temperature Experiment simulation assuming initial uniform pool temperature.

5.3.2 The RELAP5 simulation of the Pool Temperature Experiment including the prior transient of pool cooling

It was decided to simulate the pre-experiment cooling using the RELAP code to determine the pool temperature profile at the shutdown of the secondary pump. For this purpose, the primary system initial temperature was set to the relatively hot state before the cooling process began. The pool temperature was set to 28.5°C and it was considered uniform. The secondary system was configured based on reactor measurements on secondary flow and inlet/oulet heat exchanger temperature. This allowed for cooling the primary system in a manner similar to how it was conducted in the reactor prior to the execution of the experiment. It is essential to highlight that the intention is not to validate this cooling period but rather to assess its impact during the subsequent heating ramp.

Figures 5.18 and 5.19 illustrate the core temperature evolution and its derivative. Notably, RELAP temperatures in this scenario are notably higher than the experimental values, indicating an overestimation by RELAP. This discrepancy stems from an inadequate representation of the pool stratified profile at the experiment initiation. Although the heating slope in the linear region aligns closely with experimental values, the non-linear zone exhibits an abrupt temperature rise, leading to significant disparities between predicted and measured temperatures.

Table 5.5 presents RELAP maximum core outlet and inlet temperatures, alongside the derivative of the inlet temperature during the stable period (linear temperature increase). Here, RELAP core temperatures show a difference of 9.2% (inlet) and 8.5% (outlet) from the MNR measurements, while the heating slope in the linear region displays an error of 0.76%.

These observations underscore the limitations of RELAP in accurately predicting the reactor pool stratification, directly impacting the primary system heating rate at the onset of the Pool Temperature Experiment. These findings emphasize the necessity of incorporating CFD to model three-dimensional thermohydraulic phenomena within the pool.

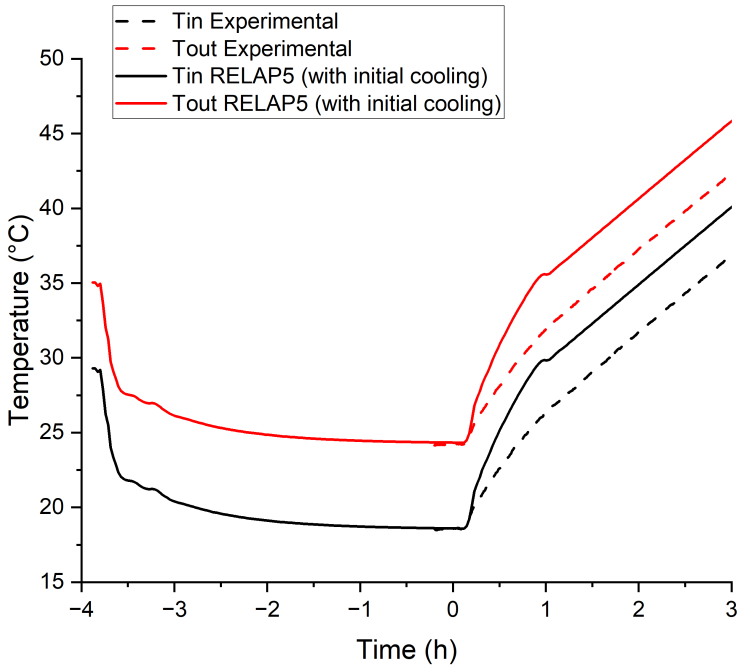

Figure 5.18: Core inlet and outlet temperature over time, considering the pool cooling process.

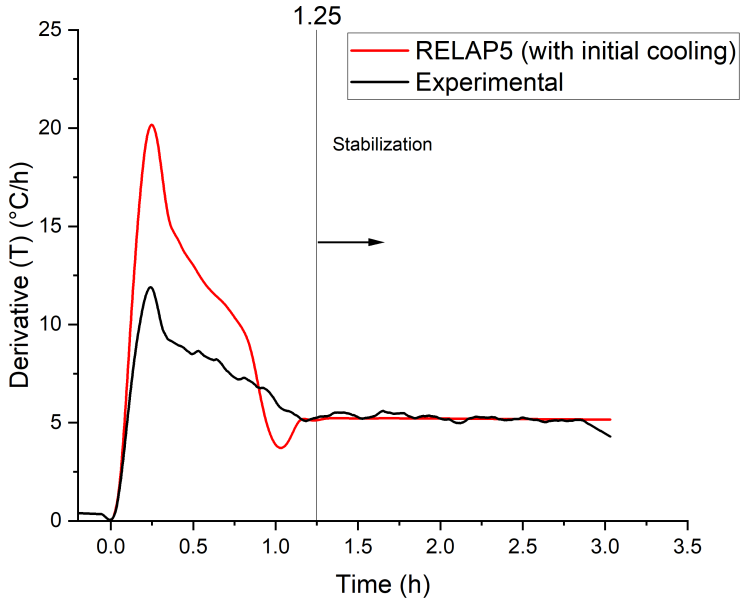

Figure 5.19: Derivative of the core inlet temperature over time, considering the pool cooling process.

Pool Temperature Experiment (RELAP Stratification)			
Parameter	**MNR**	**RELAP5**	**|Error|**
Maximum temperature at core inlet (°C)	36.9 ± 0.1	40.3	9.2%
Maximum temperature at core outlet (°C)	42.4 ± 0.1	46.0	8.5%
Heating rate (in linear region) (°C)	5.25 ± 0.14	5.21	0.76%

Table 5.5: RELAP results and comparison with experimental measurements in the Pool Temperature Experiment simulation considering the pool cooldown process previous to the start of the experiment.

5.3.3 Comparison of different simulation approaches for the Pool Temperature Experiment

The simulations conducted for the Pool Temperature Experiment using various approaches—incorporating CFD-derived stratification, assuming homogeneous pool temperature, and attempting to simulate stratification within RELAP—present intriguing insights into the impact of initial pool temperature profiles on subsequent predictive accuracy. Figure 5.20 offers a comparative analysis depicting the evolution of core inlet temperatures based on the assumptions outlined in the sensitivity analysis. These findings are juxtaposed against the optimal scenario obtained with the CFD stratification and experimental measurements. Meanwhile, Figure 5.21 illustrates the derivative of these temperature profiles, providing a comparative perspective across the datasets.

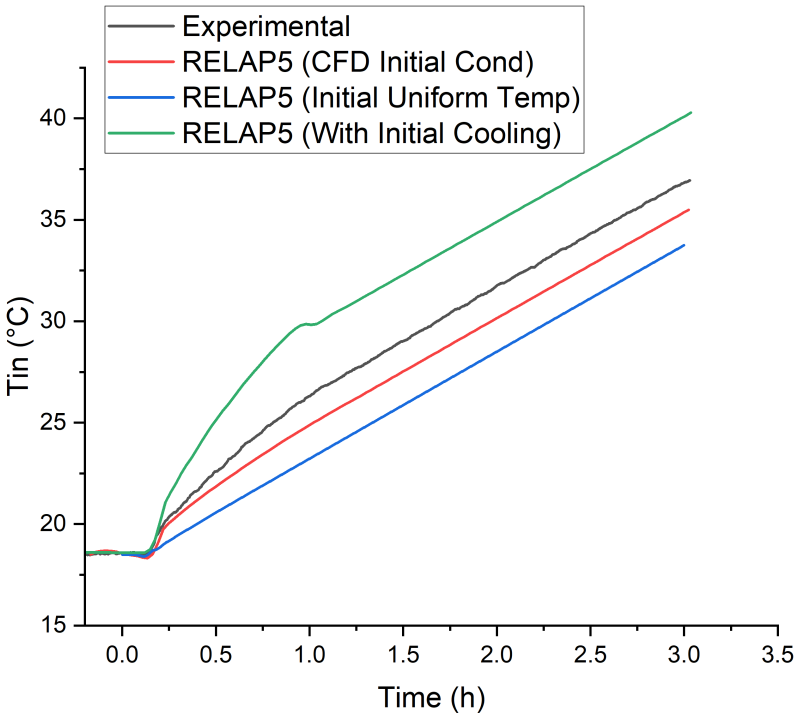

Figure 5.20: Comparison of the core inlet temperature over time with the different assumptions.

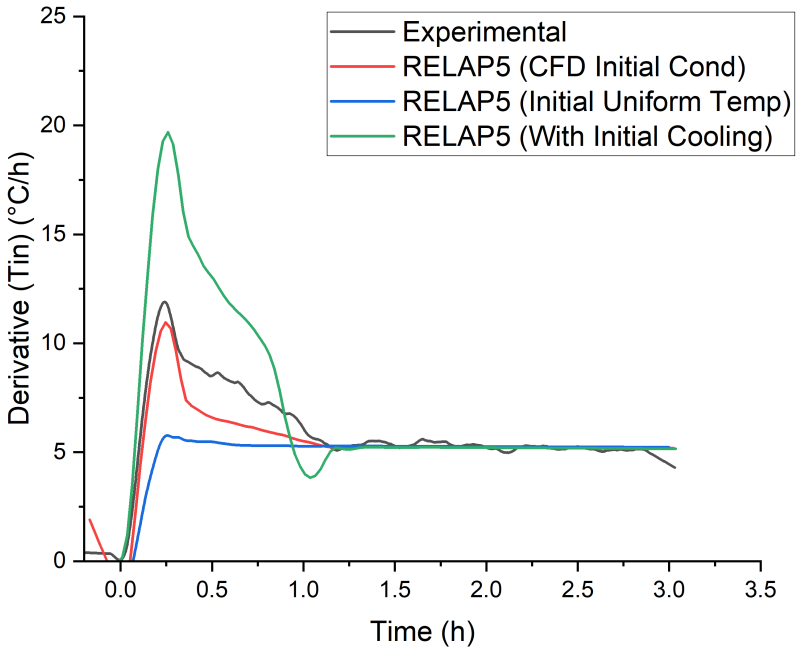

Figure 5.21: Comparison of the core inlet derivative over time with the different assumptions.

The utilization of CFD-derived stratification data unveiled the significance of capturing three-dimensional thermal stratification for accurate simulation of transient events. A notable discrepancy emerged when assuming a homogeneous pool temperature in the simulation, resulting in underestimated heating rates during the initial stages of the experiment. This highlights the importance of integrating sophisticated stratification data into thermal-hydraulic codes like RELAP for enhanced predictive accuracy.

Comparatively, attempting to simulate pool stratification within RELAP led to temperature overestimations. While RELAP provided reasonable heating rates in the linear phase of the experiment, discrepancies arose due to inaccuracies in predicting the initial stratified profile. RELAP overestimated temperatures, resulting in a marked deviation from experimental measurements during the non-linear phase.

This indicates the challenge in capturing the complex thermal stratification dynamics solely within RELAP without leveraging more detailed CFD insights. However, it can be argued that in the scenario where pool stratification is estimated by RELAP, the temperature results appear to be the most conservative among all considered cases.

The findings emphasize the need for a symbiotic integration of CFD and RELAP, leveraging the strengths of both methodologies. Combining CFD-validated stratification models with RELAP5 can refine initial temperature profiles, crucial for capturing accurate heating rates and thermal behavior during transient events. This integration presents a promising path toward more precise and reliable nuclear reactor simulations.

5.3.4 Pool nodalization

The mixing in the pool is a phenomenon that directly depends on the nodalization of this component. Various studies suggest that the effects that the nodalization of the reactor pool can have on the results can be very significant; therefore, special care must be taken when designing this nodalization. This is especially crucial when there are no experimental measurements available to assist in a comprehensive qualification of the nodalization [18].

The nodalization of the pool has a significant impact when simulating natural circulation and mixing. This is because RELAP5 is a one-dimensional code, so the nodalization must be created with the intended flow patterns in mind. The nodalization should be able to accommodate natural circulation loops in the pool volume, which, for example, cannot be achieved using a single vertical pipe to represent the pool. Therefore, the pool must be discretized into multiple vertical pipes so that the

natural circulation loops can form, allowing for a more accurate simulation of mixing.

In the analysis of the first heating cycle of the Pool Temperature Experiment, it is observed that the pool initiates with a stratified temperature profile. At the bottom, there is relatively cold water (around 18°C), while relatively warmer water concentrates at the top (approximately 26°C). Upon commencing the heating stage (i.e., shutting down the secondary system, thereby interrupting heat removal from the primary), hot water starts to be injected from the bottom of the pool (Pool 2). This inflow of hot water tends to rise and mix due to its lower density, leading to the formation of natural circulation patterns within the pool. The ascending hot water mixes with the cold water, achieving an equilibrium temperature and closing the loop in a downward direction. To capture this phenomenon using RELAP5 model nodalization, the pool must be conceptualized as a series of vertical pipes, allowing natural circulation loops to form within volumes and junctions.

A pool with a single vertical pipe allows flow in only one direction. When the pool is divided into two vertical pipes (while conserving parameters such as total area and length), the pathway for the existence of a natural circulation loop is opened, where hot fluid ascends through one pipe and descends through the other. Taking it a step further, subdividing the pool into four vertical pipes allows for an even finer description of the formation of natural circulation loops. However, due to the lack of transverse conservation equations, the actual transverse flows are only crudely approximated through hydraulic connections and loss factors.

This study aimed to assess the impact of various pool nodalizations on the simulation outcomes of the Pool Temperature Experiment. The baseline MNR model, outlined in this thesis and encompassing results from sections 5.1 and 5.2, adopts a

configuration with 2 vertical pipes for the pool, as detailed in section 4.3. This investigation specifically concentrated on evaluating two distinct nodalization approaches: the first employing a single vertical pipe for the entire pool, and the second utilizing a total of four pipes, with two dedicated to representing Pool 1 and the remaining two for Pool 2. The subsequent section provides an in-depth description of each nodalization strategy implemented, coupled with the corresponding simulation results.

It is important to highlight that, in both scenarios, the initial condition for the pool involved utilizing the stratified temperature profile derived from the Computational Fluid Dynamics (CFD) simulation. This temperature distribution is illustrated in Figure 5.11.

1-pipe Pool nodalization

In this simple model, only one pipe represents the entire pool. This pipe has 21 axial volumes that add up to a total of 9.3 m of water column. The upper volume of the pipe (volume 1) is connected to a time-dependent volume that represents the air in the containment. The lowest volume (volume 21) in the pipe represents the bottom of the pool and receives the returning water from the heat exchanger. At 1.97 meters of height from the bottom of the pool (volume 16), water is extracted to cool the core.

For illustrative purposes, Figure 5.22 depicts the nodalization of the pool isolated from the rest of the heat transport system. The connection to the heat exchanger (Pool inlet) and to the core (Pool outlet) is symbolized with time-dependent junctions and time-dependent volumes. This nodalization was integrated into the complete MNR reactor model, and the Pool Temperature Experiment simulation was

conducted. This methodology is repeated in the other sections when presenting the results of nodalizations with 2 and 4 vertical pipes; the isolated nodalization of the system is illustrated, but the simulations were carried out taking into account the entirety of the heat transport system.

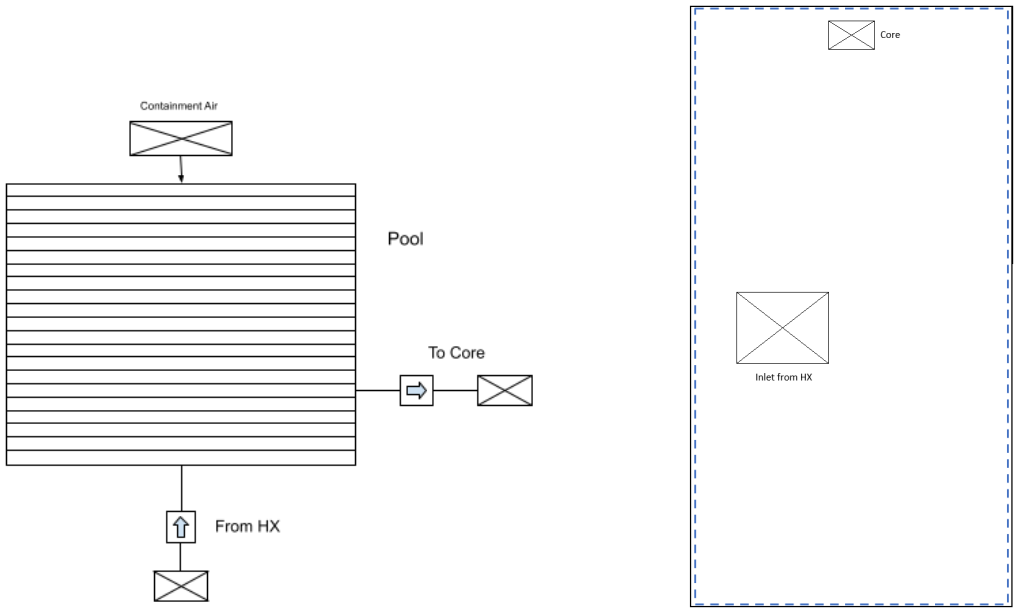

(a) Nodalization of the 1-pipe pool model. (b) Top view of pool nodalization.

Figure 5.22: Representation of the 1-pipe nodalization of the Pool.

The Pool Temperature Experiment was simulated using a 1-pipe nodalization, and the results are illustrated in Figure 5.23. This study primarily focuses on analyzing the axial temperature profile of the pool and its evolution throughout the experiment.

As the hot water enters the pool, its temperature rises solely between volumes 21 and 16, encompassing the section below the core entrance. This implies that all the heated water injected into the pool is subsequently extracted to cool the core, leaving the remainder of the water column above the core unaffected. The entire water column above the core maintains the stratified temperature since there is no

mixing with the rest of the pool.

It's crucial to note that the simulation results in this case do not represent the reality. In the MNR pool, when this heating phenomenon occurs, all water eventually reaches a uniform/mixed temperature. Consequently, the 1-pipe model falls short in accurately representing the intricate mixing phenomenology observed in the reactor pool. Therefore, it is not recommended for simulating events such as a loss of heat sink.

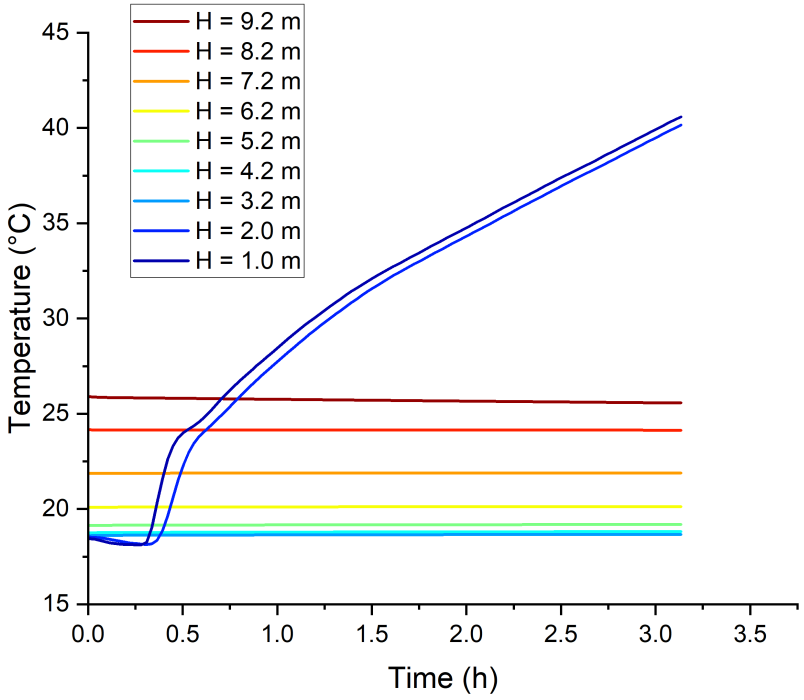

Figure 5.23: Pool temperature across height with a 1-pipe nodalization.

2-pipe Pool nodalization

This is the reference nodalization used for the pool model in this research. Comprehensive results provided so far show the performance of this nodalization in the

various simulations. But for completion, the results for this nodalization will be presented again as a review to compare with the two other nodalizations in this sensitivity analysis.

In this case, 2 pipes represent the entire pool, 1 pipe for Pool 1 and 1 pipe for Pool 2 (see Figure 5.24). Both pipes have 21 axial volumes that add up to a total of 9.3 meters of water column. The upper volumes of the pipes (volume 1) are connected to 2 different time-dependent volumes that represent the air in the containment. The lowest volume (volume 21) in the Pool 2 is where the water from the heat exchanger is injected. At 1.97 m of height from the bottom of the Pool 1 (volume 16), water is extracted to cool the core.

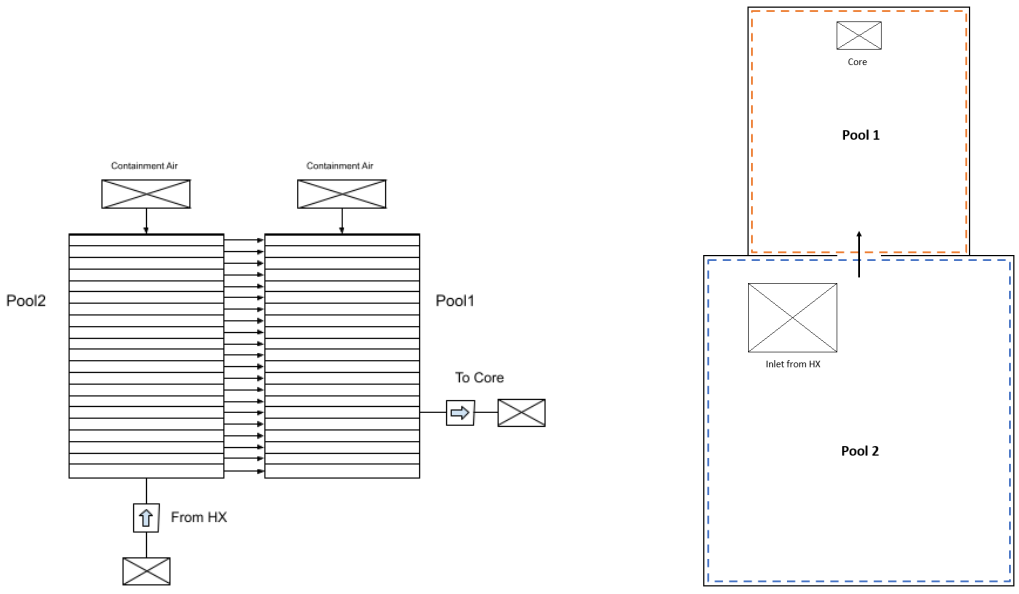

(a) Pool 2-pipe nodalization. (b) Top view of the 2-pipe nodalization.

Figure 5.24: Representation of the 2-pipe nodalization of the Pool.

Examining the model configured with 2 pipes representing the Pool reveals more

promising results in terms of mixing and overall temperature predictions. The evolution of the axial temperature profile of the pool was presented earlier in Figure 5.15. These values were derived by averaging the temperature of both sub-pools between adjacent nodes at the same height.

The temperature profile within the pool undergoes expected changes over time as the hot water ascends to the surface. Significantly, the upper sections of the pool require more time to attain a uniform equilibrium temperature compared to the lower sections. This highlights the temporal aspect of the mixing process, emphasizing the duration it takes to homogenize the temperature in the entire pool. Approximately 1.25 hours are needed to achieve a uniform temperature throughout the pool.

This 2-pipe pool model demonstrates highly promising results, allowing for a clear observation of the mixing phenomenon across the entire pool. It effectively showcases how hot water diffuses from the bottom to the surface, and concurrently, it maintains a relatively low computational cost compared to the model with 4 vertical pipes.

4-pipe Pool nodalization

In this nodalization, the entire pool is represented by four pipes, with two dedicated to Pool 1 (Pool 1A and Pool 1B) and the other two to Pool 2 (Pool 2A and Pool 2B). The upper volumes of these pipes are linked to distinct time-dependent volumes, symbolizing the air in the containment. The lowest volume (volume 21) in Pool 2B serves as the connection to the Heat Exchanger (HEX). At a height of 1.97 m from the bottom of Pool 1B (volume 16), water is extracted for the purpose of core cooling.

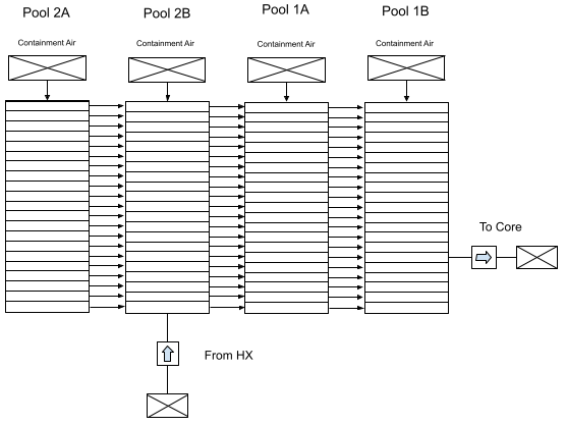

(a) Pool 4-pipe nodalization.

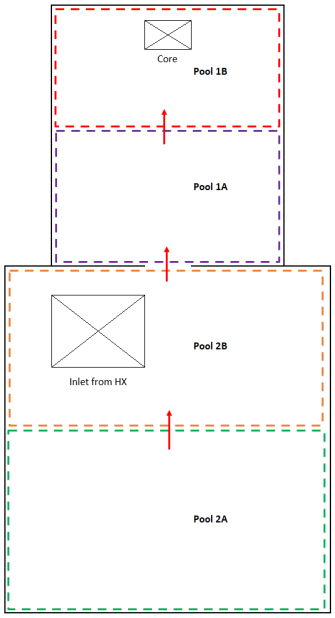

(b) Top view of the 4-pipe nodalization.

The transient behavior of this pool model closely resembles that observed in the 2-pipe model. Initially, there is a temperature increase at the bottom of the pool while the rest of the water maintains a temperature close to the initial stratified level. Subsequently, water diffuses, causing a rise in the temperature of other volumes, leading to mixing and the eventual uniformity of temperature. Approximately 0.75 hours are required to achieve a uniform temperature throughout the pool, representing a shorter time compared to the 2-pipe model (which was around 1.25 hours).

A distinguishing feature between the 4-pipe model and the 2-pipe model is that the 4-pipe model can predict temperature distribution with higher resolution. However, it's important to highlight that despite this increased resolution, the averaged values remain very similar between the two models. Additionally, the computational cost of this model is significantly higher than that of the other two. Moreover, since

conservation of momentum is not included in lateral connections, any additional segmentation does not provide significant benefits.

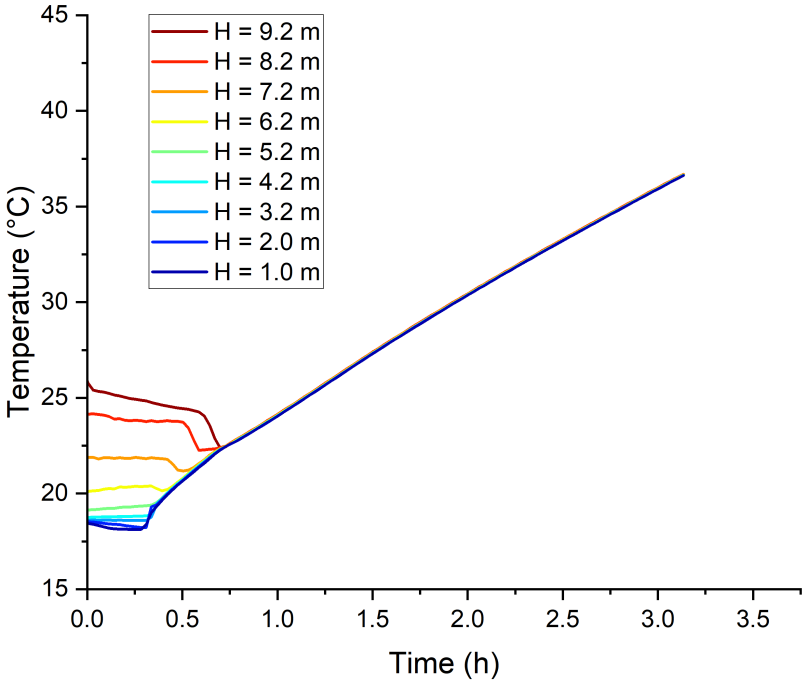

Figure 5.26: Pool temperature across height with 4-pipe nodalization.

Comparison between Pool nodalizations

In Figure 5.27, the temporal evolution of the average temperature across the entire pool is depicted using various models, as previously discussed. Notably, the average temperatures for models employing 2 and 4 pipes exhibit a distinctive similarity. In contrast, the 1-pipe model displays a considerable disparity, attributed to the heterogeneity in the temperature distribution. Furthermore, the 1-pipe model manifests a distinct behavior characterized by lower temperature values than those observed in the other two models.

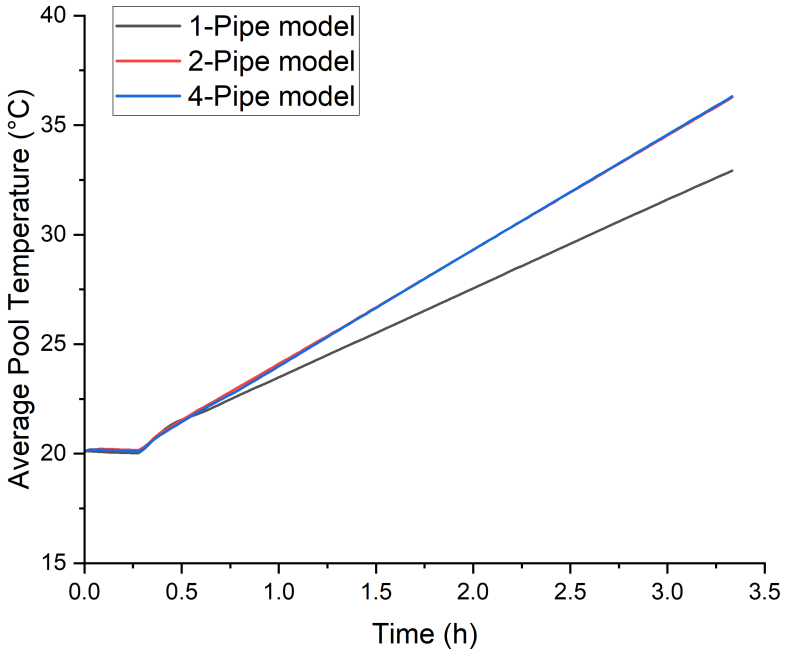

Figure 5.27: Comparison of the Pool average temperature obtained with the three different nodalizations.

Figure 5.28 depicts the core inlet temperature over time using three different nodalizations for the Pool (1, 2, and 4 pipes), alongside experimental measurements from the Pool Temperature Experiment. The 1-pipe model proves inadequate in capturing the thermal phenomenology within the pool, leading to a significant discrepancy between predictions and measurements. In contrast, both the 2-pipe and 4-pipe models demonstrate robust agreement with experimental values. The marginal difference between these models suggests negligible impact on their ability to accurately represent the thermal phenomena.

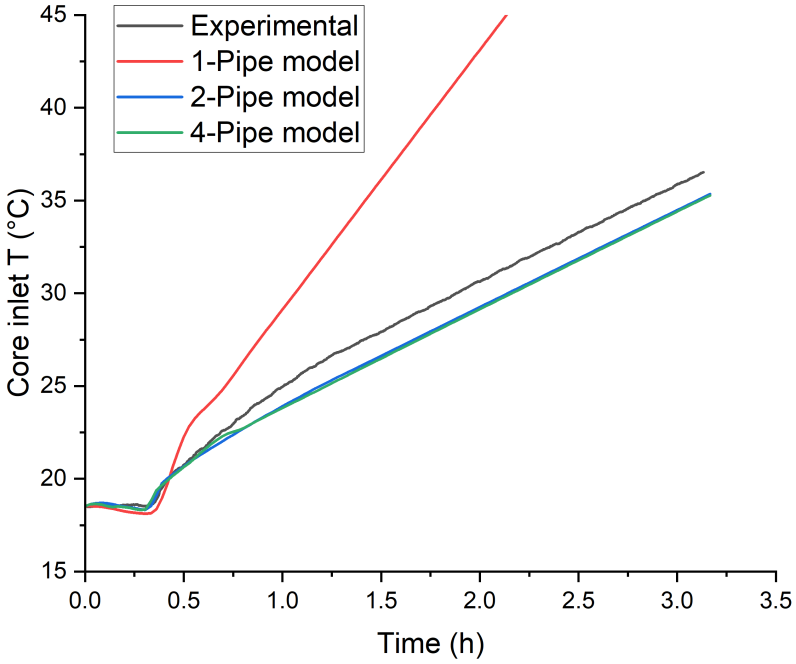

Figure 5.28: Comparison of the core inlet temperature obtained with the three different nodalizations and the experimental measurements.

In Figure 5.29, the derivative of the core inlet temperature is displayed. It becomes evident that the 1-pipe model fails to accurately capture the system behavior, resulting in a significant deviation from experimental values in terms of heating rate. Initially, the derivative experiences a sharp increase before stabilizing around 14°C/h, which notably diverges from the experimental measurements. This disparity underscores the inadequacy of this nodalization for simulating such scenarios.

In contrast, both the 2-pipe and 4-pipe nodalizations demonstrate satisfactory performance. In both cases, the evolution of the derivative closely mirrors experimental trends, though stabilization occurs more rapidly with the 4-pipe nodalization, around t=0.75h, compared to the 2-pipe nodalization, where stabilization is achieved at approximately t=1.25h. Remarkably, the stable heating rates for both models

closely match experimental values.

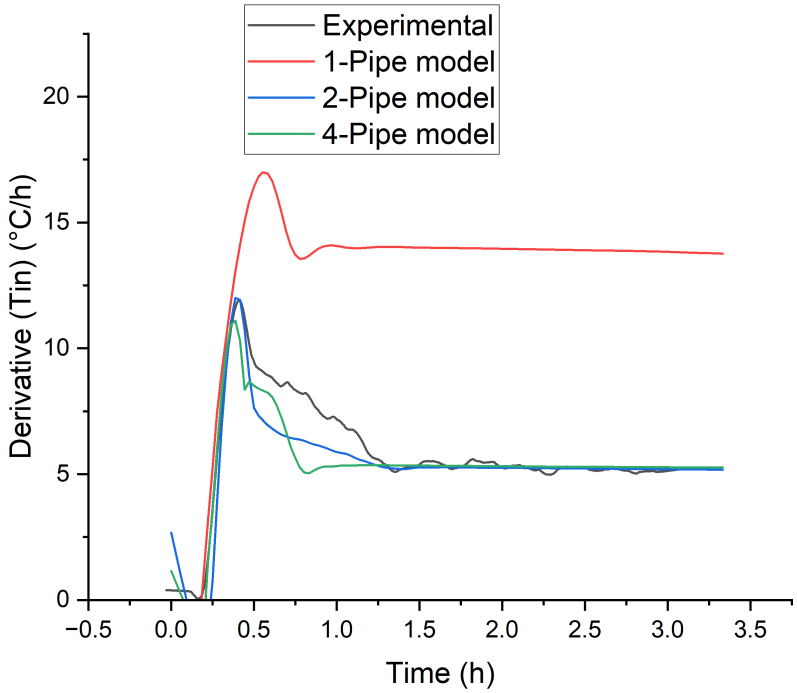

Figure 5.29: Comparison of the derivative of the core inlet temperature obtained with the three different nodalizations and the experimental measurements.

In conclusion, for an accurate depiction of phenomenology during a Loss of Heat Sink event, it is advisable to employ a Pool nodalization with at least 2 vertical pipes. The simplistic 1-pipe model lacks the precision required for obtaining representative results. Conversely, a finer nodalization, such as 4 pipes, does not significantly enhance accuracy and also entails higher computational costs. Therefore, a 2-pipe model emerges as the preferred choice for simulating such scenarios.

5.3.5 HUT nodalization

The HUT serves a critical role by introducing a time delay into the coolant flow, allowing radioactive isotopes to decay and reducing the radiation dose in the pump

room. In the real system, this delay typically spans around 10 minutes. In addition to this, the HUT adds a significant volume of water to the primary loop, enhancing the system thermal inertia. This characteristic slows down the heating and cooling processes within the primary loop, providing operators with ample time to control the reactor under various conditions. Another key feature of this component is that it maintains atmospheric pressure on its surface, forcing the coolant to flow from the reactor pool into the HUT.

The nodalization of the HUT must account for these factors to accurately represent the real system. In this model, estimating the total water volume within the HUT (thermal inertia) and maintaining atmospheric pressure on the tank surface were the main priorities. To achieve this, vertical pipes connected with lateral cross-flow junctions were employed, as detailed in the "Model Development" chapter 4.6.

However, this nodalization approach has limitations, particularly in accurately estimating the delay time, as lateral cross-flow junctions provide only a crude approximation of the transverse flow behavior. With this in mind, three different nodalizations were explored, all meeting the criteria of thermal inertia and atmospheric pressure on the surface but varying in delay time:

- A single vertical pipe with two connections at the bottom for inlet and outlet flow, as depicted in Figure 5.30.
- Two vertical pipes connected laterally with cross-flow junctions, where the first pipe bottom represents the inlet and the second pipe bottom represents the outlet, as shown in Figure 5.31.
- Seven vertical pipes connected laterally with cross-flow junctions, with the first

and seventh pipes representing the inlet and outlet, respectively. This nodalization, detailed in the "Model Development" chapter 4.6, was defined as the reference model. This nodalization was previously illustrated in Figure 4.23.

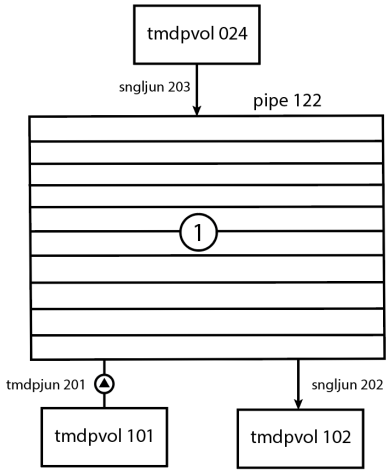

Figure 5.30: HUT nodalization considering a single vertical pipe.

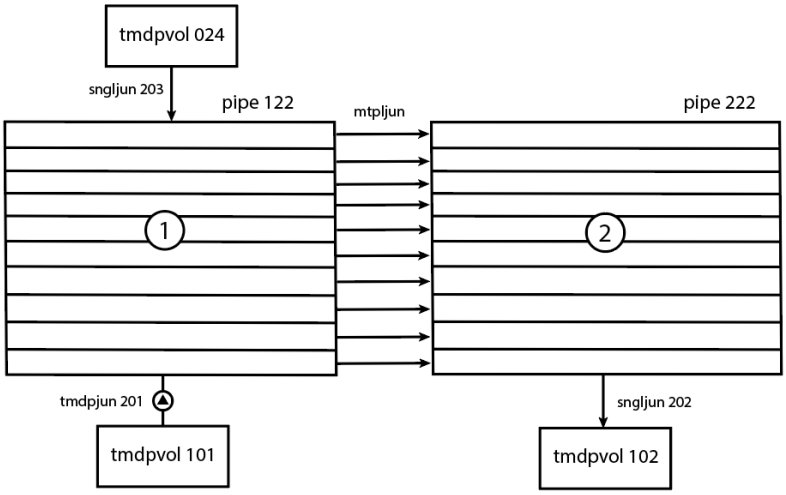

Figure 5.31: HUT nodalization considering a 2 vertical pipes connected laterally with cross-flow junctions.

The flow was regulated using a time-dependent junction at the inlet. All volumes

and pipes were initially set to a temperature of 20°C. The flow rates at the inlet and outlet were maintained at 125 l/s, representing a nominal operating condition at 3MW of power. Following a 2-minute period of steady-state simulation, water at 30°C was introduced into the inlet of the HUT. Subsequently, the time taken for the hot water to reach the outlet of the tank was recorded for analysis.

Figure 5.32 displays the results of the analysis. The inlet temperature curve represents the temperature at the inlet time-dependent volume (tmdpvol 101), initially set at 20°C and adjusted to 30°C after the first 2 minutes of steady-state simulation, following the prescribed boundary conditions.

For the nodalization with only one vertical pipe, the temperature increase at the outlet occurs almost instantly. This is because the bottom volume of this model functions as both inlet and outlet simultaneously, resulting in no modeled time delay.

When employing two pipes in the nodalization, the temperature rise at the outlet also happens rapidly following the injection of hot water at the inlet. However, the temperature increase is less pronounced compared to the single-pipe case. It takes over 30 minutes for the HUT outlet to reach 30°C in this configuration, whereas with a single pipe, the outlet temperature reaches 30°C in just 12 minutes.

Conversely, the nodalization featuring seven pipes exhibits a delay in the onset of temperature at the outlet. During the initial 6 minutes of the transient, no hot water reaches the outlet. Only after this period does the outlet temperature begin to rise gradually. Consequently, it takes over 30 minutes for the outlet temperature to reach 30°C. This nodalization closely aligns with the estimated 10-minute delay observed in the real HUT, thus justifying its implementation in the reference MNR RELAP model, as detailed in the "Model Development" chapter 4.6.

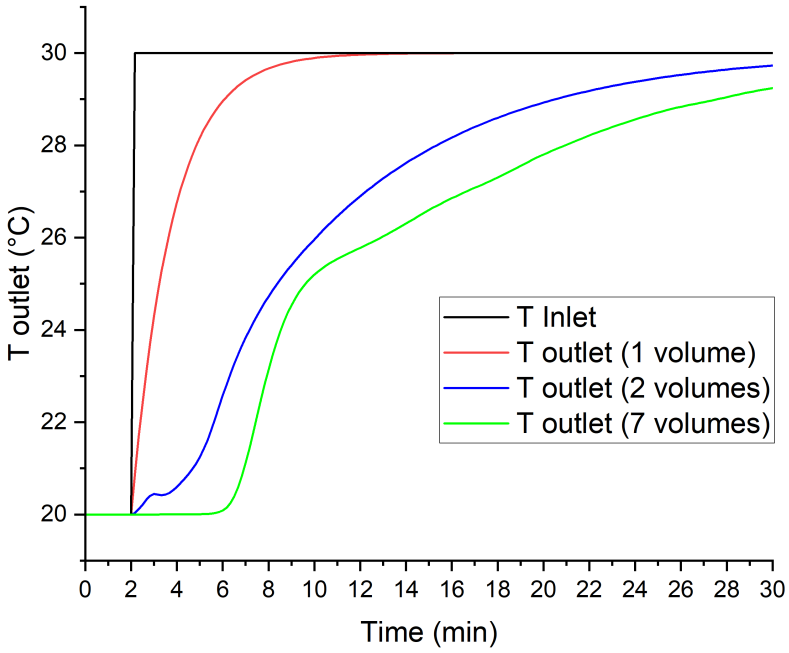

Figure 5.32: Comparison of the coolant time delay in the HUT with three different nodalizations; considering 1, 2 and 7 vertical pipes.

It's worth noting that as the number of vertical pipes in the nodalization increases, so does the computational cost of the simulation. Consequently, the 7-pipe nodalization requires significantly more computational resources compared to the 1-pipe and 2-pipe nodalizations. In contrast, the 1-pipe nodalization stands out as the faster and less computationally demanding option.

5.3.6 Impact of heat losses in the system

When modeling the primary heat transport system, it is crucial to account for heat losses, as they can significantly impact the heating rate during a loss of heat sink (LOHS) event. In this study, heat loss refers to the extraction of heat from the primary system by heat sinks in the environment surrounding the reactor. Incorporating heat

loss into the model helps prevent the overestimation of the heating rate during a LOHS event. Therefore, the decision was made to investigate the impact of heat losses considered in the MNR RELAP model.

In the previous chapter titled "Model Development," detailed thermal models for heat losses were explained, encompassing the reactor pool (4.3), primary piping (4.5), and HUT (4.6). To assess the effect of heat losses, simulations of the Pool Temperature Experiment were conducted using the reference model, as presented in sections 5.1 and 5.2, while disregarding all heat losses. It is noteworthy that the initial condition for the pool involved setting the stratified temperature profile derived from Computational Fluid Dynamics (CFD) simulations. This temperature distribution was illustrated in Figure 5.11.

Figure 5.33 displays the evolution of core inlet and outlet temperatures over time with and without the implementation of heat losses in the system model. As anticipated, the maximum temperature at the end of the heating ramp is higher when heat losses are not considered. Specifically, the maximum core inlet temperature obtained was 35.5°C with heat losses and 36.7°C without heat losses. Similarly, the core outlet temperature with heat losses is 41.2°C, while it reaches 42.4°C when heat losses are ignored.

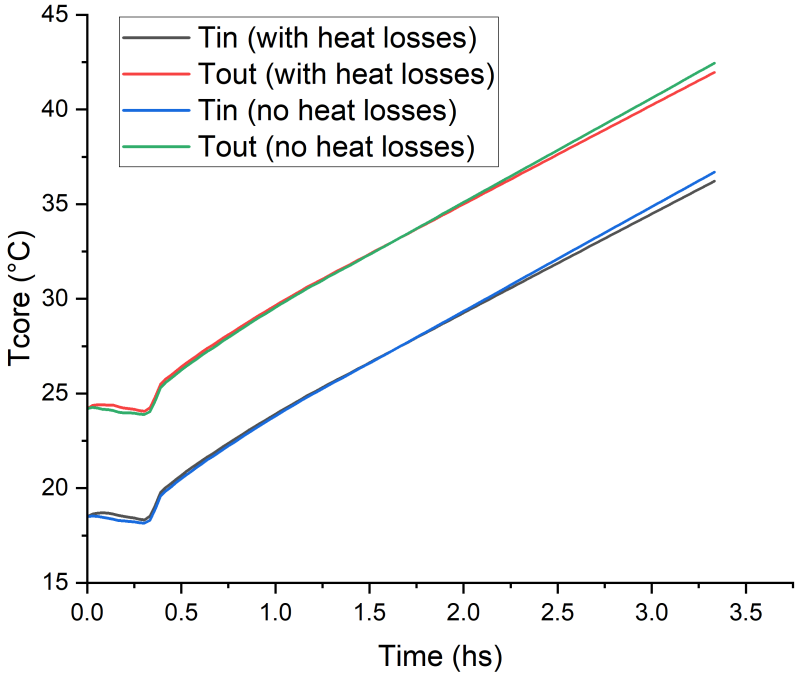

Figure 5.33: Core temperature evolution with and without heat losses.

Figure 5.34 illustrates the derivative of the core inlet temperature over time for both cases, with and without considering heat losses. This graph clearly demonstrates the impact of heat losses on the heating rate. Specifically, the heating rate with the model that includes heat losses is 5.24°C/h, whereas with the model that ignores heat losses, the heating rate is 5.51°C/h, representing a difference of 5%. It's noteworthy that experimental measurements for the experiment yielded a heating rate of 5.25 ± 0.14 °C/h. Table 5.6 provides a summary of the findings from this analysis.

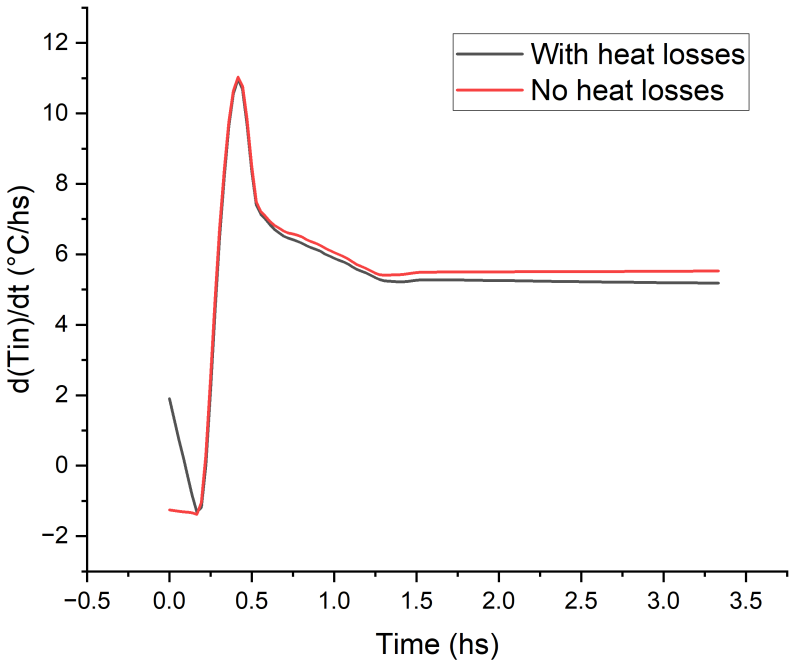

Figure 5.34: Evolution of the core inlet derivative with and without heat losses.

Impact of Heat Losses (Pool Temperature Experiment)			
Parameter	RELAP5 (w/ heat losses)	RELAP5 (no heat losses)	MNR
Max temp at core inlet (°C)	35.5	36.7	36.9 ± 0.1
Max temp at core outlet (°C)	41.2	42.4	42.4 ± 0.1
Heating rate (linear region) (°C)	5.24	5.51	5.25 ± 0.14

Table 5.6: RELAP results and comparison with experimental measurements considering the effect of heat losses.

Chapter 6

Conclusion

In conclusion, the analysis and simulations conducted using RELAP5 to model heat sink loss events at the MNR yielded valuable insights into the system behavior and the code capabilities. The comparison between RELAP5 predictions and experimental data during steady-state operation before the secondary pump trip exhibited good agreement. Specifically, the core and heat exchanger temperatures, along with primary and secondary coolant flows, showcased differences below 1% compared to the reactor measurements, validating the accuracy of the model under normal operational conditions.

Moreover, the simulations of transient events—such as the 2020 secondary pump trip and the Pool Temperature Experiment in 2023—provided deeper understanding and validation of the model predictive capabilities. During the 2020 event, the RELAP5 model effectively captured the core temperature evolution after the pump shutdown, demonstrating a consistent heating rate and closely resembling experimental measurements. The transient results exhibited an error margin below 1% just like the steady state estimations.

The Pool Temperature Experiment simulations provided valuable insights into RELAP5 performance, especially regarding the reactor pool cool-down phase preceding the experiment. This phase induced thermal stratification within the pool, a challenging phenomenon for RELAP5 to simulate accurately. The integration of a three-dimensional Computational Fluid Dynamics (CFD) model significantly bolstered the simulations' accuracy by estimating the pool stratified temperature profile. This profile was then utilized as the initial condition in RELAP5 for simulating the experiment.

By incorporating the CFD results into the RELAP5 model, a maximum error range of approximately 3-4% for peak temperatures and 0.19% for heating rates was achieved. These error margins appear reasonable given the complexity of the problem.

Further sensitivity analyses revealed challenges in accurately reproducing the pool stratified profile with RELAP5, affecting the initial heating rates observed during the experiments. Although RELAP5 could predict linear heating trends well once the pool reached equilibrium, the model encountered difficulties in accurately forecasting heating rates at the event onset.

Notably, when simulating the pool pre-experiment cooling process with RELAP5, the predicted temperatures during the loss of heat sink event consistently exceeded the measured values, suggesting a conservative bias in these predictions.

The outcomes of this research underscore the central role of the pool initial mixing state in influencing heating rates during a loss of heat sink accident. A thermally stratified pool, at the onset of the event, demonstrates a non-linear temperature response, resulting in higher temperatures than anticipated compared to a uniformly heated pool. Consequently, safety analyses for pool-type reactors during Loss of Heat

Sink (LOHS) events, assuming uniform pool temperatures as an initial condition, may lack conservatism, particularly when considering scenarios similar to the Pool Temperature Experiment.

This study highlights the significance of integrating multi-dimensional modeling techniques to enhance the accuracy and reliability of nuclear reactor safety analyses. The combined use of RELAP5 and CFD offers a promising approach to comprehensively model thermal-hydraulic behaviors, ensuring a more thorough understanding of reactor responses to transient events and optimizing safety assessments in nuclear power plants.

The sensitivity analysis conducted on the pool nodalization indicates that using a single vertical pipe does not adequately capture the thermal phenomena within the pool during a LOHS scenario. Conversely, employing 2 pipes appears to provide a more accurate representation for the pool model. However, nodalizations featuring 4 pipes do not significantly enhance the model accuracy and also increase computational costs. Therefore, opting for 2 vertical pipes emerges as the preferred choice for the pool nodalization, as it yields satisfactory results without imposing excessive demands on computational resources.

The analysis on the HUT nodalization revealed that the number of vertical pipes in the model can impact the delay time. When employing a single pipe, no delay in the coolant flow is modeled. With a 2-pipe model, the temperature increase is less pronounced compared to the single-pipe case. Conversely, a 7-pipe model (the reference model used in this study) can simulate a time delay of 6 minutes, which closely aligns with the 10-minute delay observed in the real HUT.

Lastly, the impact of heat losses in the primary heat transport system was analyzed. The results indicate that when simulating the Pool Temperature Experiment without considering heat losses in the reactor pool, primary piping, and HUT, the estimated heating rate is 5% higher compared to the model that incorporates these heat losses.

Chapter 7

Future Work

It is recommended to conduct a complementary test to the Pool Temperature Experiment, focusing on the cooling stage of the pool and its effect on the subsequent heating cycle. This test should allow the experimental determination of the axial temperature gradient within the pool and its evolution over time. To execute this experiment, a set of vertical probes with various thermocouples spaced axially should be constructed and strategically positioned in different sections of the pool. This instrumentation will enable the experimental measurement of temperature at various heights of the pool over time, thus providing a dataset for validating the CFD model used to predict the phenomenon of thermal stratification within the pool. These measurements would also help reduce uncertainty in the stratified temperature profile used in RELAP5 to predict the progression of the transient event, which has been demonstrated in this study to be significantly important in terms of the primary heating rate once the heat sink loss event is initiated.

Furthermore, it is suggested to conduct more validation studies on the RELAP5 model of the MNR, covering various types of transient events such as pool draining

accidents, loss-of-coolant accidents (LOCA), loss-of-flow accidents (LOFA), etc. The more validation cases performed on the model, the greater its reliability for subsequent reactor safety analyses.

A proposal is made to test a new nodalization of the Hold-up tank using a horizontal pipe that covers the entire length of the actual component, instead of using a series of laterally interconnected vertical pipes. This horizontal pipe should be connected at one of its ends (preferably the inlet end) to a vertical pipe, which in turn connects at its upper zone with a time-dependent volume that sets atmospheric pressure in the HUT. This would allow the flow between the reactor pool and the HUT to occur normally, driven by the height difference between the two tanks (gravitational head). Thus, greater precision could be achieved in estimating the delay time of the fluid within the real system.

It is suggested to add the piping line associated with valve V-13, which was omitted in the current model due to time constraints. This line is used during normal operation to control the inflow rate to the reactor pool. Therefore, adding it to the MNR model would enable a more realistic control of this flow.

Another proposal is to develop a detailed model of the Secondary Heat Transport System of the MNR. In the current reactor model, the secondary system is represented in a very simplified manner. A more detailed model would not only provide information on the thermohydraulic conditions of this system during a transient event but also allow for the evaluation of the performance of secondary components such as cooling towers. This detailed model would also enable the assessment of transients related to valve closures or failures on the secondary side.

Additionally, a more detailed and comprehensive model of the reactor core is

proposed, as it could be useful for analyzing certain types of accidents, such as events related to partial or total blockage of coolant channels or complete assemblies. A core model containing each assembly modeled as a separate pipe would enable the simulation and analysis of heterogeneous phenomena in the core and their impact on the entire Heat Transport System.

Finally, a research line focusing on the multiphysics coupling between RELAP5 and neutronic codes is proposed. This would enable the coupled calculation of accidents presenting strong feedback between the reactor thermohydraulics and core neutronics. In this case, RELAP5 could provide information about the fluid temperature and density, as well as core material properties, while the neutronic code would estimate the power distribution in the core. Additionally, RELAP5 could be coupled with subchannel thermohydraulic codes to simulate the core behavior in much greater detail. In this scenario, RELAP5 would provide primary and secondary system parameters, while the subchannel code would use boundary conditions from RELAP5 to perform a detailed calculation of the core thermohydraulics.

Appendix A

CFD model of the MNR pool

Some background on CFD is given in this section. Furthermore, the description of the CFD model, including the boundary conditions is provided.

Background on CFD

The CFD software used in this work is Ansys CFX. Ansys CFX is a commercial general purpose CFD software, part of Ansys suite of products. It is a vertex-based finite volume code, and it is capable of modelling laminar and turbulent flows. Several turbulence models are available in CFX; however, the most used and robust turbulence models are based on the Reynolds Averaged Navier-Stokes (RANS) equations. The RANS equations involve the splitting of variables such as velocity into the time-averaged and fluctuating components. In order to offer a closure relation to RANS equations, the Boussinesq approximation is used, which expresses a linear dependence between the turbulence shear stress and strain rate. Two-equation turbulence models such as $\kappa - \epsilon$, $\kappa - w$, and Shear Stress Transport (SST) are available in CFX. As the

name implies, these models solve two equations for two different turbulence quantities, such as turbulence kinetic energy, turbulence dissipation rate and turbulence frequency.

Model development

A representation of the CAD model used in the CFD calculations is shown in Figure A.1. Three assumptions were made to the CAD model:

- The installations located in the pool are not taken into account in this work.
- The gate that separates the core from the rest of the pool in reality is broader at the bottom compared to the top part. In this work, the gate is assumed to have the same width regardless of the height, while preserving the flow area through the gate.
- Based on the intention of this transient and its longevity, the core was modelled as a water cuboid. This means that the fuel assemblies are not included in this model.
- The concrete container of the pool is also not included in the calculations.

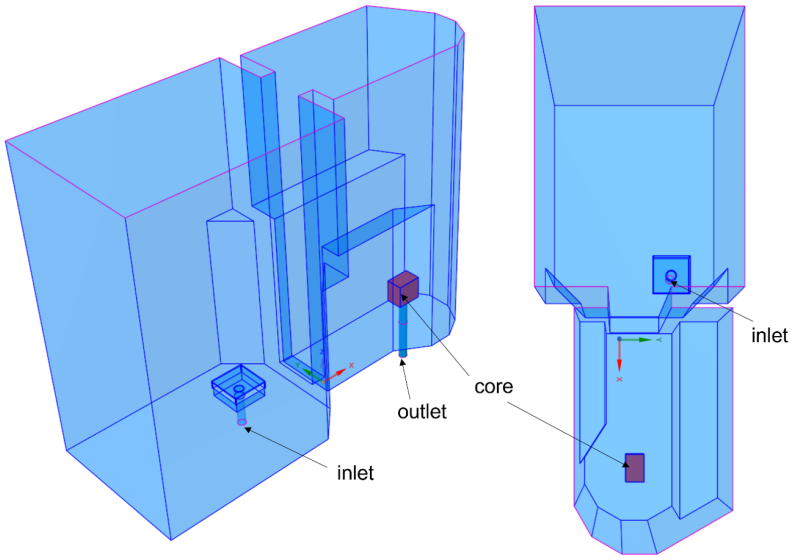

Figure A.1: CAD model of the MNR pool. The core is shown in red. The Inlet of the pool is shown both figures, while the outlet is only shown on the left-hand side figure. In the right-hand side figure, the outlet is located below the core.

The geometry was meshed using Ansys Meshing. The mesh used for this calculation results from a mesh sensitivity analysis study, in which three meshes with different mesh densities were examined (see Table A.1).

Mesh	**Node number**	**Min. element quality (-)**	**Max. Courant number core (-)**	**Max. Courant number pool (-)**
Mesh 1	559011	0.23	639.1	518.9
Mesh 2	3952586	0.47	316.5	260.9
Mesh 3	8432299	0.48	316.0	260.0

Table A.1: Mesh sensitivity analysis parameters for three meshes.

Based on the element quality, the Courant number and the node number, Mesh 2 was chosen for further calculations due to its satisfying ratio between quality and computational effort.

The boundary conditions for the transient include the inlet mass flow of 126 kg/s, and outlet pressure of 1.8 bar. Additionally, the walls of the pool are modelled as no

slip adiabatic wall, while the top of the pool is free slip and adiabatic. The transient runs for about 14000 s, with a 0.2 s time step for the first 5 seconds, and a 10 second time step for the remaining time.

Bibliography

[1] *McMaster Nuclear Reactor Safety Report, Rev. 1.* McMaster Nuclear Reactor, 2012.

[2] *Safe Operating Envelope of McMaster Nuclear Reactor, Rev.5, MNR Technical Note MNR TN-2001-03 R5.* McMaster Nuclear Reactor, 2020.

[3] *Safety Assessment for Research Reactors and Preparation of the Safety Analysis Report.* Number SSG-20 (Rev. 1) in Specific Safety Guides. IAEA, Vienna, 2022. ISBN 978-92-0-141521-9.

[4] H. Abou Yehia, J. Bastos, H. Boado Magan, A. D'Arcy, F. D'Auria, A. Doval, V. Garea, A. Guba, A. Hainoun, S. Lee, et al. Safety analysis for research reactors. 2008.

[5] M. Adorni, A. Bousbia-Salah, T. Hamidouche, B. Di Maro, F. Pierro, and F. D'Auria. Analysis of partial and total flow blockage of a single fuel assembly of an MTR research reactor core. *Annals of Nuclear Energy*, 32(15):1679–1692, 2005.

[6] A. Bousbia-Salah, F. D'Auria, and T. Hamidouche. Analysis of typical transients in the generic 10 MW IAEA MTR research reactor by RELAP5/3.2. 2005.

[7] A. Bousbia-Salah, A. Jirapongmed, T. Hamidouche, J. R. White, F. D'Auria, and M. Adorni. Assessment of RELAP5 model for the University of Massachusetts Lowell research reactor. *Nuclear Technology and Radiation Protection*, 21(1): 3–12, 2006.

[8] S. Chatzidakis and A. Ikonomopoulos. Phenomenological investigation of loss of coolant accident in a research reactor facility. *Nuclear Engineering and Design*, 256:341–349, 2013.

[9] S. Day. McMaster Nuclear Reactor - Reactor Specification", Rev.2, January 2011, as part of IAEA CRP 1496, Innovative Methods for Research Reactors: "Benchmarking against Experimental Data of the Neutronic and Thermalhydraulic Computational Methods and Tools for Operation and Safety Analysis for Research Reactors. Technical report, MNR, 2008-2012.

[10] S. Day, R. Prinsloo, and F. Van Heerden. Development of the MNR OSCAR-5 core follow and reload calculational model for operational support.

[11] F. Dittus and L. Boelter. Heat transfer in automobile radiators of the tubular type. *International communications in heat and mass transfer*, 12(1):3–22, 1985.

[12] N. El-Sahlamy, A. Khedr, and F. D'Auria. Thermal hydraulic analysis of reactivity accidents in MTR research reactors using RELAP5. *Kerntechnik*, 80(6): 557–562, 2015.

[13] C. Fletcher and R. Schultz. RELAP5/MOD3 code manual. Technical report, Nuclear Regulatory Commission, Washington, DC (United States), 1992.

[14] W. J. Garland. Thermalhydraulic modelling of the McMaster Nuclear Reactor. Technical report, MNR Technical Report 97-04, 1997.

[15] T. Hamidouche, A. Bousbia-Salah, M. Adorni, and F. D'Auria. Dynamic calculations of the IAEA safety MTR research reactor benchmark problem using RELAP5/3.2 code. *Annals of Nuclear Energy*, 31(12):1385–1402, 2004.

[16] T. Hamidouche, A. Bousbia-Salah, F. D'Auria, et al. Overview of accident analysis in nuclear research reactors. *Progress in Nuclear Energy*, 50(1):7–14, 2008.

[17] F. P. Incropera, D. P. DeWitt, T. L. Bergman, A. S. Lavine, et al. *Fundamentals of heat and mass transfer*, volume 6. Wiley New York, 1996.

[18] A. Khedr and F. d'Auria. Nodalization effects on RELAP5 results related to MTR research reactor transient scenarios. *Nuclear Technology and Radiation Protection*, 20(2):3–9, 2005.

[19] C. S. Kim. Thermophysical properties of stainless steels. Technical report, Argonne National Lab, 1975.

[20] S.E. Day, K.S. Ruiz. MNR Facility Specification Thermal-Hydraulics, Rev.1, February 2024, as part of IAEA CRP 1496, Innovative Methods for Research Reactors: "Benchmarking against Experimental Data of the Neutronic and Thermalhydraulic Computational Methods and Tools for Operation and Safety Analysis for Research Reactors. Technical report, MNR, 2024.

[21] H. V. Soares, I. D. Aronne, A. L. Costa, C. Pereira, and M. A. F. Veloso. Analysis of loss of flow events on brazilian multipurpose reactor using the RELAP5 code. *International Journal of Nuclear Energy*, 2014, 2014.

[22] G. Stander, R. H. Prinsloo, E. Müller, and D. Tomaševic. OSCAR-4 code system application to the SAFARI-1 reactor. In *Proceedings of the International Conference on the Physics of Reactors*, pages 1179–1187, 2008.

[23] F. M. White. *Fluid mechanics*. The McGraw Hill Companies, 2008.